

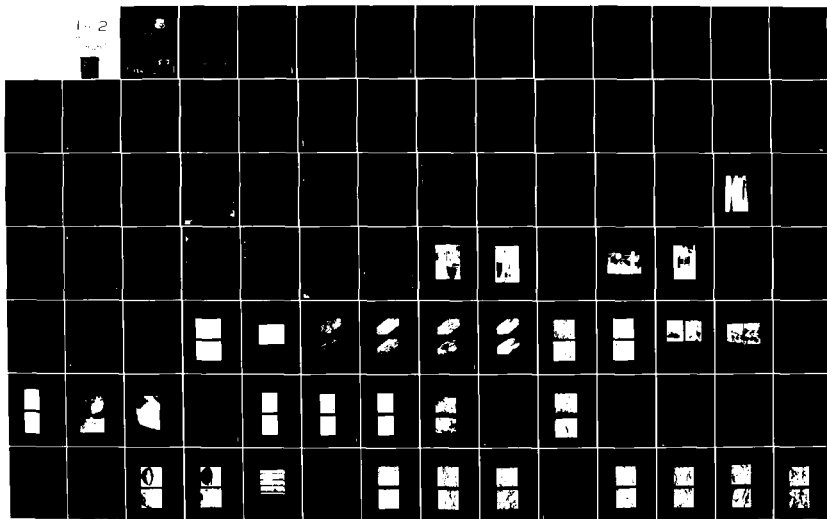
AD-A118 280

AIR FORCE WRIGHT AERONAUTICAL LABS WRIGHT-PATTERSON AFB OH F/G 11/6
A COMPARISON OF MICROSTRUCTURE AND PROPERTIES OF EQUIVALENT STR--ETC(U)
AUG 81 S M DOERR
AFWAL-TR-81-4068

UNCLASSIFIED

NL

1-2



12

AFMAL-TR-81-4068



**A COMPARISON OF MICROSTRUCTURE AND PROPERTIES
OF EQUIVALENT STRENGTH INGOT METALLURGY AND
POWDER METALLURGY 7XXX ALUMINUM ALLOYS**

Structural Metals Branch
Metals and Ceramics Division

Stephen H. Doerr, Capt, USAF

August 1981

Final Report for Period August 1979 - September 1980

Approved for Public Release; Distribution Unlimited

DTIC FILE COPY

AD A118280

MATERIALS LABORATORY
AIR FORCE WRIGHT AERONAUTICAL LABORATORIES
AIR FORCE SYSTEMS COMMAND
WRIGHT-PATTERSON AIR FORCE BASE, OHIO 45433

DTIC
ELECTE
AUG 17 1982
F

88 08 17 001

NOTICE

When Government drawings, specifications, or other data are used for any purpose other than in connection with a definitely related Government procurement operation, the United States Government thereby incurs no responsibility nor any obligation whatsoever; and the fact that the government may have formulated, furnished, or in any way supplied the said drawings, specifications, or other data, is not to be regarded by implication or otherwise as in any manner licensing the holder or any other person or corporation, or conveying any rights or permission to manufacture use, or sell any patented invention that may in any way be related thereto.

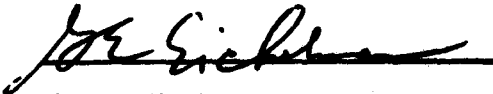
This report has been reviewed by the Office of Public Affairs (ASD/PA) and is releasable to the National Technical Information Service (NTIS). At NTIS, it will be available to the general public, including foreign nations.

This technical report has been reviewed and is approved for publication.



LT. RANDALL JÄHREN
Project Engineer

FOR THE COMMANDER



G.E. RICHELMAN
Chief,
Structural Metals Branch
Metals & Ceramics Division

"If your address has changed, if you wish to be removed from our mailing list, or if the addressee is no longer employed by your organization please notify AFMIL/MLIS, W-PAFB, ON 45433 to help us maintain a current mailing list".

Copies of this report should not be returned unless return is required by security considerations, contractual obligations, or notice on a specific document.

UNCLASSIFIED

SECURITY CLASSIFICATION OF THIS PAGE (When Data Entered)

REPORT DOCUMENTATION PAGE		READ INSTRUCTIONS BEFORE COMPLETING FORM
1. REPORT NUMBER AFWAL-TR-81-4068	2. GOVT ACCESSION NO. AD A118280	3. RECIPIENT'S CATALOG NUMBER
4. TITLE (and Subtitle) A COMPARISON OF MICROSTRUCTURE AND PROPERTIES OF EQUIVALENT STRENGTH INGOT METALLURGY AND POWDER METALLURGY 7XXX ALUMINUM ALLOYS		5. TYPE OF REPORT & PERIOD COVERED Final Report August 1979-September 1980
7. AUTHOR(s) Stephen H. Doerr, Capt, USAF		6. PERFORMING ORG. REPORT NUMBER
9. PERFORMING ORGANIZATION NAME AND ADDRESS Materials Laboratory (AFWAL/MLLS) AF Wright Aeronautical Laboratories, AFSC Wright-Patterson AFB, OH 45433		8. CONTRACT OR GRANT NUMBER(s)
11. CONTROLLING OFFICE NAME AND ADDRESS Materials Laboratory (AFWAL/MLL) AF Wright Aeronautical Laboratories, AFSC Wright-Patterson AFB, OH 45433		10. PROGRAM ELEMENT, PROJECT, TASK AREA & WORK UNIT NUMBERS 24180207
14. MONITORING AGENCY NAME & ADDRESS (if different from Controlling Office)		12. REPORT DATE August 1981
		13. NUMBER OF PAGES 181
		15. SECURITY CLASS. (of this report) Unclassified
		15a. DECLASSIFICATION/DOWNGRADING SCHEDULE
16. DISTRIBUTION STATEMENT (of this Report) Approved for public release; distribution unlimited.		
17. DISTRIBUTION STATEMENT (of the abstract entered in Block 20, if different from Report)		
18. SUPPLEMENTARY NOTES		
19. KEY WORDS (Continue on reverse side if necessary and identify by block number) High Cycle Fatigue CT91 Powder Metallurgy 3-Point Bend Toughness 7075 Exfoliation Corrosion Crack Initiation Aluminum Alloy Forgings		
20. ABSTRACT (Continue on reverse side if necessary and identify by block number) Microstructure and property relationships of equivalent strength ingot and powder metallurgy (I/M and P/M) 7XXX aluminum alloy die forgings were examined. Fatigue, toughness and corrosion behavior are discussed. Unlike the I/M product, the P/M material did not exhibit a reduction in S-N fatigue behavior in the transverse orientation. Since toughness anisotropy is not similarly dependent upon crack initiation variables, no such anomaly occurred in this property. P/M material was more resistant to exfoliation corrosion in.		

DD FORM 1473 EDITION OF 1 NOV 65 IS OBSOLETE

UNCLASSIFIED

SECURITY CLASSIFICATION OF THIS PAGE (When Data Entered)

Cont'd

UNCLASSIFIED

SECURITY CLASSIFICATION OF THIS PAGE(When Data Entered)

any condition of heat treatment than the most resistant heat treatment condition of the I/M material.

Accession For	
NTIS GRA&I	<input checked="" type="checkbox"/>
DTIC TAB	<input type="checkbox"/>
Unannounced	<input type="checkbox"/>
Justification	
By	
Distribution/	
Availability Codes	
Dist.	Avail and/or Special



UNCLASSIFIED

SECURITY CLASSIFICATION OF THIS PAGE(When Data Entered)

PREFACE

This technical report was prepared by the Structural Metals Branch, Metals and Ceramics Division, Materials Laboratory, Air Force Wright Aeronautical Laboratories, Wright-Patterson Air Force Base, Ohio. The research was conducted under Project No. 24180207. This report includes work performed during the period August 1979 to September 1980. The research was performed by Capt. Stephen H. Doerr.

Mr. Leroy Kennard and Col. Dana Brabson are acknowledged for their timely recommendations and assistance in the authors' transfer from a contract management division to a research division of the Materials Laboratory. The author also recognizes the inspiration he drew from Dr. John Hyzak to accelerate the work. Thanks are due to Dr. Lawrence Otto of the Alcoa Technical Center for the donation of ingot stock used for this project. The author gratefully acknowledges Walter Griffith for furnishing the powder billet needed to pursue the project, for the suggestion of the project itself, for valuable discussions during the course of the enterprise, and for the loan of a considerable amount of reference material. The author also thanks Mr. Francis Jones, Mrs. Jacqueline March, and Mr. Paul Osterday all of the Air Force Wright Aeronautical Laboratories Technical Information Services Division for considerable contributions of time and effort in the exhaustive literature searches conducted over the past two years. The author appreciates the contributions of Dr. Ivan Martorell, and Messrs. Robert Sweeney, Marion Myers, Thomas Jones, James Heil and Roy LeBlanc for forging and machining the material. The author is indebted to Robert Brodecki for photographic assistance and for enlisting the aid of others to expedite the work. Messrs. Marlin Cook and William Houston, Daniel Allen and Gary Teeters are also thanked for their support and instruction in metallographic procedures. Mr. Richard Bacon has the author's gratitude for a most thorough instruction in the operation of a scanning electron microscope. The author is also grateful to Mr. Richard Klinger for thorough instruction in the use of an Instron mechanical testing machine. Mr. Clayton Harmsworth is acknowledged for the permission to have access to the RUMUL resonating fatigue testing machine. The author is indebted to Mr. Samuel Macy for calibration and

electrical circuitry trouble-shooting of the RUMUL machine and to Mr. Donald Wolesslagle for patient instruction in its proper use. Messrs. Robert Lewis and James Paine are also thanked for technical assistance in MTS operation, toughness testing, data reduction and procedural documentation. The author thanks Lt. Randall Jahren for assistance in the corrosion testing. The technical assistance of Messrs. Ralph Omlor, Walter Custer and Brewster Strobe in the performance of optical and transmission electron microscopy, electron microprobe analysis and other laboratory procedures is also acknowledged. The author recognizes the considerable contributions of Ms. Cheryl Conley to all aspects of the extensive photographic documentation. In this regard, thanks are also due to the Technical Photographic Processing Division of the 4950th Test Wing, Air Force Systems Command. The author acknowledges the assistance of Mr. Gail Weisenberger of the Foreign Technology Division, Air Force Systems Command for assistance in translation of the German article used in statistical evaluation of the fatigue data. The author thanks Captain Arsenio Illoreta for imaginative use of computer plotting techniques in manifestation and interpretation of the fatigue data. The author's appreciation extends to Mr. William McConehea of the Air Force Wright Aeronautical Laboratories Graphic Support Services for the generation of mechanical test specimen drawings. Drs. Terrence Ronald, Lawrence Bidwell and Francis Froes, Captain David Voss and Messrs. Gail Eichelman and Lawrence Hjelm has the author's appreciation for helpful advice, discussions and recommendations as well as overall support. The author is appreciative of the typing and other manuscript preparation efforts of Ms. Tonya Bright. Finally, the author gratefully acknowledges the patient guidance and understanding of Professor Gordon Powell during the performance of the research and the composition of this thesis.

TABLE OF CONTENTS

SECTION		PAGE
I	INTRODUCTION	1
II	LITERATURE SURVEY	4
	1. Precipitation-Strengthened Al P/M Alloys	4
	2. Crystallographic Structure and Stacking Fault Energy	6
	3. Microstructural Effects	7
	4. Fatigue Behavior	10
	a. High and Low Cycle Fatigue	10
	b. Relationships Between Monotonic and Cyclic Properties	13
	c. Practical Considerations in Fatigue Evaluation	15
	5. Corrosion Behavior	19
III	EXPERIMENTAL PROCEDURE	21
	1. Materials	21
	a. Primary Processing	21
	b. Chemical Analysis	23
	c. Deformation Processing	23
	d. Heat Treatment	23
	2. Metallographic and Fractographic Characterization	29
	a. Optical Microscopy	29
	b. SEM Microscopy	31
	c. TEM Microscopy	31
	3. Mechanical Behavior Evaluations	32
	a. Monotonic Tension Testing	32
	b. Toughness Testing	34
	c. Fatigue Testing	38
	4. Statistical Evaluation of Fatigue Data	42
	5. Corrosion Behavior Assessment	43
	a. Hardness Testing	43
	b. Electrical Conductivity Testing	44
	c. Exfoliation Corrosion Testing	44
IV	RESULTS AND DISCUSSION	45
	1. Microstructure	45
	2. Mechanical Properties	67

TABLE OF CONTENTS (Concluded)

SECTION		PAGE
	2. Mechanical Properties (Cont'd)	
	a. Strength and Ductility	67
	b. Toughness	67
	c. Fractography of Tensile and Toughness Specimens	72
	d. Fatigue	86
	(1) Stress Concentrations	86
	(2) Fatigue Strength Anisotropy	92
	e. Fractography of Fatigue Specimens	97
	(1) Macroscopic Features	97
	(2) Initiation Sites	97
	(3) Striations	112
	3. Corrosion Resistance	121
	a. Hardness	121
	b. Electrical Conductivity	121
	c. Exfoliation Corrosion	125
V	SUMMARY AND CONCLUSIONS	133
VI	RECOMMENDATIONS FOR FUTURE WORK	134
	APPENDIX A	135
	APPENDIX B	136
	APPENDIX C	137
	REFERENCES	148

LIST OF ILLUSTRATIONS

FIGURE		PAGE
1	Forging Die	27
2	Specimen Extraction Plan	33
3	Toughness Testing Apparatus	36
4	3-Point Bend Jig	37
5	Fatigue Testing Machine	39
6	Close-up of Fatigue Specimen in Grips	40
7	Fatigue Specimen Drawing	41
8	As-Cast I/M Optical Micrographs	46
9	As-Compacted P/M Optical Micrograph	47
10	As-Forged 3-D Optical Micrographs	48
11	Higher Magnification Views of Features in Figure 10	49
12	Heat Treated 3-D Optical Micrographs	50
13	Higher Magnification Views of Features in Figure 12	51
14	Heat Treated Longitudinal SEM Micrographs	52
15	Heat Treated Long Transverse SEM Micrographs	53
16	Heat Treated Longitudinal TEM Micrographs	54
17	Heat Treated Long Transverse TEM Micrographs	55
18	EDAX Analyses of Light and Dark Contrast Areas	57
19	Heat Treated I/M Precipitates TEM Micrograph	58
20	Heat Treated P/M Precipitates TEM Micrograph	59
21	EDAX Analyses of Grain Boundary Precipitates	61
22	EDAX Analyses of Grain Boundary Precipitates and Matrix	62
23	EDAX Analyses of Matrix Precipitates	63
24	As-Cast I/M and As-Compacted P/M TEM Micrographs	64
25	Matrix Precipitate EMPA Micrographs	66
26	Longitudinal Tensile Specimen SEM Fractographs	73
27	Long Transverse Tensile Specimen SEM Fractographs	74
28	Toughness Specimen Optical Fractograph	75
29	Longitudinal Tensile Specimen SEM Fractographs	77
30	Long Transverse Tensile Specimen SEM Fractographs	78
31	Flat Fracture and Shear Lip Area SEM Fractographs	79
32	LT Toughness Specimen SEM Fractographs	81
33	TL Toughness Specimen SEM Fractographs	82

LIST OF ILLUSTRATIONS (Cont'd)

FIGURE		PAGE
34	Higher Magnification Views of Features in Figure 32	83
35	Higher Magnification Views of Features in Figure 33	84
36	S-N Plot	87
37	Y.S.-Normalized Re-Plot of Figure 36	93
38	U.T.S.-Normalized Re-Plot of Figure 36	94
39	Fatigue Specimen SEM Fractographs	98
40	Load Arrest Line SEM Fractographs	99
41	Region B Initiation Site SEM Fractographs	100
42	Higher Magnification Views of Region B Initiation Sites	101
43	Region A Initiation Site SEM Fractographs	102
44	Typical Fatigue Striation SEM Fractographs	105
45	Higher Magnification Views of Region B Initiation Site	106
46	Region C Fatigue Specimen SEM Fractographs	107
47	Higher Magnification Views of Region C Initiation Site	108
48	Region A Initiation Site SEM Fractographs	109
49	EDAX Analyses of Region B Initiation Site Particles	111
50	Low Magnification SEM Views of Striation-Containing Areas	113
51	Typical I/M Striation SEM Fractographs	114
52	Typical P/M Striation SEM Fractographs	115
53	Higher Stress Intensity P/M Striation SEM Fractographs	118
54	Transition to All-Dimple Fracture SEM Fractographs	120
55	Lower Magnification View of Transition in Figure 54 and and Large Cracked Particle SEM Fractographs	122
56	Higher Stress Intensity I/M Striation SEM Fractographs	123
57	EXCO Coupons After Test	126
58	EXCO Test Beakers During Test	127
59	EXCO Test Coupon Optical Micrographs	129
60	EXCO Test Coupon Optical Micrographs	130
61	EXCO Test Coupon Optical Micrographs	131
62	Higher Magnification Views of Features in Figure 61	132

LIST OF ILLUSTRATIONS (Concluded)

FIGURE		PAGE
C-1	Stress vs. Probability of Failure at 10^7 Cycles Plot	142
C-2	Y.S.-Normalized Re-Plot of Figure C-1	143
C-3	U.T.S.-Normalized Re-Plot of Figure C-1	144
C-4	Stress vs. Probability of Failure at 3×10^5 Cycles Plot	145
C-5	Y.S.-Normalized Re-Plot of Figure C-4	146
C-6	U.T.S.-Normalized Re-Plot of Figure C-4	147

LIST OF TABLES

TABLE		PAGE
1	Powder Particle Oxide Chemistry	24
2	P/M Billet Predensification Data	24
3	P/M Cold Compaction Data	24
4	P/M Can Evacuation Data	25
5	P/M Hot Compaction Data	25
6	Overaged Radial P/M Billet Properties	25
7	I/M Billet Practice	25
8	Chemical Analysis	25
9	Forging Procedure	26
10	P/M Dimension Sequence	26
11	I/M Dimension Sequence	26
12	Heat Treatment Procedure	30
13	Tensile Data	68
14	Toughness Data	68
15	Hardness Data	124
16	Conductivity Data	124
C-1	P/M Fatigue Data	140
C-2	I/M Fatigue Data	141
C-3	Mean Fatigue Strengths	141

SECTION I

INTRODUCTION

Grain size refinement has long been known to increase the strength of metals (Reference 1). Numerous approaches to accomplishing this refinement in ingot metallurgy (I/M) aluminum (Al) alloys have been investigated (References 2,3). Thermomechanical treatments of I/M materials have resulted in grain refinement but without significant gains in mechanical properties (References 4-7). The powder metallurgy (P/M) approach to grain refinement represents a dramatic departure from conventional I/M techniques.

Investigators have probably always realized that superior mechanical integrity (fatigue, toughness, ductility, and corrosion resistance) of P/M materials could never be achieved without the complete elimination of porosity and the existence of metal-to-metal bonding everywhere within the product (References 8,9,10). Pressure alone is insufficient to accomplish this. In fact, the determination of satisfactory processing parameters for P/M products has been the subject of several investigations in recent years (References 11,12). Solid state sintering cannot achieve sufficient metal-to-metal bonding in Al P/M because of the highly stable oxide on the surface of the powder particles. Liquid-phase sintering would defeat the purpose of the greater supersaturation of alloying elements desirable to enhance subsequent precipitation strengthening. Hot vacuum compaction results in a somewhat higher degree of product soundness but still does not achieve the kind of maximum integrity which is only imparted from substantial amounts of hot deformation (Reference 13). Dendritic solute segregation is known to increase as solidification rate increases; however, dendrite cell size decreases as the solidification rate increases. The resulting segregation is, therefore, easier to homogenize because the diffusion distances are shorter. This is one of the key factors giving the P/M approach its advantage (Reference 14). Obviously, solidification rates achievable for an "ingot" on the order of 15 microns in size will be greater than those for an ingot 15 centimeters in size. The greater homogeneity, finer grain size and diffusion-limiting oxide, all inherent with the P/M process, provide the advantages

of higher solution and deformation temperatures without "hot shortness" (eutectic melting), lower deformation loads for hot working, and greater resistance to fracture during forging because of enhanced hot ductility.

The U.S. Army was first in supporting research and development efforts in fully dense Al P/M products for intended replacement of brass alloys in munitions applications. Subsequent U.S. Air Force interest in such products was with the intent of Al P/M applications as replacements for selected I/M Al primary, load-carrying airframe structures. Strength-to-weight ratio, toughness and corrosion behavior were the primary standards for performance evaluation. The CT-91 Al P/M alloy was superior in all these properties to the best Al I/M materials (7075 and 7050) (Reference 15). Other advances have been encouraging but not dramatic and so efforts continue to make incremental advances as well as to understand the fundamental potential and limitations of the P/M approach for Al, Fe, Ni and Ti-base alloy materials (References 16,17).

At least one author (Reference 18) has noted that of the four critical properties in structural Al I/M alloy design and selection (strength, toughness, corrosion resistance and fatigue), only in the last have significant improvements not been made. The resistance to use of Al P/M as a substitute for Al I/M has been based largely on lack of adequate fatigue design data.

The material used for the present work is one of the few commercially available, off-the-shelf advanced technology, P/M Al alloys. Both longitudinal (most flow) and long transverse (least flow) directions of die forgings were tested. The 7075 ingot material used for comparison was worked in three axes of orientation at 90° to each other (ABC), as is standard practice when upsetting is the preliminary processing procedure; whereas, the powder material was only worked in one direction.

The following were the incentives for this work: Air Force interest in better materials, Materials Laboratory's interest in new materials, the already demonstrated strength superiority of the CT-91 Al P/M alloy, the need for additional property data on this alloy, and the need for an understanding of the relationships between microstructure and

AFWAL-TR-81-4068

properties. The specific objectives were a comparison of the micro-structure, high cycle fatigue, toughness and corrosion behavior of equivalent strength 7XXX I/M and P/M aluminum alloys. Optical, SEM, EDAX, TEM and EMPA microscopy, notched round tension-tension fatigue, slow-bend Charpy toughness and exfoliation corrosion tests were employed to provide these comparisons.

SECTION II

LITERATURE SURVEY

1. PRECIPITATION STRENGTHENED Al P/M ALLOYS

Aluminum alloys 2024 and 7075 are the most widely used of all high strength Al alloys. For this reason, they have been selected more than any others for scientific and engineering study. Moreover, 7075 and 2024 are recognized within the R&D community as the standards with which new Al alloys must be compared (Reference 19). Both of these alloys achieve their strength from the precipitation of very fine particles within a solid solution alloy matrix. However, 2XXX alloys simply cannot achieve the strength levels of 7XXX alloys. Moreover, 7XXX alloys heat treated to an overaged, lower strength condition but equivalent to the peak strength condition of 2XXX, out-perform them in fatigue, toughness and corrosion behavior (Reference 20). The powder metallurgy (P/M) 7XXX Al alloys offer the potential for increased precipitate volume from higher alloy content without risk of segregation or ingot cracking problems during solidification. P/M material may be "solution" treated at higher temperature than I/M material without fear of grain growth by virtue of the presence of recrystallization restricting oxide dispersion. As the result, even more of the alloying elements can be driven into solution and become available for subsequent precipitation. An added benefit of the shorter diffusion distances inherent in P/M products is the greater effectiveness of homogenization in shorter times. Additionally, with no Cr or Zr dispersoids (required in ingot metallurgy (I/M) to inhibit grain growth) to serve as added sites for detrimental heterogeneous precipitation and alloying element consumption, a larger proportion of beneficial precipitates should result. This may partially explain the superior strengthening capability of the P/M materials. Evidence to support such a theory is contained in the fact that additional artificial aging beyond standard ingot metallurgy practices is required to achieve maximum strength in the P/M material. The comparison between equivalent strength 7XXX P/M and 7XXX I/M alloys should be made. That is, for an optimum combination of strength, toughness, fatigue and corrosion; heretofore, the 7XXX-T7 (lower strength) condition was selected over 2XXX alloys. Now, with the advent of P/M,

fatigue and strength can be improved upon without sacrifices in toughness or corrosion properties.

It is generally observed in most materials that a decrease in all mechanical properties is experienced in the transverse orientations. This anisotropy has historically been accounted for by the unfavorable distribution and orientation of inclusions, by crystallographic texture, or by inadequate deformation processing in a given orientation (Reference 21).

Other work undertaken to understand the real origins of this anisotropy has indicated that in contrast to Ti alloys, very little of the anisotropy effects observed in these P/M Al alloys is the result of crystallographic texture (Reference 22). Instead, anisotropy of strength and toughness is probably more induced in I/M materials by the distribution of constituent particles and in P/M materials, by the distribution of oxide particles. It is doubted whether such anisotropy can be easily or economically eliminated in commercial products (References 23, 24).

It is important to understand that the primary processing procedures for forging I/M alloys, let alone for the new P/M alloys, are not at all definitive. The amount of work required to achieve optimum microstructure and properties is simply unknown. In many cases, the achievement of final geometry from the forging process is the only criterion employed in following a given forging schedule. For this reason, common practice to achieve adequate working simply involves preliminary working by extrusion or multiple orientation upsetting. In this way, most of the adverse effects of directionality in flow are overcome. Unlike a cast ingot microstructure, as-vacuum-hot-compacted powder metallurgy billets possess a completely homogeneous microstructure. The only reason powder materials must be worked at all is that some, as yet unestablished, amount of shearing, tearing and re-welding of powder particles is essential for product soundness. That is, because of the inherent oxide layer surrounding each powder particle, metal-to-metal contact in the as-compacted powder billet condition, though fully dense, is less than required to result in good toughness and cyclic mechanical properties. Aside from their restriction of recrystallization and grain growth, the oxides in P/M material are not believed to produce any other effects except at much

higher volume fractions where they can produce substantial increases in strength of otherwise low strength aluminum alloys (References 25, 26).

As with the oxide, cobalt dispersoid particles may play some role in inhibiting recrystallization and grain growth. However, no significant mechanical or chemical effects have thus far been observed from their presence. Historically, they had been credited with the enhanced resistance to stress corrosion cracking of the CT-91 Al P/M alloys, but this contribution is now uncertain and in the process of re-evaluation (References 27, 28).

2. CRYSTALLOGRAPHIC STRUCTURE AND STACKING FAULT ENERGY

Because aluminum alloys are face-centered-cubic (FCC) and have a high stacking fault energy (SFE), they do not display a fatigue endurance limit, do not normally twin, cleave nor fail intergranularly, and do not exhibit a significant grain size dependence in fatigue crack growth rate (References 29-44). Commercial aluminum alloys cyclically soften and develop coherent, wavy slip bands in the $\{111\}\langle 110 \rangle$ crystallographic orientation but never initiate failure in these bands. Instead, fatigue crack initiation always occurs at grain boundaries, pores or particles greater than one micron in size (References 45-75).

Fatigue crack propagation (FCP) can itself be considered to progress through three growth rate transition stages. First, the microstructure and perhaps the environment initiate the process at some finite threshold of changing stress intensity (ΔK_{th}). Second, the process continues in a more linear fashion dependent upon the alternating stress intensity and the aggressiveness of the environment. Third, the process becomes unstable and accelerates rapidly to failure in a mode dependent only upon static stress conditions. The material properties which control the first two of these transitions have been much speculated about. For the third stage, it has generally been agreed that fracture toughness is the only material property of significance (References 76, 77). Stage I FCP occurs along preferred crystallographic slip planes at a 45° angle to the applied tensile axis (planes of maximum shear stress). Its propagation rate is more rapid for "wavy" than for "planar" slip materials.

Stage II FCP occurs at 90° to the applied tensile axis after a certain crack growth rate has been reached (References 78-80). The transition from Stage I to Stage II FCP occurs at approximately the beginning of the linear portion of the fatigue crack growth rate (da/dN vs. ΔK) plot. This also roughly coincides with the onset of "striation" (radially emanating lines of crack advance roughly perpendicular to the origin) formation (Reference 31). This transition occurs when a crack length of a few hundred microns is reached and has been considered a more practical definition of the transition between FCI and FCP (Reference 82). Investigators have noted that crack growth rates in this range of crack lengths are extremely slow (Reference 83).

3. MICROSTRUCTURAL EFFECTS

The fine grain size contribution to strengthening of P/M materials permits them to be used in the overaged condition without a loss in strength below the level of I/M-T6 condition. The lack of a greater relation between grain size and strength has been explained in terms of the action of dispersoids and semi-coherent precipitates promoting slip and reducing the influence of grain boundaries. Grain size should not begin to exhibit a significant effect on strength until the grain size approaches the dispersoid size. Subgrain size in any aluminum alloy, either I/M or P/M, reaches an equilibrium size with deformation which is dependent upon SFE. Therefore, subgrain size does not significantly affect strength either. What remains then, in the difference between the strength of pure aluminum and aluminum alloys are a combination of the effects of solid solution, dispersion and precipitation strengthening. The incremental gains in strength of fully-strengthened P/M alloys over their fully-strengthened I/M counterparts have been relatively small, which fact is fully in line with these considerations.

Grain size has been observed to be related to fatigue strength for low SFE (high strain hardening) materials. Grain size also has some effect on fatigue strength for high SFE (low strain hardening) materials but the effect is much smaller. Longer fatigue lives in either case have been attributed to longer FCI lives with fine grain size material (Reference 84). Although grain size normally has its greatest effect in

constant amplitude HCF conditions, the dislocation cell structure of high SFE materials totally masks the effect (Reference 85).

In large-grained materials, cracks are initiated at relatively higher stresses than in small-grained materials. However, a low stress that "initiated" a crack in the fine-grained material may be insufficient to propagate it. Hence, the crack has not really initiated (Reference 86). A possible explanation is that the myriad of small grain boundaries, each acting as a free surface, serve to distribute and relieve the stress concentration thereby lowering the effective stress level and retarding transition to Stage II FCP. So, on the one hand, grain boundaries are believed to inhibit fatigue microcrack growth since slip systems are discontinuous across them. On the other hand, grain boundaries can serve as the initiation sites in fatigue and as crack paths in fracture because of their inherent discontinuity and function as a sink for constituent segregation (Reference 87). Stage II FCP is found to be proportional to SFE (Reference 88). Since both I/M and P/M Al alloys have the same SFE and form cells which do not impede FCP, Stage II crack growth rates should be the same for I/M and P/M materials. At low amplitudes in Stage I, coarse grain size does in fact retard crack advance. Investigators have found such a relationship between coarse grain size and slow Stage I crack growth rates. This fact is supported by the lower value for threshold stress intensity (ΔK_{th}) for the finer grain size P/M materials (References 89-91). But again, grain size effects are only important at these very low ΔK levels (References 92, 93). At least in Stage II, fine grain size does not accelerate FCP. Note that this fact is not inconsistent with the experimental observation that overall FCP is slower in a single crystal than in a polycrystal. Most materials are used in polycrystalline form and therefore, exhibit the second stage of FCP which is more sensitive to material properties (References 94-99). It has been demonstrated that aggressive environmental conditions can completely eliminate such effects (Reference 100).

In conjunction with the decrease in importance of grain size in FCP for large plastic zone sizes and increasing crack growth rates, there is an increase in the importance of second phase constituent particles (References 101, 102).

Others have shown that as solidification rate decreases, the amount of equilibrium constituents formed and their segregation increases and transverse mechanical properties decrease (Reference 103). Large second phase particles formed during solidification or solution treatment of high strength Al alloys do not provide significant strengthening by comparison with the finer precipitates formed during subsequent low temperature aging. In fact, these large second phase particles are detrimental to fatigue and toughness properties in much the same manner as manganese sulfide inclusions in steels, which are a primary cause for anisotropy in these materials (Reference 104). Unlike fatigue strength, great success has been met in efforts to improve the toughness of aluminum I/M alloys over the past 15 years. The approaches taken have generally involved controlling the second phase particle size and distribution (References 105-107). But, as with fatigue, other microstructural features as well as deformation mode play a significant role in determination of the toughness of a given material. The smaller precipitates do not affect FCP and their behavior is nearly indistinguishable from that of the aluminum matrix which acts like a continuous field. In constant amplitude cycling conditions, the effect of large inclusions in Stage II growth is minimal. These inclusions are really only important in initiation. But these inclusions do become important in spectrum loading conditions where they assist in crack growth retardation following overloads. Since such large inclusions are not present in P/M materials, this effect is not observed (Reference 108).

Since the plastic zone size is at the outset already much larger than the P/M grain size, a faster fatigue crack rate and a lower ΔK_{th} are expected and have been observed (References 109, 110). One theory attributes these observations to the decreased potential for dislocations to retrace their paths across many grain boundaries (Reference 111). If the plastic zone size is smaller than the grain size, slip is not reversible because the number of available slip systems is restricted. Under these conditions, crystallographic or "Stage I" cracking occurs (Reference 112). When the plastic zone size approaches the grain size, microstructural features cease to affect FCP. This coincides more or less with the transition to Stage II, and striation formation in the Paris Law

region of the crack growth rate vs. ΔK plot. X-ray microbeam and electron channeling contrast techniques for measuring plastic zone size at different ΔK levels have found a linear relation. More than this, it has been concluded that subgrain size and crack opening displacement (COD) are related neither to each other nor to fatigue crack growth rates (Reference 113).

4. FATIGUE BEHAVIOR

a. High and Low Cycle Fatigue

In the name of "Damage Tolerant Design Philosophy", fatigue crack growth resistance has been receiving the "lion's share" of attention from the aerospace design community in recent years (Reference 114). Such an approach completely obscures consideration of fatigue crack initiation resistance; which, in fact, actually controls fatigue life. The fine grain size which permits gains in all static properties and even in fatigue crack initiation resistance and total fatigue life, may be eclipsed by the inferior fatigue crack growth behavior inherent in fine-grained material at low stress intensities. The recent shift in design emphasis to tolerance of assumed pre-existent cracks nearly stifles the historical trend of fine grain material selection. The historical superior in-service fatigue performance of fine-grained I/M materials has not sufficient evidence to support the open-armed acceptance of P/M materials in fatigue-critical applications.

Fatigue can be defined as the localized accumulation of plastic deformation from cyclic loading. Improvement in fatigue crack initiation (FCI) resistance should theoretically be obtainable by increasing the homogeneity of plastic deformation. It is also theorized that if dislocations are required to "loop" around rather than "shear" through strengthening precipitates, such homogeneity is enhanced. Grain size reduction is yet another means considered to promote homogeneous plastic deformation (Reference 115). An "overaged" P/M alloy with its fine grain size and non-shearable precipitates should therefore possess optimum FCI resistance. If fatigue crack propagation (FCP) is really dependent on elastic or shear modulus (E or G), little improvement can ever be hoped for in that respect. Notches should be viewed as they really are...sites for crack initiation but not actually "cracks". Microstructure

and deformation behavior have different effects on fatigue performance under different conditions of stress and strain cycling. Therefore, both low amplitude, long life or "high cycle fatigue" (HCF) and high amplitude, short life or "low cycle fatigue" (LCF) types of testing are valuable for materials evaluation (Reference 116).

The following general and non-mechanism dependent conclusions have been reached by several investigators about the nature of fatigue crack initiation (FCI) and fatigue crack propagation (FCP) in metallic materials (References 117-121).

High strains promote homogeneous (uniform) deformation and can initiate failure at "intrusions" and "extrusions" generated by "persistent slip band" (PSB) formation. More often, however, LCF testing tends to concentrate deformation heterogeneously at pre-existing discontinuities, any of which become possible initiation sites and the cause of failure depending on size and coincidental location in the specimen. LCF may not identify the very worst actor(s) however, since fracture is nearly always initiated at a free surface and therefore, typically, the external surface. This is a consequence of the state of biaxial or plane stress that exists there, as well as of the impossibility of a truly perfect surface (Reference 122). For a crack to initiate internally in preference to the specimen surface, the stress concentration must, by definition, be greater there. Such a situation occurs occasionally in LCF at gross defects (Reference 123). But, as the depth below the surface increases, the size of the defect required to initiate failure increases markedly (Reference 124). For this reason, the P/M material should be inherently superior in fatigue than I/M material because of the inherently smaller inclusion size; which should be limited to the maximum prior powder particle size in P/M material assuming no additional contamination is introduced in handling. In LCF then, the effects of such discontinuities should be somewhat less significant than in HCF. Moreover, internal initiation is likely to occur only for materials possessing very low levels of defects (References 125, 126). In fact, there is little difference in life expectancy between defective and defect-free material under LCF loading conditions (Reference 127).

For this reason, and in general for any alloy system in LCF, fatigue crack initiation (FCI) can be considered to be dependent on defect size and distribution while fatigue life can be considered to be more a function of fatigue crack propagation (FCP) because LCF life is mainly crack growth. These assertions are supported by the general observation that cracks typically initiate at approximately 1% of total life in LCF as can be determined by the first electronically detectable load drop above experimental error (Reference 128). Low strains tend to promote only heterogeneous (localized) deformation at pre-existing stress concentrating discontinuities, and initiate fatigue failure at these. In HCF, initiation is always at the worst defect on the surface of the specimen. If there are relatively few inclusions of acute shape, they could conceivably be expected not to be found at the surface. In such an instance, crack initiation could be internal even in HCF. However, since most engineering aluminum alloys are known to contain large numbers of relatively brittle (therefore typically acute in shape from fracture during processing) inclusions, initiation is expected and virtually always occurs at the external surface (Reference 129). The statistical probability of FCI in Al alloys decreases rapidly as inclusion size decreases (Reference 130). Significant differences in fatigue life are observed between defective and defect-free material. In general, for any alloy system in HCF, fatigue crack initiation (FCI) can be considered to be a function of FCI since HCF life is mainly crack initiation (References 131-133). The assertion that defect shape rather than size or distribution control FCI in HCF is supported by the fact that investigators have observed that only a certain fraction of even the very largest pores or particles ever initiate cracks. That fraction is also observed to increase as the nominal stress or strain increases (Reference 134). These facts are completely consistent with the differences observed in FCI between LCF and HCF behavior. Others have shown that defect (pore or particle) shape and/or orientation with respect to the gross stress/strain axis, more than defect size or distribution within the bulk material, are the keys to whether a given defect initiates a crack (Reference 135). That is, two defects of equal size may not develop equal stress concentrations. In other words, minimum defect size is a necessary but insufficient criterion for crack initiation. The actual stress concentration

developed for a given applied stress/strain because of shape and/or orientation, constitutes the precise criterion for FCI.

"Scatter" in fatigue data is inherently larger in HCF than in LCF test results. This is due, in part, to the change in importance from FCP and bulk static mechanical properties in LCF to the greater importance of FCI in HCF as previously discussed (Reference 136). Defects and particles in the bulk material are only important in LCF because of their effect on FCP and toughness. In HCF, defects and particles have little or no effect on FCP for most of the fatigue life as evidenced by the absence of their interference with fatigue striations. Only at very high fluctuations in stress intensity, approaching the fracture toughness of the material, do such particles affect FCP (References 137, 138). The smaller amount of scatter in LCF data is believed to be due to shorter initiation periods prior to FCP which is consistent with the multiple initiation sites generally observed. The first of these to initiate by virtue of its size and proximity to the surface, causes failure. The larger amount of scatter in HCF data is conversely believed to result from a longer period of initiation prior to FCP which is consistent with the single initiation (at the worst defect) typically observed. Hence, failure becomes an increasingly statistical phenomenon in HCF (References 139-141).

b. Relationships Between Monotonic and Cyclic Properties

Because fatigue is the accumulation of plastic strain, fatigue thresholds and strengths should increase with increasing yield strength ($\sigma_{y.s.}$) of materials. This makes sense because the amount of stress that can be accommodated before a permanent (plastic) strain results is obviously greater for a material with greater yield strength. But, yield and ultimate strengths are not very predictive of fatigue strengths because they represent only an engineering contrivance. In fact, very little relationship between either FCI or FCP and strength or microstructure exists (References 142, 143). Research has shown that large differences in y.s. and u.t.s. do not affect FCI or FCP (References 144-146). Stage II FCP seems to be governed by elastic modulus (E) and the strain hardening

exponent. The effect of temperature on these is observed to have the same effect on FCP rate (Reference 147). As noted earlier, structural features do become important at high ΔK levels due to the fact that K_{\max} approaches K_{IC} or K_C (depending on whether plane strain or stress conditions respectively, are prevailing). Crack growth rates in tougher materials will be slower (at high ΔK levels) than in brittle materials. This is consistent with superior LCF behavior of higher toughness materials (Reference 148).

In contrast to aluminum alloys, some pure metals, for example, copper, exhibit a direct correlation between fatigue strength and yield strength. Similarly, other alloy systems that rely on precipitation strengthening, for example, iron base alloys, exhibit a higher ratio of fatigue to yield strength reflecting their greater microstructural stability in cyclic loading at room temperature. This is related to the higher temperature of precipitation for ferrous alloys (Reference 149). In certain strength ranges, ferrous alloy fatigue strength is about half the yield strength. For Al, Mg, Cu and Ni-base alloys, fatigue strength is about a fourth to a third of the ultimate strength (References 150, 151). The ratio of smooth fatigue strength to ultimate monotonic tensile strength is sometimes called the "fatigue ratio" (Reference 152). It has been known for many years, that neither smooth or notched fatigue strengths of aluminum alloys are greatly affected by product type, alloy chemistry, strengthening mechanism, grain size or static strength (References 153-155). However, as static strength increases, smaller and smaller inclusions can give rise to failure since critical crack length decreases because toughness does not increase as rapidly as strength. Therefore, the inherently smaller inclusions in P/M material should make it superior in fatigue to I/M material at equal strength.

Correlations of fatigue strength with elastic modulus are found to be more universally applicable than correlations with static strengths (References 156-159).

All theoretical and empirical approaches used to account for FCP behavior incorporate the shear or elastic modulus (G or E) or a factor the size thereof in their calculations (References 160-164).

The inverse relationship between crack growth rate and modulus is common to all materials and all crack growth predictions models. Unfortunately, the value of E can only be increased by about 10% (Reference 165). SFE and ΔK_{th} cannot be significantly increased either (References 166, 167). Note that E increases only 3% due to precipitate coherency, while any remaining increase is due to the enriched solid solution (Reference 168). Historically, it was found that high solid-solution concentrations; for example 25% Zn in Al alloys, resulted in both higher modulus and fatigue strength. Such highly concentrated I/M alloys were unstable and tended to segregate. Aluminum-lithium alloys present one of the greater potentials for increasing modulus and commensurate fatigue strength. The P/M approach avoids the stability and segregation difficulties. But, unfortunately, Al_3Li precipitates, which increase the modulus, substantially lower the toughness and LCF properties (Reference 169).

c. Practical Considerations in Fatigue Evaluation

The stresses created in real engineering structures are produced by the strains they are designed to withstand in the performance of their function. However, in HCF, load and strain control become practically synonymous because cycling is occurring in the nominally elastic load range; wherein, stress is directly proportional to strain as defined by "Hooke's Law":

$$\sigma = E\epsilon \quad (1)$$

It is reasonable to expect then, that the same mechanical properties and microstructural features that produce the effects experienced in strain-controlled fatigue, will also produce those same effects in load-controlled fatigue. Therefore, load-controlled HCF testing is a relevant approach for investigation of FCI (References 170-172). A significant advantage of load-controlled testing is that rapid generation of data becomes possible. Strain-controlled testing by virtue of experimental apparatus limitations, is capable of cycling at a maximum rate of approximately 30 cycles/second. Load-controlled testing, on the other hand, can be

performed at rates up to approximately 170 cycles/second without significant effects on the mechanism of FCI (Reference 173).

The presence of notches in fatigue test specimens mainly affects the FCP and not the FCI contribution to total life. FCP is generally predictable from geometry and linear elastic fracture mechanics (LEFM), whereas, FCI is dependent upon the more specific material properties which determine mechanisms and is not dependent upon gross geometrical features (Reference 174). The assertion that even notched HCF life is mainly determined by the FCI portion of total life, is strongly supported by the observations of others that the number of cycles to FCI at a defined crack length is approximately the same for both smooth (theoretical, geometrical stress concentration factor, $K_t^{\Delta} \equiv 1$) and notched ($K_t=4.5$) specimens (Reference 175). The generation of notched HCF data for the purpose of understanding FCI behavior, is therefore easily justifiable. Cracking in notches is characteristic of nearly all real-life failures of engineering structures (Reference 176). As mentioned previously, K_t is merely a theoretical value. It is intended to be a conservative multiplication factor which, when applied to the prevailing nominal stress, determines the effective stress seen by a component with a certain geometry. The effective stress seen by a real component seems always to be less than or equal to this value and to be dependent on material properties as well. Another such factor (K_N) proposed by Neuber, represents an empirical approach to take these into account (Reference 177). A third factor specifically applicable to fatigue (K_f) has also been widely used to describe the effects of notches on fatigue behavior (Reference 178). This last factor is really just the ratio of unnotched to notched fatigue strength and is less than or equal to unity. A defining equation to empirically quantify dependence on material properties is given as:

$$Q \triangleq \frac{K_f - 1}{K_t - 1}; \text{ where,} \quad (2)$$

Q is called the fatigue notch sensitivity factor and is greater than or equal to zero. It is not necessarily good for Q to equal zero and K_f to equal unity since this could indicate a material so poor in fatigue

properties that notches do not degrade them further; as is the case with white cast iron (Reference 179).

Fatigue failure is primarily governed by maximum tensile stresses. Constant amplitude testing is nearly equivalent to variable amplitude or "spectrum" testing for low strain-hardening, rapid subgrain stabilizing materials like Al alloys. Such materials exhibit relatively history-independent responses (Reference 180). Fatigue strength is observed to decrease with decreasing mean stress. Conversely, increases in mean stress result in longer lives. Therefore, the addition of any compressive stress will tend to degrade total life (Reference 181). FCP is governed only by the change in maximum stress intensity (ΔK_{\max}), and for a given load, the severity of the test increases as ΔK_{\max} increases and as the R-ratio decreases. It must be noted that, at the same time, no significant change in fatigue crack growth rate ensues for decreasing R-ratios.

For 7XXX Al alloys, because of their low strain hardening ability, fatigue crack growth (FCG) rates for fully reversed loading do not differ significantly from FCG rates for tension-tension loading. This confirms the fact that the compression portion of fully-reversed loading does little to advance the crack (Reference 182). A number of investigators have demonstrated that fatigue response of materials subjected to negative R-ratios can be approximated by simply ignoring the negative portion of a load excursion with no loss in the accuracy of life prediction since the cracks are closed for compressive loads (References 183-185). Note that cracks may even be partially closed for low positive R-ratios (Reference 186). To review then, it is an experimentally determined fact that as the R-ratio is increased from its possible values of -1 to +1, the fatigue strength increases. That is, a non-zero mean stress ($R \neq -1$) will always increase measured fatigue strength (Reference 187). But few real engineering structures are subjected to completely reversed ($R=-1$) cycling. Considering the already dismal fatigue strength limitations of high strength aluminum alloys, such a fatigue condition would be unnecessarily conservative in the evaluation of their suitability for critical aerospace applications.

In reality, a typical fighter aircraft lower wing experiences cyclic loading conditions approximating $R=.1-.3$. A typical transport aircraft lower wing experiences cyclic loading conditions approximating $R=.5$ with a ΔK_{max} of only 11 to 16 MPa \sqrt{m} . An $R=.1$ condition, being more severe than either of these conditions, is therefore more frequently selected for testing and evaluation of materials intended for use in such applications. Note that upper wings see only compressive loads in HCF but do experience failures from LCF tensile loads which result from rough landings. It may also be noted that most of these loading conditions are axial in nature and so the use of axially loaded specimens to simulate service conditions that involve direct loading with non-zero mean stress as an important variable is quite realistic (Reference 188). Although it has been noted that R-ratio greatly affects total life, it has been shown not to have any significant effect on the FCI mechanism itself and hence is not a significant test variable with regard to comparisons between material all tested at the same R-ratio. That is, relative ranking of materials will remain constant for any R-ratio (Reference 189). Another point often made is that negative R-ratios obliterate fractographic information making subsequent analysis more difficult (Reference 190). Others have used positive R-ratios merely to avoid such difficulties (Reference 191).

Investigators have found little difference in fatigue crack growth rates at relative humidities between 5 and 100% for aluminum alloys; that is, very large differences in fatigue crack growth rates have been observed between less than 5% and greater than 5% which represents a transition point (References 192, 193). Any fatigue testing performed at relative humidities greater than 5% (typical of all but the most sophisticated controlled atmospheric conditions) should correlate fairly well. Therefore, room temperature, laboratory air (~50% relative humidities with presence of hydraulic oil vapors from test machines) can be considered a fairly aggressive environment for precipitation-strengthened aluminum alloys (References 194, 195). It is an environmental condition of practical relevance in that it does not differ significantly from that experienced by a typical engineering structure. It is believed that corrosive environment affects primarily the propagation of fatigue cracks and not their initiation mechanisms (Reference 196).

5. CORROSION BEHAVIOR

Aluminum is one of the most highly reactive of all the elements but rapidly develops a protective oxide film. Cathodic electrode potentials of metals in contact with aluminum alloys may or may not cause "galvanic" (electrolytic) attack depending on the current flow, which is limited by polarization. The constituent phases $(\text{CuAl}_2)_2\text{FeAl}_3$, CuAl_2 , FeAl_3 , (Al-Fe-Si) , and Mg_2Si are cathodic to the aluminum matrix and tend to cause it to dissolve around them. MgZn_2 is anodic and tends itself to dissolve (Reference 197). Cu is added to aluminum to increase corrosion and stress corrosion resistance (References 198, 199). Zr and Cr also increase stress corrosion resistance but limit capability for thick section strengthening. Fe and Si do not affect corrosion behavior to any significant extent. Mg is generally detrimental to corrosion properties because of its inherently anodic nature (References 200-202).

The terms stress corrosion cracking (SCC) and corrosion fatigue merely refer to the combination of aggressive chemical environmental conditions with static or cyclic mechanical stresses respectively. Precipitation-strengthened aluminum alloys can be more or less susceptible to these attacks depending on their specific heat treatments and microstructures (Reference 203).

The overaged heat treatment condition for 7XXX aluminum alloys reduces their susceptibility to all forms of corrosion (Reference 204). Overaging drives the precipitation reaction toward chemical equilibrium and so its beneficial effect on corrosion behavior is easily understandable. As particle size and spacing increase, thermal and electrical conductivity are observed to increase (Reference 205).

Although relative importance of microstructural features and conductivity is still controversial, one thing remains certain and universally agreed upon. That is, the highest strength (T6) condition of 7XXX I/M Al alloys is inferior to the lower strength (T7) condition (References 206-215). Adequate corrosion resistance has not been shown to depend on the presence of any element (References 216, 217). Like CT-91 P/M overaged material, I/M alloy 7050-T73 is almost comparable to

AFWAL-TR-81-4068

7075-T6 in strength. This is probably the result of its finer grain size as well as lower quench sensitivity (owing to the use of Zr instead of Cr for control of grain growth and recrystallization). However, 7050-T73 is inferior to 7075-T73 in SCC resistance (Reference 218). In contrast, the CT-91 Al P/M alloy heat treated to the fully overaged condition, nevertheless, is left equal in strength to 7075-T6 with the SCC resistance of 7075-T73. These advantages for the P/M material have already been largely documented (Reference 219).

Like resistance to SCC, resistance to corrosion fatigue is enhanced in the overaged heat treated condition of 7XXX Al alloys (Reference 220). One of the reasons for this is apparently the higher toughness of the overaged condition. The increase in plastic zone size permits greater crack retardation during the overloading conditions to which structures are typically subjected in real engineering life spectra (References 221-223). Additionally, overall reduced susceptibility to corrosion of the microstructure has been shown to be a significant contributing factor to fatigue crack propagation. The P/M material which has equal strength to I/M material even while in the overaged condition, has the advantage of resistance to environmental acceleration of FCI and FCG (Reference 224). Numerous reviews of corrosion theories were published in the early 1970's (References 225-228). But for all the theories of environmentally assisted cracking, basically all that one can really be sure of is that moisture is somehow deleterious and overaging heat treatment is somehow beneficial to the corrosion resistance of precipitation-strengthened aluminum alloys (Reference 229).

SECTION III

EXPERIMENTAL PROCEDURE

1. MATERIALS

a. Primary Processing

In conventional ingot metallurgy (I/M) processing, a molten metal alloy is poured into some sort of mold for solidification to a convenient shape. In powder metallurgy (P/M) processing, a molten metal alloy is poured in a restricted flow and atomized by the blast of a gaseous stream. Air atomization rather than inert gas is used for aluminum alloys for several reasons. First, unlike Cu, Fe, Ni or Ti, aluminum is capable of spontaneously forming a thin (.005 to .01 μ m) protective oxide scale around each solidifying particle which effectively prevents further oxidation. Virtually no practical atmosphere can be devised to prevent the oxidation of aluminum. Second, the irregular shape of air-atomized powders, though less conducive to high "tap" densities than perfectly spherical particles typically produced by inert gas methods, enhances capability for pore closure during compaction. Third, air is free (Reference 230). The high rate of heat extraction in atomization produces a high solidification rate and a resulting fine grain and constituent size (Reference 231). Considering the free energies of formation of the various possible oxides that might be formed in a 7XXX Al alloy; that is, Al, Mg, Zn, Cu, Fe, Si, Cr, Co, one would expect mainly MgO, Al₂O₃ and ZnO in that order of formation and such a hypothesis has been verified by Auger analysis (Table 1).

An average particle diameter (APD), as measured by Fisher Subsieve Sizer, of about 15 microns has been determined to be optimum in aluminum alloys for good compaction and retention of sufficient unoxidized alloying elements to achieve good mechanical properties. Whereas, given reasonable quality control, conventional solidified ingots originate as fully dense products, solidified powder particles must be compacted to achieve full density. To accomplish this, the powder is first cold isostatically pressed in a "wet bag" to approximately 75% of theoretical density. Although higher densities are easily achievable, this density

optimizes "green" strength for handling and interconnected porosity for satisfactory "out-gassing" prior to hot compaction to full density. If extraneous moisture and gases are not driven off prior to hot compaction they can create internal porosity, blistering and delamination upon subsequent expansion during solution heat treatment. The next procedure is encapsulation of the "green" compact in a welded aluminum alloy container of adequate hot strength, and preheating, at as high a temperature as possible short of eutectic melting, for several hours while maintaining a dynamic vacuum. The evacuation tube is then sealed off and the hot compact is pressed to full density in a heated, closed-end ("blind") extrusion die. Following an air cool to room temperature the "canning" material is removed by "scalping" (machining). Porosity is not a significant factor in the structure of Al P/M products fabricated in this fashion but that final forging is certain to eliminate it even if it were. Nevertheless, density is always checked using the constant temperature water bath Archimedeian technique (Reference 232). The principle, though quite simple, is also quite valid. If equal weights of P/M and I/M materials displace equal volumes of water, they must be of equal density. All of the procedures outlined here were actually performed at the Alcoa Technical Center outside Pittsburgh, PA., under contract with the Air Force (References 233-235). Additional details are included in Tables 2, 3, 4, and 5. Besides the density measurement, both P/M forgings and several of the finish machined P/M test specimens were non-destructively tested for internal voids by radiographic (X-ray) methods. No porosity was indicated. Mechanical property data for some of the as-compacted P/M billet material tested under the aforementioned contract at Alcoa are also given in Table 6.

As is standard practice, the I/M material was given a high temperature treatment (Table 7) to help homogenize the solute elements (Reference 236). Homogenization leads to more efficient utilization of solute elements; particularly copper, which is one of the more slowly diffusing species, and leads to relatively higher strength and ductility after subsequent deformation and heat treatments.

b. Chemical Analysis

Aqueous mixed acids dissolution chemical analysis of the as-received billet materials was performed in accordance with standards established here at the Materials Laboratory (Reference 237). However, the oxide in P/M material is very fine and so standard wet-filter analysis methods for oxygen can yield oxygen content results up to 100X too low. Therefore, neutron activation analysis for oxygen content was selected (References 238, 239). Chemical compositions are indicated in Table 8.

c. Deformation Processing

Investigators have only recently found that approximately 85% reduction in height of 7075 I/M Al warm-rolled plate results in maximum grain refinement (Reference 240). Forging is generally accomplished at a relatively warm temperature to prevent extensive recrystallization and grain growth as well as to reduce the flow stress of the material and so permit higher reductions. A forging ratio, defined as the final area divided by the original area, of about 2 or 3 to 1 is typically recommended to obtain optimum short transverse mechanical properties (Reference 241). A ratio of height to base of the forging of less than 2 to 1 ensures that even with "sticking" friction conditions, no buckling instability could occur (Reference 242). These few guidelines were used in the processing of materials for the present work. Additional details can be found in Tables 9, 10 and 11 and Figure 1.

d. Heat Treatment

After forging, an additional homogenizing or "solution" heat treatment was accomplished at a high enough temperature and for a long enough time to redissolve precipitates but not coarsen grains or result in an inordinately slow quench rate through the 400 to 300°C critical precipitation range. Below 300°C, precipitation is sufficiently slow that the quench rate to below the G.P. zone formation temperature (approx. 100°C) is unimportant. Cooling rates depend upon both the temperature of the quenching medium and the heat transfer conditions at the interface. High surface-to-volume ratio and blackbody (non-reflective) conditions are obviously most effective. Cooling rates below 550°C/second

AFWAL-TR-81-4068

TABLE 1
POWDER PARTICLE OXIDE CHEMISTRY

<u>Mole %</u>	<u>ΔG_f @ 626°C Kcal/mole O_2</u>	<u>Min. Oxid. Conditions</u> P_{O_2} (atm)
50% Al_2O_3	-220	10^{-53}
27% MgO	-245	10^{-58}
18% ZnO	-125	10^{-30}
6% Cu_2O	- 50	10^{-11}

TABLE 2
P/M BILLET PRÉDENSIFICATION DATA

<u>U.S. Standard Screen Analysis Wt%</u>				<u>(APD) Avg. Particle Diameter</u>
- 50	-100	-200	-325	14.63 micron
<u>+100</u>	<u>+200</u>	<u>+325</u>	<u>-</u>	
0.2	1.2	10.6	87.6	

TABLE 3
P/M COLD COMPACTION DATA

<u>Maximum Pressure</u>	<u>Compact Weight</u>	<u>Compact Dimensions</u>
207 MPa	66 Kg.	18.7cm in. dia. x 109.2cm high

TABLE 4

P/M CAN EVACUATION DATA

<u>Time to Reach Max. Temp.</u>	<u>Max. Temp.</u>	<u>Time @ Max. Temp.</u>	<u>Vacuum</u>
7 hours	521°C	1 hour	10µm Hg.

TABLE 5

P/M HOT COMPACTION DATA

<u>Max. Pressure</u>	<u>Time @ Max. Pressure</u>
620MPa	1 minute

TABLE 6

T6 + 14 HR. OVERAGE RADIAL P/M BILLET PROPERTIES

<u>U.T.S.</u>	<u>Y.S.</u>	<u>% El.</u>	<u>% R of A</u>	<u>N.T.S/Y.S.</u>
75Ksi	66Ksi	12	22	1.27

TABLE 7

I/M BILLET PRACTICE

Direct Chill Cast
Homogenized 860+870°F for 8+10 hours

TABLE 8

CHEMICAL ANALYSIS; WT. %

<u>Element</u>	<u>CT-91 P/M (Experimental)</u>	<u>CT-91 P/M (Commercial)</u>	<u>7075 I/M (Commercial)</u>
Zn	6.3	6.4	5.8
Mg	2.4	2.4	2.4
Cu	1.6	1.6	1.7
Fe	.06	.06	.16
Si	.06	.06	.10
Mn	.005	.005	.03
Co	---	.35	---
Cr	---	---	.2
Ti	.005	.005	.016
B	---	---	.001
O	.337	.288	.009
Al	Bal.	Bal.	Bal.

TABLE 9

FORGING PROCEDURE

Preheat tool steel die and Al blocks at 700°F for 2 hours.

Forge at 3 inches per minute in heated chamber at 700°F

using colloidal graphite lubricant.

Cool to room temperature.

Trim square (I/M blocks - between upsets).

Remove flash with belt grinder.

350-400 tons final reduction forging load required

TABLE 10

P/M DIMENSION SEQUENCE

2 in.	x	3.5 in.*	x	3.5 in.
-------	---	----------	---	---------

70% reduction in height

6 in.	x	3.5 in.*	x	8 in.
-------	---	----------	---	-------

* 3.5 in. = width of channel die.

TABLE 11

I/M DIMENSION SEQUENCE

2 in.	x	3.5 in.	x	3.5 in.
-------	---	---------	---	---------

40% reduction in height

2.7 in.	x	2.1 in.	x	4.3 in.
---------	---	---------	---	---------

trim square

trim square

trim square

40% reduction in height

3.5 in.	x	2.7 in.	x	2.4 in.
---------	---	---------	---	---------

trim to 3.2 in.

trim square

trim square

>80% reduction in height

.6 in.	x	3.5 in.*	x	7 in.
--------	---	----------	---	-------

* 3.5 in. = width of channel die.

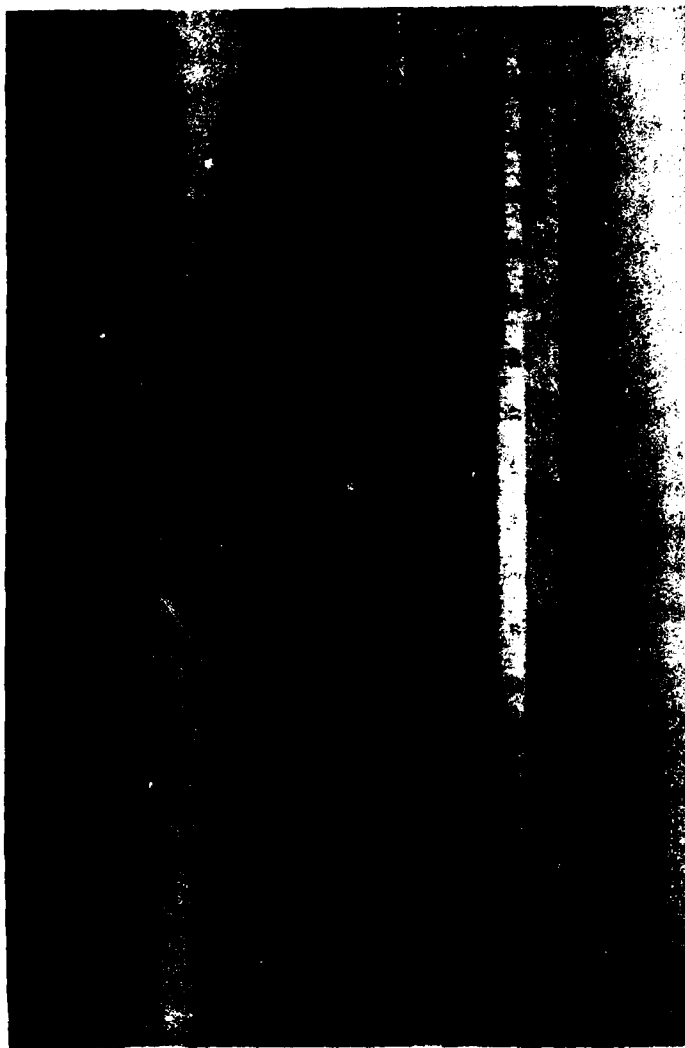


Figure 1. Configuration of I/M or P/M Forging Stock Positioned in H-13 Tool Steel Channel Die Prior to Final Forging.

for 7XXX alloys prevent attainment of maximum strengths in subsequent aging heat treatments. Cooling rates above $105^{\circ}\text{C}/\text{second}$ are necessary to achieve immunity to intergranular corrosion in alloys heat treated to the maximum strength (T6) condition. Such rates are not achievable in thick sections because quench rates are limited principally by the thermal conductivity of the metal; which is essentially uncontrollable. For this reason, 7XXX alloys are not generally used in the T6 "temper" in service environments conducive to stress corrosion. Instead, the weaker, overaged (T7) temper is used (References 243, 244). For 7XXX forgings which are subsequently heat treated to T6 condition, quenching in 80°C rather than 10°C water results in a slight loss in strength but a significant gain in toughness and resistance to stress corrosion cracking (Reference 245). Quenching in 80°C water can be considered either a simulation of quench rates for the interior of a thicker section quenched in a lower temperature medium, or representative of commercial quenching practice for thinner, complex sections subject to severe warpage from residual stresses induced by cold water quenching (Reference 246). Quenching in 80°C water, as was done for the materials in the present work, is known to result in approximately 75% lower residual stresses than can be induced by cold water quenching (References 247-249). In any case, the quenching method employed for the present work can be considered commercially relevant.

A standard "stress relieving" practice is to plastically compress forgings by 1 to 3% after quenching (Reference 250). However, it was elected not to do this in the interests of expediency for the present work. Instead, the flash was ground off the forging and then the forgings were merely cut into small bars prior to solution heat treating as an additional measure to minimize the effects of any residual stresses from quenching.

Unlike 2XXX alloys, which can arrive at maximum strength while remaining at room temperature within a single day, and become completely stable after only four days, 7XXX alloys cannot be used in the so-called "naturally aged" condition, but must instead be "artificially aged" at an elevated temperature. The reason for this difference is that the nucleation and/or growth kinetics of the (MgZn) zones in 7XXX alloys are

more sluggish at room temperature than those of the (CuAl) zones in 2XXX alloys. This fact is believed to be the cause of the observed smaller G.P. zones in 7XXX alloys and their resultant greater strength. Unfortunately, yield strength increases much more slowly than ultimate strength with elevated temperature aging and so ductility, as measured by percentage elongation in a tensile test, decreases. "Overaging" to lower strength generally does not recover this loss (Reference 251). Details of the heat treatments employed in the present work are given in Table 12.

2. METALLOGRAPHIC AND FRACTOGRAPHIC CHARACTERIZATION

a. Optical Microscopy

The optical metallographic examination procedures observed in the present work were as follows:

1. Section specimen with water-cooled abrasive cut-off wheel.
2. Mount with heat/pressure curing plastic.
3. Grind with water on 240, 320, 400 and 600 grit SiC or emery papers rinsing clean and rotating scratch direction 90° between each grit size.
4. Ultrasonically clean in acetone.
5. Polish with oil and 6 micron diamond paste on a rotating wheel covered with no nap nylon cloth.
6. Wash with soap and water and ultrasonically clean in acetone.
7. Final polish with distilled water and 1 micron magnesium oxide powder on a rotating wheel covered with medium nap microcloth.
8. Rinse with tap water and then methanol and blow dry with a light blast of compressed air.
9. Immerse in solution of:
 - a. 90ml H₂O, 10ml H₃PO₄ (80%) at 50°C for four minutes, or
 - b. (Keller's etchant) 95ml H₂O, 2.5ml HNO₃ (conc.), 1.5ml HCl (conc.), 1ml HF (conc.) at room temperature for ten seconds.
10. Rinse in tap water.
11. Neutralize with a dilute solution of bicarbonate of soda.
12. Rinse with tap water and then methanol and blow dry with a light blast of compressed air.

TABLE 12
HEAT TREATMENT PROCEDURES

	<u>I/M - T6*</u>	<u>P/M - T7*</u>
Solution Treat	880°F - 1hr./1/2-in.	920°F - 1 hr./1/2-in.
Quench	180°F water	same
Natural Age	5 days at room. temp.	same
Artificial Age	250°F - 24 hours	same
Overage	None	325°F - 14 hours

*Note: forgings were cut into 3" x 2/3" x 2/3" rectangular specimen blanks prior to heat treatment to avoid residual stress variations due to the geometry of the forging.

**To simulate quenching of larger/thicker pieces.

	<u>I/M - T73***</u>	<u>P/M - T6***</u>
Solution Treat	880°F - 1 hr./1/2-in.	920°F - 1 hr./1/2-in.
Quench	180°F water	same
Natural Age	5 days at room temp.	same
Artificial Age	250°F - 24 hours	same
Overage	325°F - 10 hours	325°F - 4 hours

***Note: These heat treatments were evaluated only in exfoliation corrosion testing of forgings cut into 3-1/2" x 2-1/2" x 1/2" rectangular blanks prior to heat treatment.

Etchant a. was used for all but the microstructural evaluation of the material subjected to the EXCO (ASTM Standard Exfoliation Corrosion) test. This solution was used rather than the more standard Keller's mixture of acids (Etchant b.) because of its tendency to produce a more uniform attack. In this way, subgrain boundaries (which are of lower energy and misorientation than primary grain boundaries; Reference 252) could be clearly delineated. Etchant b. is a standard primary grain boundary etchant for aluminum alloys.

All optical micrographs were produced on 100 x 125mm Polaroid ASA 55 film and obtained with an Olympus PME metallograph. Optical fractographs of as-fabricated specimens were similarly produced with an Olympus MP-4 microscope.

b. SEM Microscopy

Scanning electron microscopy (SEM) procedures utilized in the present work were as follows:

1. A layer of carbon was shadowed onto mounted specimen surfaces at a 45° angle via physical vapor deposition after polishing and etching to simultaneously prevent charging of the non-conductive mounting material in the SEM and permit accurate electron dispersive X-ray analysis (EDAX) of material chemistry.
2. A .02µm coating of gold-palladium was sputtered on the surface at a 90° angle after repolishing and re-etching to simultaneously prevent charging on the non-conductive mounting material in the SEM and enhance the resolution capability of the features. Sputtering of Au-Pd affords greater control of coating thickness but could interfere with accurate chemical analysis with EDAX.

All SEM fractography was performed on the as-fractured surface. Fractured specimens halves were preserved by storage in an evacuated desiccator until examination. All SEM micro- and fractographs were produced on 100 x 125mm Polaroid ASA 55 film and obtained with an ETEC (Perkin-Elmer) Autoscan with KEVEX attachment. EDAX display photos were produced on 75 x 100mm Polaroid Polacolor 2 type 108 film and obtained with a hooded Polaroid 75 x 100mm land camera.

c. TEM Microscopy

Transmission electron microscopy (TEM) procedures utilized in the present work were as follows:

1. Section a 2.5mm thick, approximately 10mm square specimen with a low deformation diamond saw cut on both sides (throw the first, outer, slice away).

2. Gently remove the oil and dirt with soap and water and dab dry.
3. Wrap index finger with double side sticky adhesive tape.
4. Stick specimen to the tape.
5. Thin to 1.25mm by gently grinding both sides alternately with 240, 400 and 600 grit SiC or emery papers, rotating the scratch direction 90° between each grit size to ensure all scratches from the preceding grit are removed.
6. Rinse clean in acetone and gently wipe dry with soft cloth or facial tissue to ensure adhesive from tape and grit from grinding papers are removed.
7. Ultrasonically clean in acetone.
8. Stamp out 3mm diameter discs with "cookie cutter" designed for this purpose (not shown).
9. Perforate by means of twin jet electropolishing in bath of 20% HNO_3 (conc.) and 80% methanol at -40°C, 25 volts, 50 milliamps (fiber optics detect perforation and sound alarm in Fissione and Struers models). Time to perforate should be 1 to 5 minutes.
10. Rinse in pure ethanol.
11. Store in mechanical pump or diffusion pump evacuated desiccating chamber until ready to examine in TEM.

All TEM micrographs were produced on 75 x 100mm Kodak glass plates and printed on Kodak paper. The micrographs were obtained with a JEOL 200KV microscope with no goniometer stage. Additional qualitative and quantitative determination of particles observed in the foils was obtained through examination in an ETEC Microprobe.

3. MECHANICAL BEHAVIOR EVALUATIONS

a. Monotonic Tension Testing

Monotonic tension testing was performed in accordance with ASTM E8-69 on an Instron mechanical screw machine with a 4,540Kg. load cell (Reference 253). Standard 2/3cm diameter, 7-1/2cm long smooth, round, threaded specimens were machined from forgings as schematically illustrated in Figure 2, and tested in the as-machined condition. A crosshead speed of .127cm/min. and a 12.7cm/min. chart speed afforded

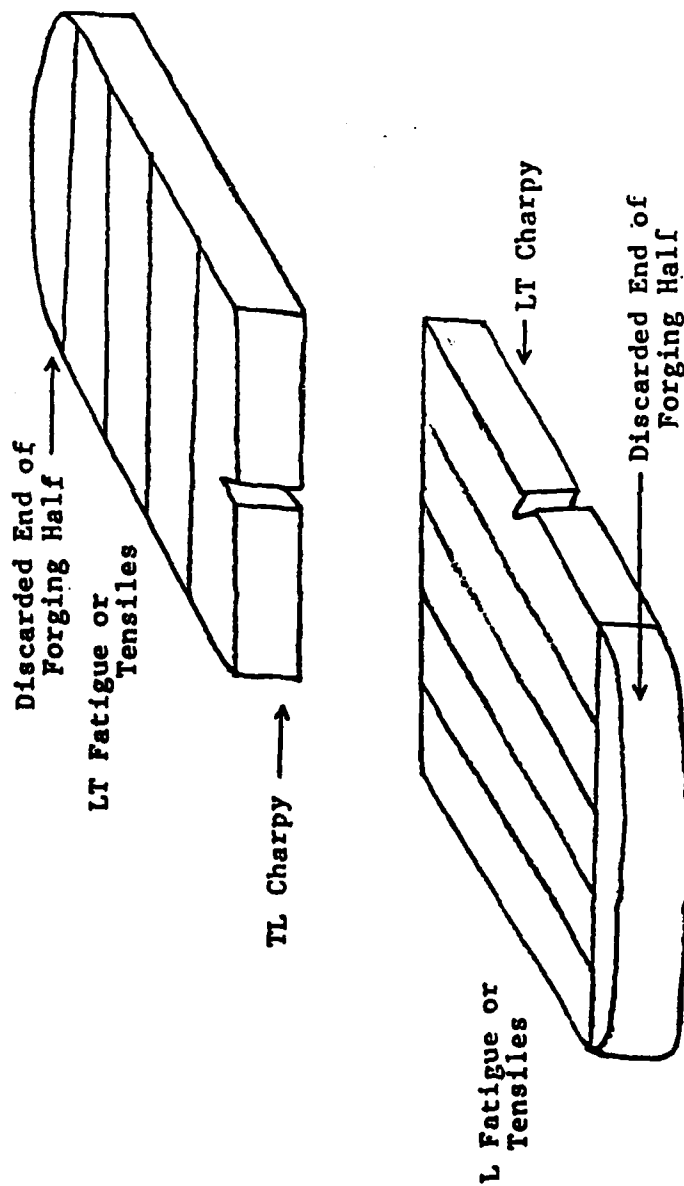


Figure 2. Mechanical Test Specimen Extraction Plan.

minimal load train lag and therefore, reasonable approximation of percentage elongation without the aid of an extensometer. This fact had been verified earlier by comparing measurements (made from circumferentially razor scribed gage marks highlighted with blue toolmaker's ink created by a special jig fixture mountable on the tool position of a horizontal lathe, not shown) before and after testing with the aid of a Gaertner toolmaker's microscope. Percentage elongation of a gage section, however, is not a very accurate nor meaningful engineering property. A better measure of material ductility is obtainable from measurement of reduction in cross-sectional area ("necking") and this also was accomplished. Sample calculations are presented in Appendix A (References 254-256).

b. Toughness Testing

Charpy impact testing, although quite useful for the evaluation of toughness in steels, is insensitive and overly conservative for the evaluation of aluminum alloys (References 257-259). Slow-bend, fatigue pre-cracked, Charpy testing can reveal differences obscured by impact testing without the need to resort to costly and time-consuming "compact tension specimen" (CTS) K_{IC} ("plane strain" opening mode (I), "critical" (C) stress intensity) toughness testing. Slow-bend Charpy testing is performed with less technical difficulty and less money than electronically instrumented, "sensitized" impact testing (Reference 260). In fact, all other tests are currently less recommended for rapid, inexpensive toughness measurement (Reference 261).

Slow, 3-point bend, fatigue pre-cracked, Charpy toughness testing was performed in accordance with ASTM E399-78 on a closed-loop electroservohydraulic Mechanical Test Systems (MTS) machine (Reference 262). Standard 1cm square, 5-1/2cm long rectangular specimens were machined from forgings as schematically illustrated in Figure 2. Razor scratching of the notches prior to pre-cracking is generally considered acceptable for soft, low strain hardening materials and so was performed in order to aid crack initiation (Reference 263). Specimens were then ground through 240, 320, 400 and 600 grit SiC or emery papers, rinsing clean with tap water and rotating scratch direction 90° at each step.

AFWAL-TR-81-4068

The final scratch orientation was perpendicular to the crack growth direction to enable easy subsequent observation and measurement of pre-crack length. Specimens were ultrasonically cleaned in acetone to remove any debris remaining in the notches that might subsequently be confused with fracture debris. Specimen widths and thicknesses were measured using a Gaertner toolmaker's microscope to an accuracy of three decimal places.

For slow-bend Charpy toughness testing, specimens are pre-cracked by fatigue loading to develop the sharpest possible crack. Slow pre-crack growth can cause uneven crack front growth problems and great care must be taken in this regard. ASTM E399 requires that crack front variation be no greater than 5%.

Since pre-crack starting at $.4K_{IC} < K < .9K_{IC}$ is recommended for aluminum alloys (K is the stress intensity in $\text{MPa}\sqrt{\text{m}}$ and K_{IC} is the "critical" mode I or "opening" mode stress intensity), all pre-cracks were started safely within this range (References 264, 265). A frequency of 30Hz was selected. For the toughness test itself, a crosshead rate of 1.27cm/min. and a ram travel of .4cm were selected so as to break but leave specimen half shear lips connected and preserve the fracture surfaces. A Datronics linear variable differential transducer (LVDT) and a Hewlett-Packard X-Y recorder were used to accurately acquire load and displacement data. See Figures 3 and 4.

Note that elastic modulus (E) cannot be accurately calculated in a tension test without the use of an extensometer because of the load train effects. However, E is known not to vary significantly for the alloys of any element. For 7XXX aluminum alloys, E is approximately 71500 MPa. E can be checked to an accuracy within 5% from the load deflection curve produced with an LVDT and X-Y recorder of a slow-bend Charpy toughness test (Reference 266). Sample calculations are presented in Appendix B.

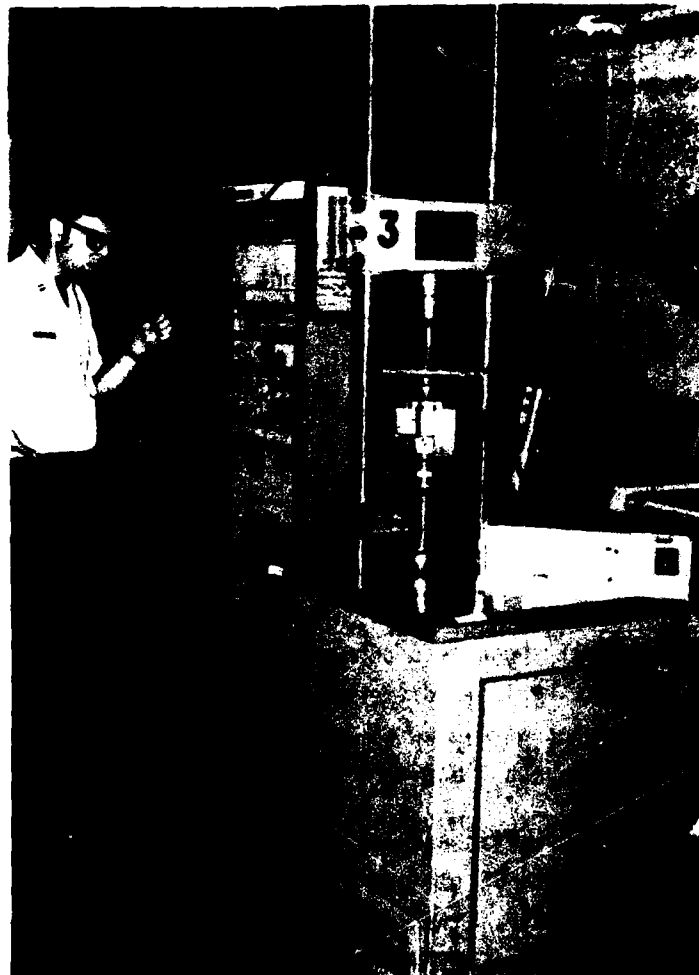


Figure 3. MTS Toughness Test Apparatus Showing Datronic LVDT Amplifier and Hewlett-Packard X-Y Recorder (Center Right). Dial Gage Used to Determine Ram Travel Required for Specimen Fracture Without Complete Separation of Halves Obscured by Left Column of MTS Frame.



Figure 4. Close-Up of Slow-Bend Toughness Jig with LVDT Piston (to the Left of the Fracturing Ram) for Acquiring Precise Displacement Data.

c. Fatigue Testing

Constant amplitude, notched axial tension-tension fatigue testing was performed in accordance with E466-72T on a Rüsenberger-Müller resonance machine (Reference 267). See Figures 5 and 6. Specimens were machined from forgings as schematically illustrated in Figure 2, to the dimensions indicated in Figure 7. A $K_t \sim 3$ was selected for the present work because of the wealth of comparable data in the literature, reproducibility of specimens, and its widespread engineering use as a practical design criterion; e.g., a round hole (References 268-273). The specimen geometry was designed to afford such a value based on the calculations of Peterson (Reference 274).

Ultrasonic degreasing in acetone both preceded and followed notch polishing with lapping oil and 600 grit SiC or emery paper. Specimens were held in a slowly rotating lathe chuck for this procedure. Following this, electropolishing was accomplished at 40-45 volts and 7-9 amps in a solution of 50 parts methanol, 30 parts ethylene glycol monobutyl ether (butyl cellosolve) and 4 parts HClO_4 (60%) with the bath temperature maintained between 0 and 10°C for 10 to 30 seconds. After electropolishing, specimens were rinsed with tap water and then methanol and blown dry. If examination at 10X magnification revealed residual scratches or pitting, specimens were reground with 400 and 600 grit SiC or emery papers and re-electropolished. Untested specimens were stored with broken specimens in an evacuated desiccator until ready to test.

It is generally recognized that fatigue behavior is relatively insensitive to both frequency and waveform (Reference 275). An R-ratio (minimum divided by maximum load) of .1 and a frequency of approximately 105Hz were selected to afford rapid testing with no damage to fractographic features. The sensitive solid state electronics of the "RUMUL" machine are capable of detecting load drops as small as 2Kgs. (approx, 1MPa). When such a load drop occurs, the machine is designed to stop cycling automatically and hold the mean tensile load until manually restarted. Some tests were permitted to be interrupted in this fashion for up to 48 hours before being restarted, while others were restarted immediately upon automatic shutdown. Still other tests were performed in



Figure 5. Rüssenberger-Müller (RUMUL) Resonance Fatigue Testing Machine.
Vertical Allen Wrench Locks and Unlocks Vibrating Platform.

AFWAL-TR-81-4068

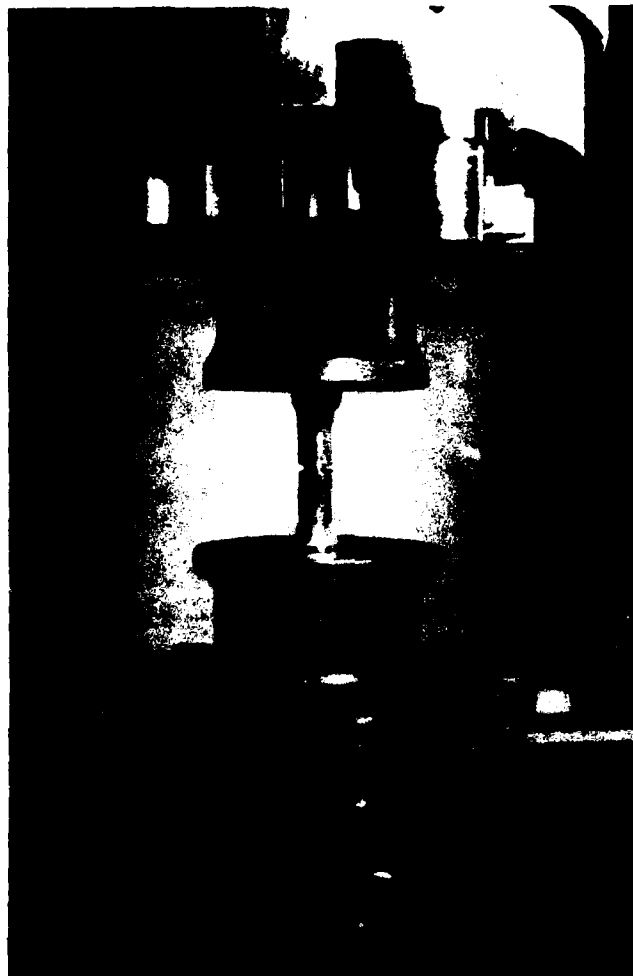


Figure 6. Close-Up of Notched Fatigue Specimen Threaded Into Grips.

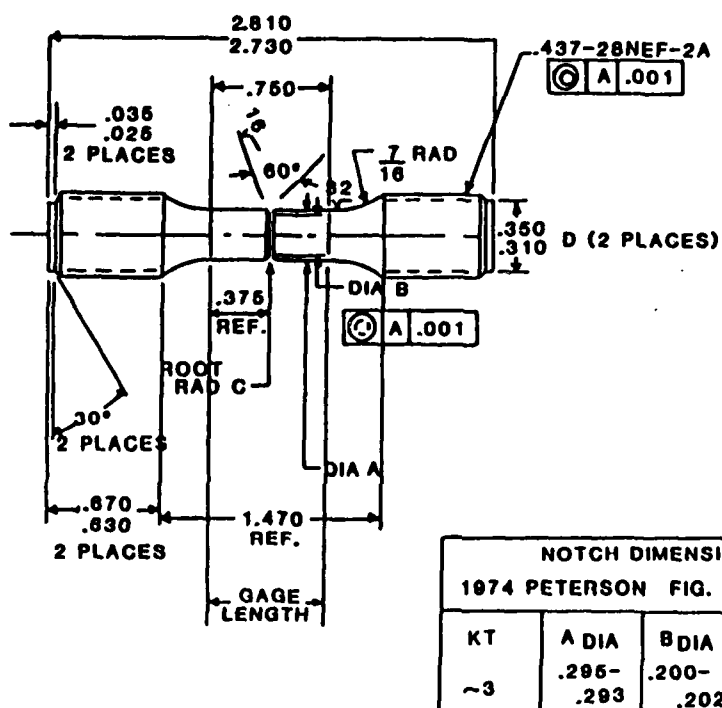


Figure 7. Notched Fatigue Specimen Drawing, Scale Approximately 1:1, All Dimensions in Inches.

the manual override mode so that no interruption of the testing was permitted to occur even after the initial load drop. None of these variables seemed to influence the outcome of the testing in any way. Even if a crack tip were blunted by a dwell at the mean load, the effect would be nullified by the return to maximum load upon restarting the test.

As the intent of the present work was not principally an assessment of such environmental factors as industrial pollution, "acid rain" and so forth, on the mechanical behavior of these alloys, the test environment selected at least represents a simple and reproducible condition. For all of the aforementioned reasons, then, constant amplitude, notched, axial, HCF in room temperature laboratory air at 105Hz in a machine which operates on the principle of resonant vibration, and an R-ratio of .1 were selected as the testing conditions for the present work. Because the fatigue strength of aluminum alloys does not change very rapidly after about 10 million (10^7) cycles (although apparently continues to decrease at least up to 500 million cycles (Reference 276)), tests were generally terminated at 10^7 cycles if no failure occurred by then simply in the interests of time.

4. STATISTICAL EVALUATION OF FATIGUE DATA

That fatigue is probabilistic has long been a recognized fact. However, in this investigation, it was felt that an estimate of the entire "S-N" (stress vs. log cycles to failure) curve in the low amplitude loading range (failure at greater than 10^4 cycles) was more important than establishing any statistically significant data such as fatigue strength at a given life. Therefore, it was decided to use the so-called "standard" fatigue test method. In this approach, several tests at each of several stress levels are run to simply "sketch-out" a rough "Wöhler" or S-N curve. A "conservative" curve was then drawn below the data which is meant to suggest a trend in fatigue behavior. Maennig suggests using a factor of .2 to increase the width of the "scatterband" in laboratory specimen testing and a factor of .6 in full-scale complex component testing. Therefore, in the range of testing performed in this study (approx. 70MPa), a 7MPa increase to the top and bottom of the bands is indicated. Such an approach is valuable for qualitative

evaluation. The primary interest of this work was concentrated at the high cycle fatigue (HCF) or "long-life" end of the fatigue life spectrum (S-N graph). It must be noted that a statistically significant analysis of fatigue behavior would have required approximately nineteen specimens per material condition per stress level. It is known that HCF distributions are not log normal because of the existence of specimens that do not fail ("runouts") and so the practice of establishing truly significant HCF data is neither economically reasonable nor practical.

Similarly, the "Quantal Response" (or "Survival" or "Mortality" or "All-or-Nothing" or "Probit") method, although superior to the constant stress level method described above in defining fatigue strength at a given life, was not used because of insufficient time and numbers of specimens available for testing.

This is unfortunate in that such analysis is very useful in defining the distribution. Several other methods were also not considered because of their requirement to use more than one stress per specimen to ensure failure. Such an approach is questionable if strain hardening or softening can occur. The "Weibull" distribution analysis was not used because it was felt that it would offer little additional insight into the data beyond that already provided by the "Staircase" and "Boundary" statistical treatments described in Appendix C (References 277-285).

5. CORROSION BEHAVIOR ASSESSMENT

a. Hardness Testing

Hardness, being a measure of the extent of precipitation in aluminum alloys, is often determined in lieu of or in conjunction with other corrosion susceptibility evaluations.

Rockwell B hardness testing was performed in accordance with ASTM Standard E18-74 (Reference 286). Specimens were ground with water on 180 grit SiC or emery paper, rinsed with tap water and blown dry.

b. Electrical Conductivity Testing

Electrical conductivity, like hardness, is also a measure of the extent of precipitation and is often similarly employed in corrosion susceptibility evaluations.

Electrical conductivity testing was performed in accordance with ASTM B342-63 (Reference 287). Specimens were ground with water on 180 grit SiC or emery paper, rinsed with tap water and blown dry.

c. Exfoliation Corrosion Testing

Exfoliation corrosion testing was performed in accordance with ASTM G34-72 on different combinations of alloy chemistry and heat treatment (Reference 288). See Tables 8 and 12. Specimens were diagonally machined from forgings to provide greater "end grain" exposure, ground with water on 180 grit SiC or emery paper, rinsed with tap water and blown dry. Specimens were suspended from nylon fishing line in a 4 Molar NaCl, .5 Molar KNO_3 , .1 Molar HNO_3 aqueous (distilled water) solution for 48 hours. Optical photographs of the test were taken at the one hour point and again at the six hour point after immersion. After 48 hours, specimens were rinsed with tap water and allowed to air dry. They were then immersed in concentrated HNO_3 for 30 minutes, rinsed with tap water and again left to air dry. Photographs of the flat and diagonally machined sides were then obtained. Weight loss is an unreliable criterion in the evaluation of exfoliation corrosion and was not measured (Reference 289). Instead, microscopic evaluations of the areas subject to what appeared to be the most severe attack were sectioned, mounted and metallographically examined.

SECTION IV

RESULTS AND DISCUSSION

1. MICROSTRUCTURE

Optical micrographs of as-cast ingot and as-compacted billet materials are presented in Figures 8 and 9. Three-dimensional optical micrographs of both as-forged and fully heat treated conditions are compared in Figures 10, 11, 12 and 13. The gross difference in grain size is readily apparent in all of these photographs. Heat treated I/M grain size is approximately $500 \times 300 \times 75\mu\text{m}$ in L, LT and ST directions respectively. Heat treated P/M grain size is approximately $60 \times 35 \times 10\mu\text{m}$ in L, LT and ST directions respectively or roughly an order of magnitude smaller. These grain dimensions are typical for both materials (References 290, 291). In the as-compacted P/M billet material, prior powder particle boundaries are conspicuous by their equiaxed shape. Comparing forged with as-compacted conditions especially in the ST direction (Figures 9 and 11) show pronounced elongation and a partially recrystallized structure. A greater degree of recrystallization seems to be present in the I/M material than in the P/M material. Dynamic recovery is the sole softening mechanism in metals where climb and cross-slip of dislocations are relatively easy. As a result, misorientation of sub-boundaries is maintained sufficiently low (on the order of 1°) so that they never become capable of migrating as grain boundaries of recrystallization nuclei. This process occurs in metals of high stacking fault energy (SFE) (References 292-294). Note that no stacking faults (generally indicative of low SFE, planar-slip type materials) were observed in any of the foils of the present work. This result is of course consistent with historical observations of precipitation-strengthened aluminum alloys (References 295, 296).

Because of the equivalence in stacking fault energy for any aluminum alloy, the subgrain sizes of P/M and I/M materials are equivalent and approximately 1 to $3\mu\text{m}$ as can be seen in optical micrographs in Figure 13, scanning electron micrographs in Figures 14 and 15 and transmission electron micrographs in Figures 16 and 17 (Reference 297).

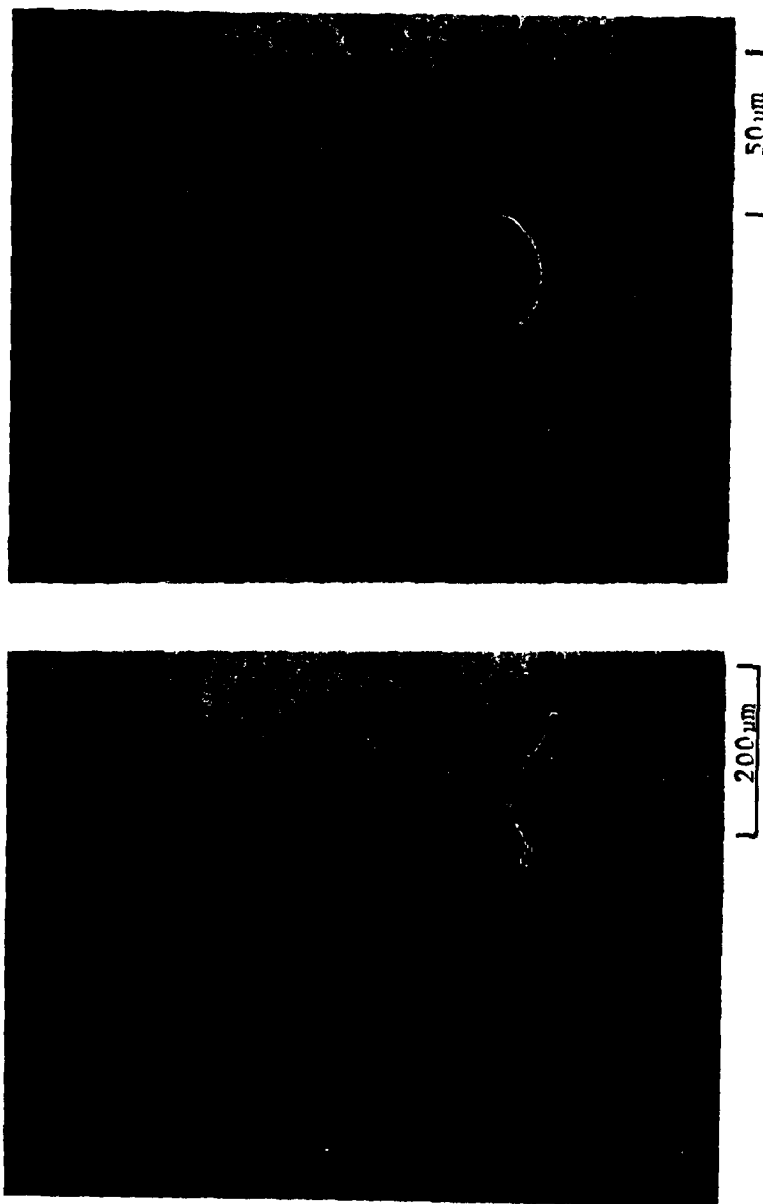


Figure 8. Optical Micrographs of As-Cast 7075 Al Ingot Metallurgy (I/M) Billet.

AFWAL-TR-81-4068



Figure 9. Optical Micrograph of As-Compacted CT-91 Al Powder Metallurgy (P/M) Billet.

AFWAL-TR-81-4068

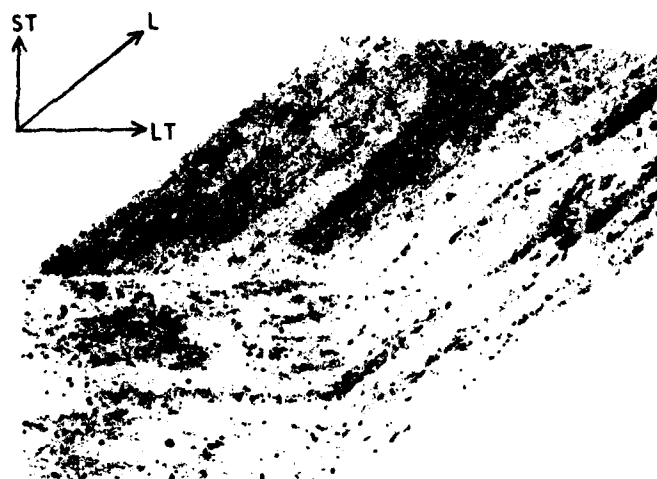
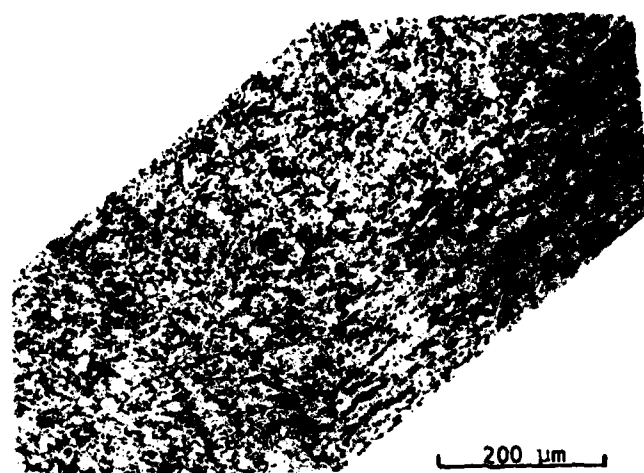


Figure 10. Three-Dimensional Optical Micrographs of As-Forged P/M (Upper) and I/M (Lower) Materials.

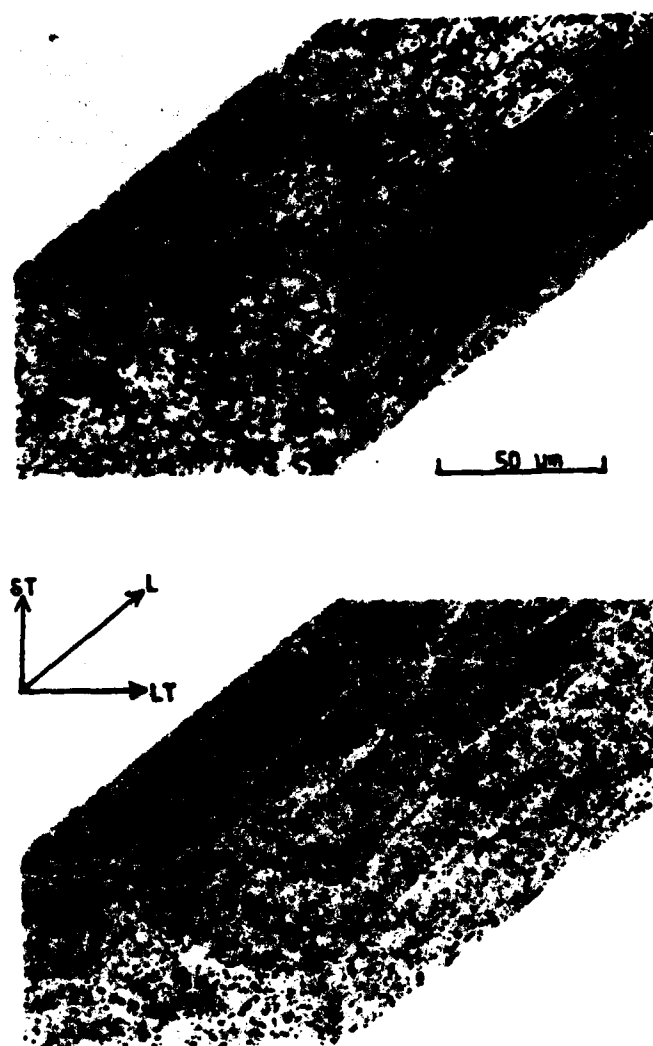


Figure 11. Higher Magnification Three-Dimensional Optical Micrographs of As-Forged P/M (Upper) and I/M (Lower) Materials.

AFWAL-TR-81-4068

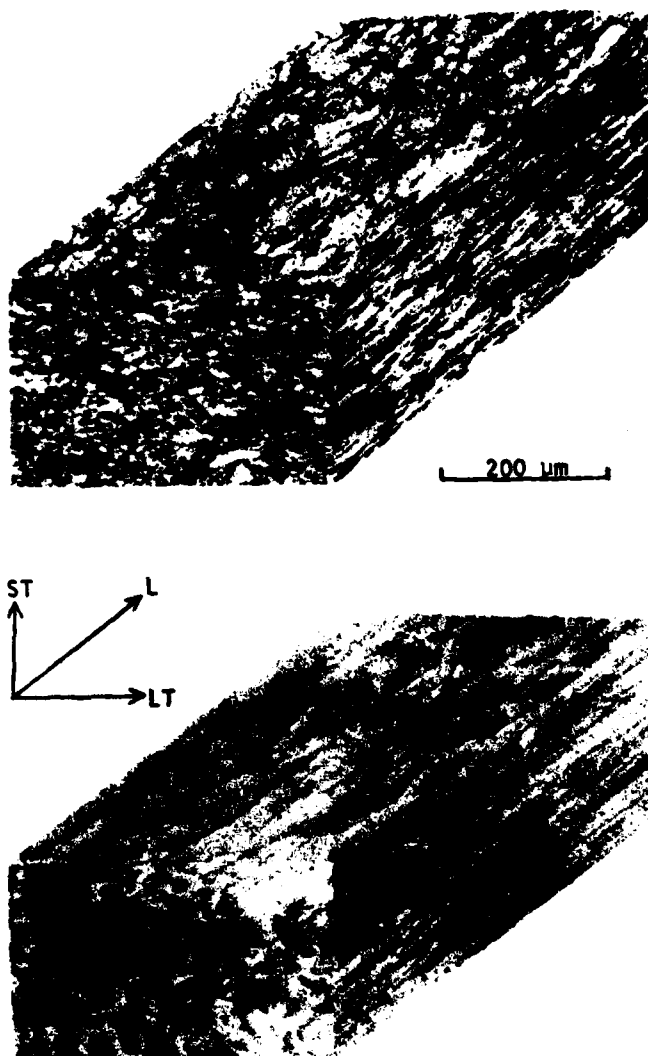


Figure 12. Three-Dimensional Optical Micrographs of Fully Heat Treated P/M (Upper) and I/M (Lower) Materials.

AFWAL-TR-81-4068

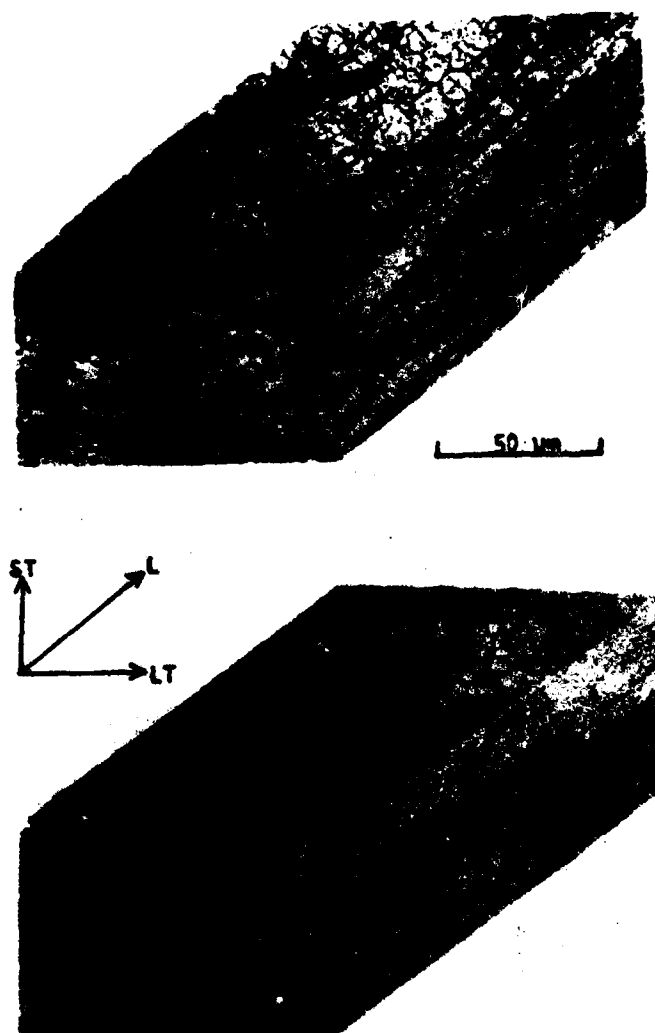


Figure 13. Higher Magnification Three-Dimensional Optical Micrographs of Fully Heat Treated P/M (Upper) and I/M (Lower) Materials.

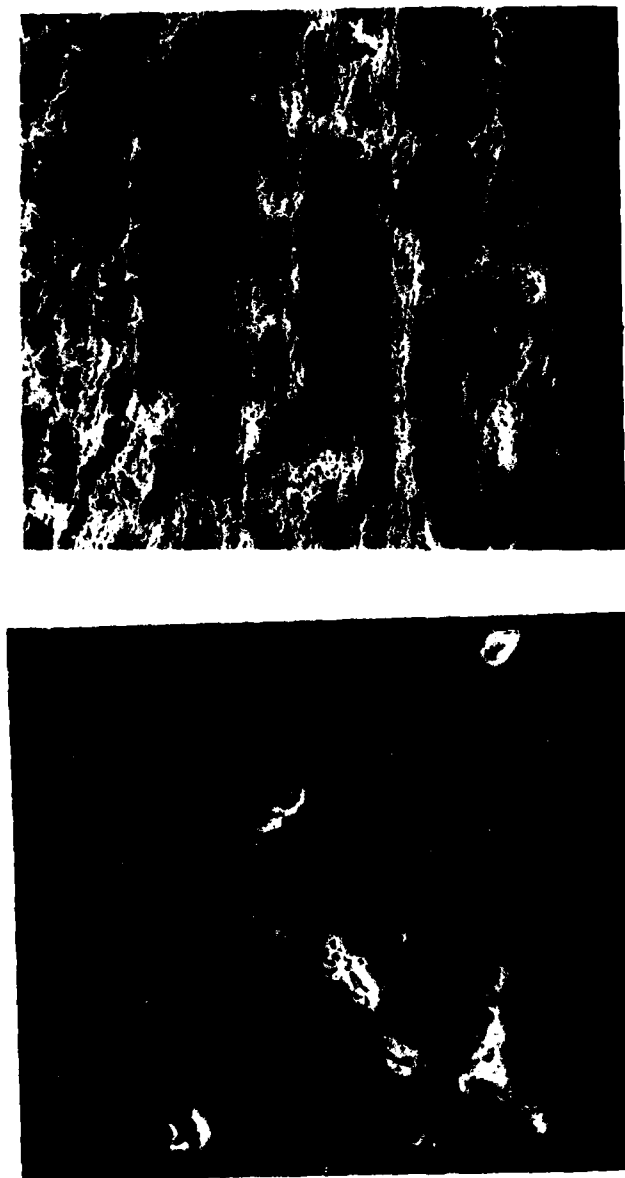


Figure 14. SEM Micrographs of Fully Heat Treated Longitudinal Faces of I/M (Left) and P/M (Right) Materials.

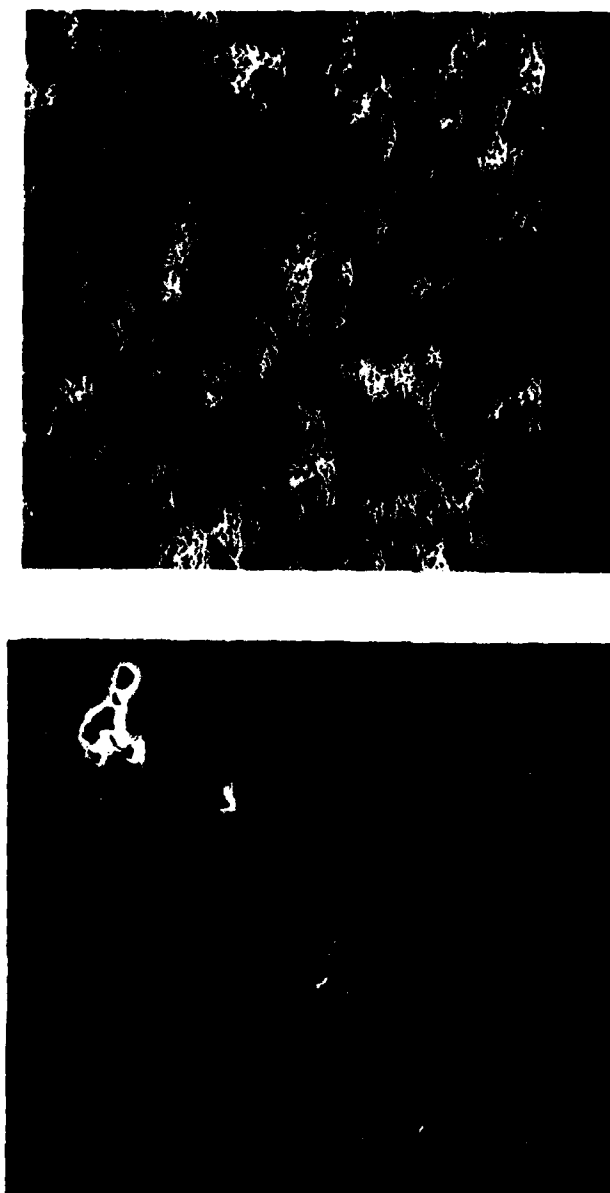


Figure 15. SEM Micrographs of Fully Heat Treated Long-Transverse Faces of I/M (Left) and P/M (Right) Materials.

AFWAL-TR-81-4068

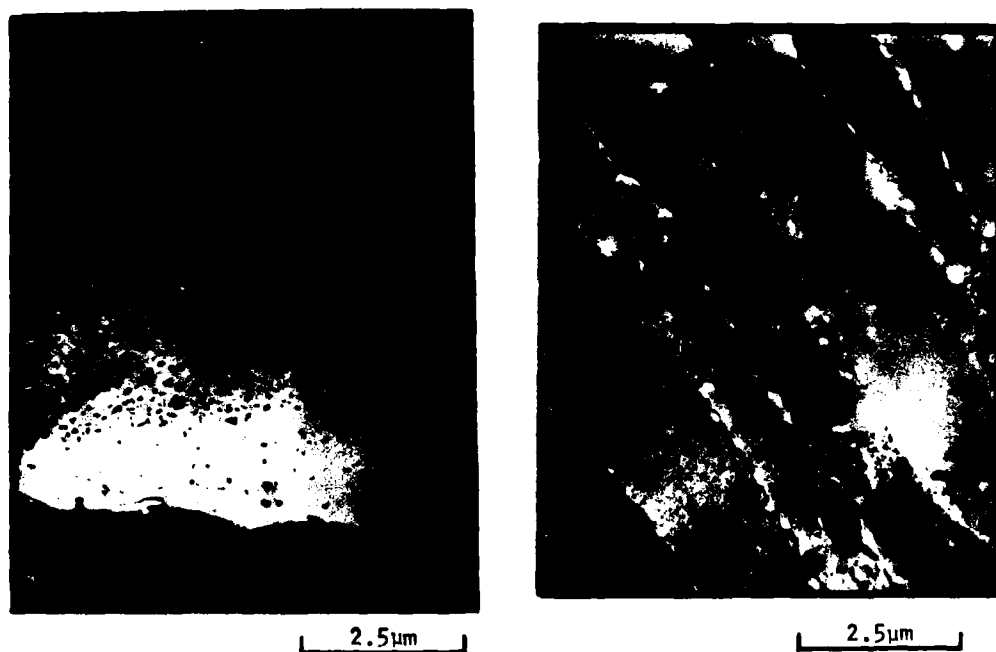


Figure 16. TEM Micrographs of Fully Heat Treated Longitudinal Sections of I/M (Left) and P/M (Right) Materials.

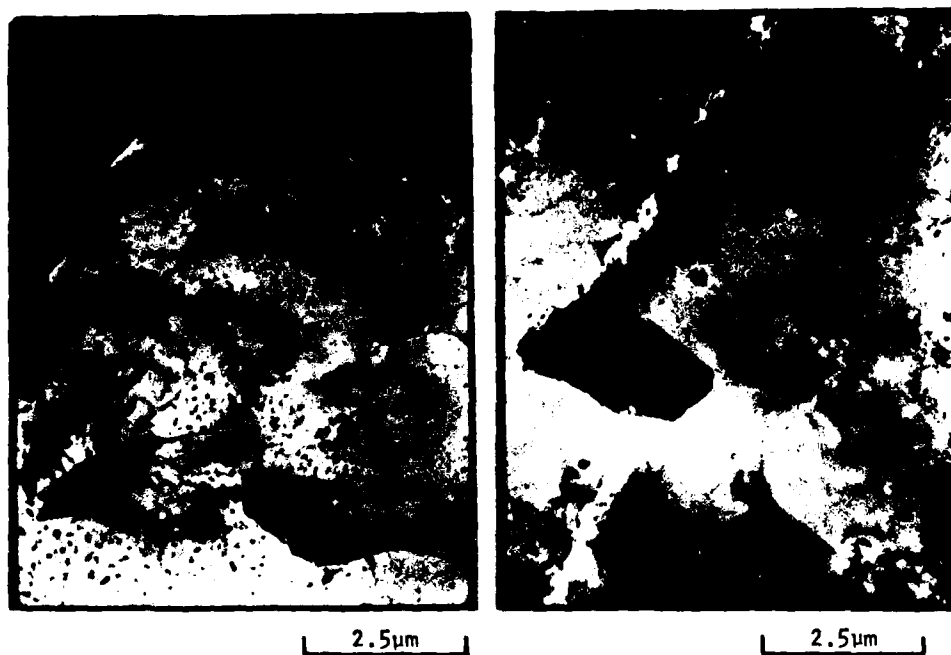


Figure 17. TEM Micrographs of Fully Heat Treated Long-Transverse Sections of I/M (Left) and P/M (Right) Materials.

Recrystallization in 7075 I/M alloy is inhibited by the presence of chromium. This fact is confirmed by noting that the recrystallized regions (subgrains not present) contained less chromium than the unrecrystallized regions (subgrains present). See Figures 14, 15 and 18. In contrast, the trapped oxides in the P/M materials nearly preclude recrystallization and grain growth (Reference 298). In fact, it is primarily pre-recrystallization recovery of subgrain boundaries that occurs in the P/M materials. Evidence to this effect can be seen in Figures 16 and 17. It may also be noted that the "recrystallized" regions contained less cobalt than the "unrecrystallized" regions. See Figures 14, 15, and 18. The walls of the subgrains apparent in Figures 16 and 17 were probably formed by the combination of "climb" and glide of edge dislocations ("polygonization") as well as screw dislocation twist boundary formation. These boundaries were observed to go in and out of contrast during tilting (a confirmation that they were not primary grain boundaries). The multiple boundaries around some of the subgrains in Figures 16, 17 and 19 were probably "bend extinction contours" from bending of the foil, because these were observed to sweep across the field of view with tilting. The smaller, discontinuous lines associated with some of the precipitate particles in this figure were probably dislocation lines. In Figure 20, it can be observed that such lines may have served as the sites for heterogeneous nucleation of η' precipitates on either side of the large rounded constituent particle (References 299, 300).

With optical microscopy, it is possible to observe $(\text{CuAl}_2)_2\text{FeAl}_3$, FeAl_3 , CuAl_2 and even Mg_2Si (in proportion to the presence of Si in the alloy; which is quite small). Of these phases Mg_2Si is the darkest, followed by $(\text{CuAl}_2)_2\text{FeAl}_3$, FeAl_3 and CuAl_2 (see Figures 8, 9, 10, 11, 12 and 13) (Reference 301). SEM examination offers not only higher magnification with resolution but also energy dispersive X-ray analysis capability. EDAX analysis verified that with optical microscopy, Si-containing compounds are darkest. However, the order reverses for $(\text{CuAl}_2)_2\text{FeAl}_3$ and CuAl_2 with the former showing brightest. For the P/M material, except in the as-compacted condition, no compounds large enough to evaluate chemistry could be found. And for the as-compacted

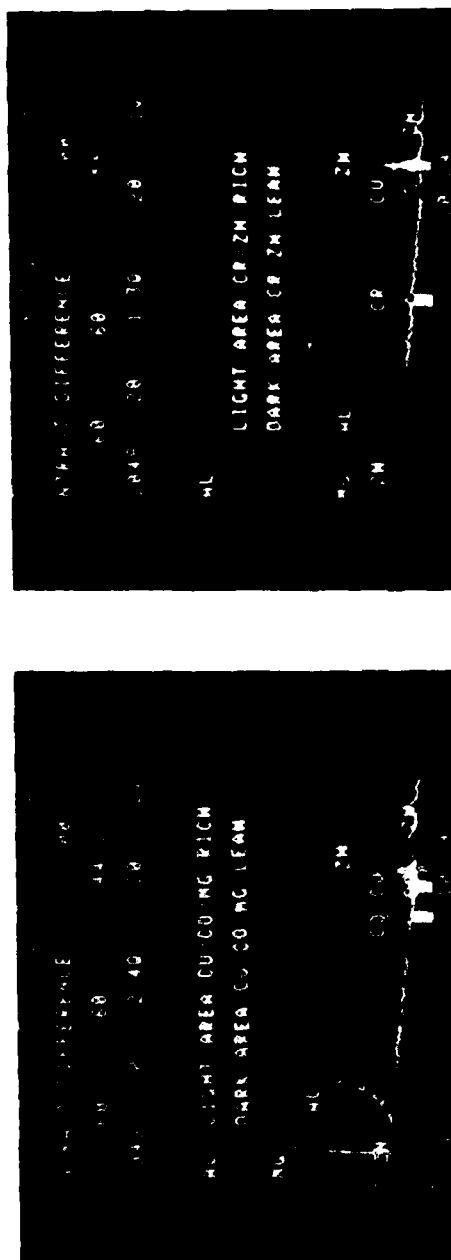


Figure 18. Photographs of EDAX Displays of Qualitative Chemical Analysis Comparisons of Light and Dark Areas of Fully Heat Treated I/M (Left) and P/M (Right) Materials.



Figure 19. Higher Magnification TEM Micrograph of Precipitates in Fully Heat Treated I/M Material.



Figure 20. Higher Magnification TEM Micrograph of Precipitates in Fully Heat Treated P/W Materials.

materials, only tiny CuAl_2 and Co_2Al_9 constituents were detectable (see Figures 8, 21, and 22). The reason why no Mg or Zn containing phases were found for either material is probably due to the fact that they have greater solubility, and the phases that are formed tend to be very small and homogeneously distributed within grains and grain boundaries alike. The presence of what seemed to be elemental Si (Figure 23) may have been merely the result of SiC polishing grit since gases and solid elements of lower atomic weight than sodium cannot be detected with energy dispersive X-ray analysis.

Figure 24 presents representative transmission electron micrographs of the I/M and P/M materials at their initial stages of processing. For the sake of expediency and because the TEM had no goniometer stage (making selected area electron diffraction (SAED) extremely tedious), no attempt was made to identify the small particles present by means of diffraction spot patterns. Hence, all "identification" of phases in the present work is by comparison with the literature. In the as-cast I/M and as-compacted P/M materials, irregular or blocky shapes on the order of $1\mu\text{m}$ or larger were probably $(\text{CuAl}_2)_2\text{FeAl}_3$, CuAl_2 , FeAl_3 , α Al-Fe-Si or Mg_2Si constituents. In the fully heat treated I/M materials (Figures 16, 17 and 19), the fairly uniform distribution of dark (high density), .1 to $.3\mu\text{m}$, low aspect ratio, irregularly shaped particles was probably the $\text{Al}_{18}\text{Mg}_3\text{Cr}_2$ dispersion. This is strongly suggested by their conspicuously complete absence in the P/M material. It is surmised (based on the TEM photomicrographs in the literature) that the light and dark .02 to $2\mu\text{m}$ needles, plates, rods and rectangles, generally present through all of the various stages of processing in both P/M and I/M materials, were probably the incoherent MgZn_2 n -phase. Similarly, the lighter .002 to $.5\mu\text{m}$ spheres and discs were probably the semi-coherent MgZn_2 n' -phase. These two phases were probably the grain and subgrain boundary phases in most cases. The darker .02 to $.3\mu\text{m}$ spheres present only in the P/M material were probably the Co_2Al_9 dispersoids. Furthermore, the randomly distributed, lightly shaded, irregular patches in the P/M material probably contained extremely fine oxide particles (References 302, 303). Even finer than these however, were the unresolvable coherent (MgZn) G.P. zones believed to be of a size less than $.002\mu\text{m}$ and spherical or disc-like in shape.

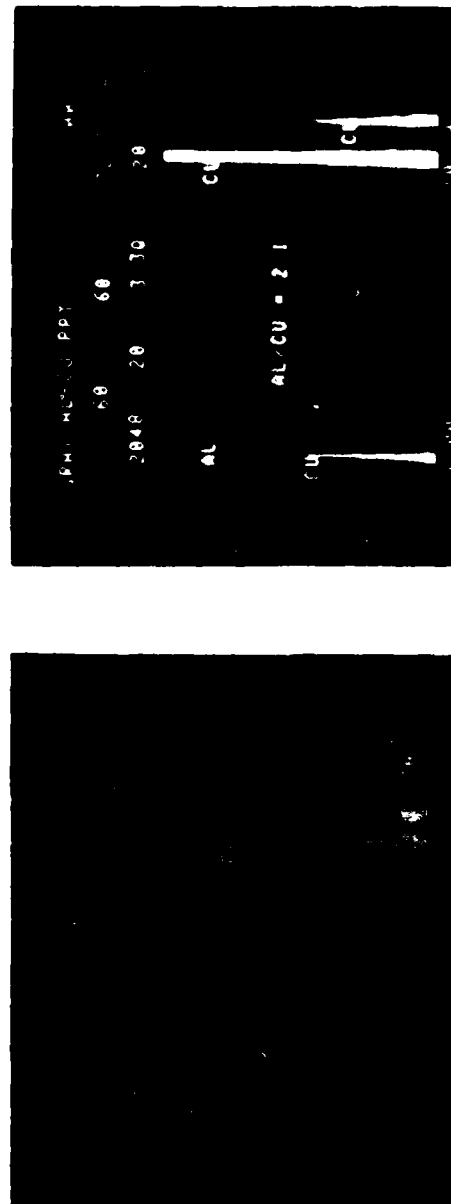


Figure 21. Photographs of EDAX Displays of Qualitative Chemical Analyses of Spherical White Grain Boundary Precipitate (Left) in As-Compacted P/M Material and Rounded Gray Precipitates (Right) in Both As-Compacted P/M and As-Cast I/M Materials.

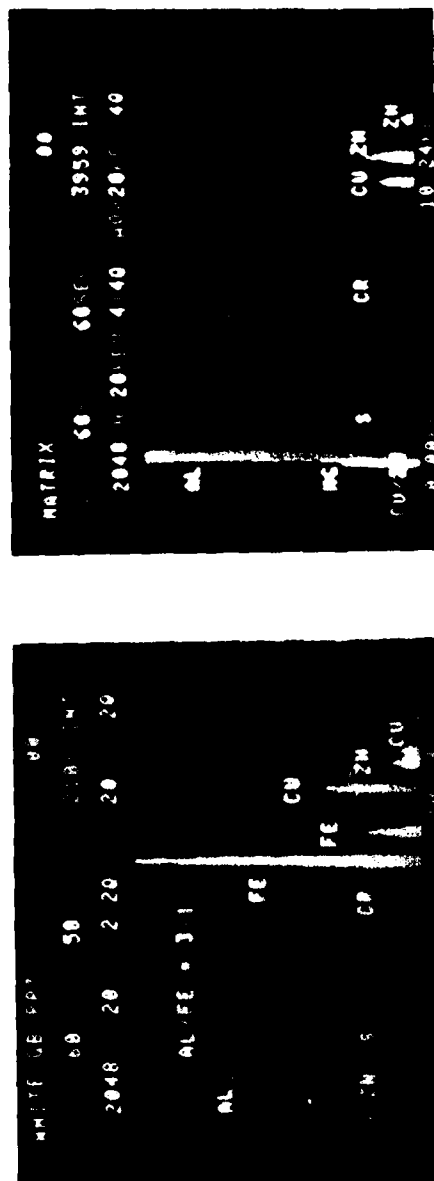


Figure 22. Photographs of EDAX Displays of Qualitative Chemical Analyses of Irregular White Grain Boundary Precipitate (Left) and the Alloy Matrix (Right) in the As-Cast I/M Material.

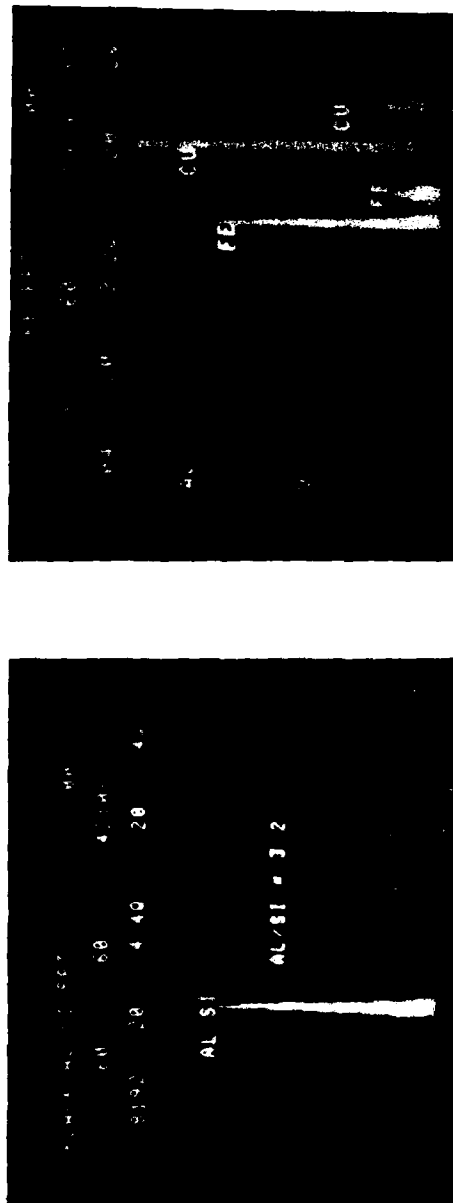


Figure 23. EDAX Displays of Qualitative Chemical Analysis of Black Particles (Left) and of Large Irregularly Shaped, Fractured White Precipitates (Right). Smaller Gray Precipitates are CuAl_2 .

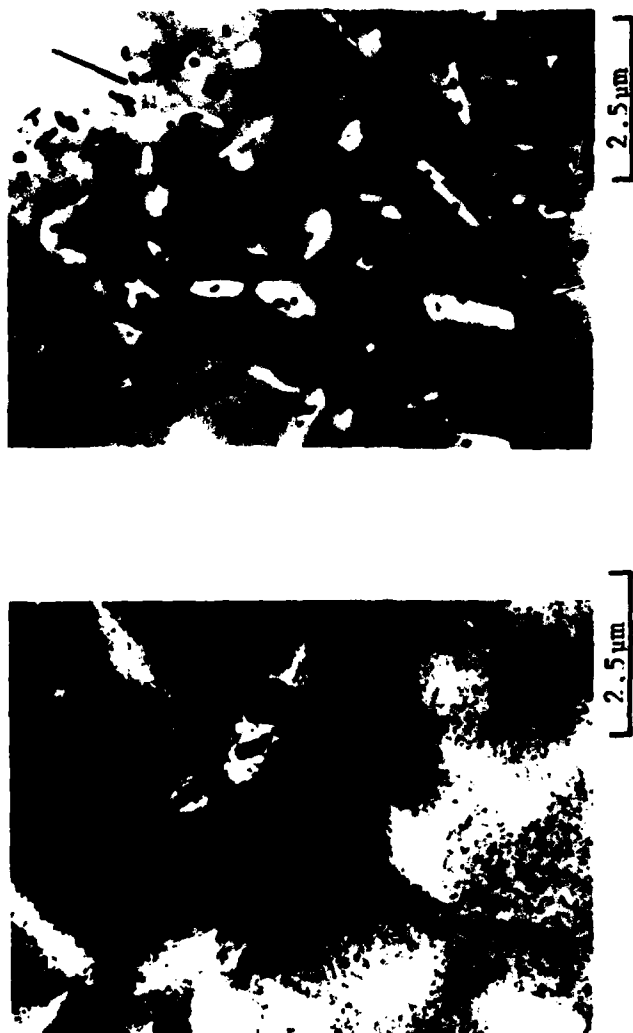


Figure 24. TEM Micrographs of As-Cast I/M (Left) and As-Compacted P/M (Right) Billet Materials.

The uniform "salt and pepper" appearance within the grains is due to n' and not G.P. zones (References 304-323). The white areas in Figures 16, 17, 19, 20 and 24 that appear to be holes created by the removal of a particle, were exactly that as was later verified by electron microprobe analysis (EMPA). Within or near the edge of the rod-shaped voids in Figure 24, there generally remains a much smaller, irregular, spherical or disc-shaped particle. This is suggestive of heterogeneous nucleation of incoherent n -phase either on ϵ or n' phases, which had been previously concluded by other investigators (Reference 324). Since this occurs in both I/M and P/M materials, it obviously does not require Cr-dispersoid particles which are present only in the I/M alloy. Other researchers have concluded that nucleation of n -phase does indeed occur on Cr-dispersoids but only if they are situated in a certain crystallographic orientation (Reference 325). This is obvious since only a small percentage of Cr-dispersoids nucleate n -phase.

Tentative identification of the largest precipitates was confirmed by EMPA of these foils (see Figure 25). The large, gray, irregularly-shaped particle in the left-hand micrograph (as-cast I/M) was determined by quantitative wavelength dispersive X-ray analysis to be $(Fe_{.7}Cu_{.3})Al_3$. The little round, white balls were determined by a 60 minute "X-ray map" (not shown) to be Si, probably from the glass container used in the electropolishing of the foils. The large, white, irregularly-shaped particle (partially removed by etching) in the right-hand photograph (as-forged I/M) was $(Cu,Zn)Al_2$, again as determined by a 60 minute "X-ray map" (not shown). The small, white rod-shaped precipitates were indeed $MgZn_2$ and the larger, black rod-shaped voids probably contained $MgZn_2$ precipitates. Several very small (approx. $.25\mu m$), round white balls (not shown) turned out to be Co_2Al_9 dispersoids as expected. As with the previous SEM investigation, no other particles large enough to analyze could be found in the P/M foils.

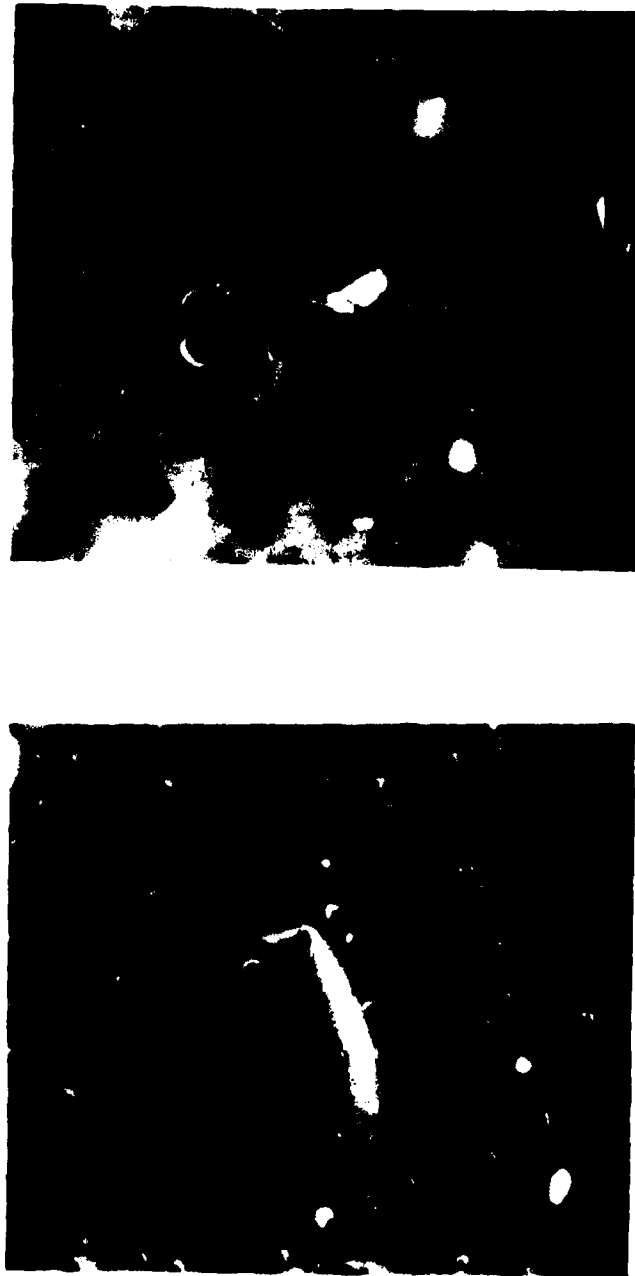


Figure 25. ENPA Micrographs of Thin Foils of As-Forged I/M Material (Left) Containing Large $(\text{CuAl}_2)_2\text{FeAl}_3$ Precipitate, As-Cast I/M Material (Right) Containing Large White $(\text{Cu,Zn})\text{Al}_2$ Precipitate and Small White Rods of MgZn_2 Precipitate.

2. MECHANICAL PROPERTIES

a. Strength and Ductility

The results obtained from tensile testing are presented in Table 13. Values agree well with other published data for these materials (References 326-332). In fact, some of the very same material used for the present work and similarly processed and tested under contract for the Air Force at Alcoa produced very similar properties (Reference 333). The static strength achieved for 7075-T6, used in the present work as control material, suggests that a maximum amount of Cu was dissolved in the matrix (Reference 334). This result is indicative of an optimum solution heat treatment for the ingot material. Note that alloying element homogenization is never totally effective in I/M materials, however, and so 2XXX and 7XXX I/M alloys are not used in the un-wrought condition. Again, this is not a concern with P/M materials for which the ductility and reduction in area measurements are more sensitive to their only possible segregation. That is, the high values obtained in these properties for the P/M material, suggest that the grain boundary oxide was adequately dispersed during forging.

It should be noted that the yield and ultimate strengths of the ingot material were only slightly higher than those of the powder metallurgy material in the longitudinal orientation. The long transverse orientation properties of the I/M and P/M materials were even closer. Such results provide the desired opportunity for a fair comparison of the other properties of these materials.

b. Toughness

Toughness testing values obtained in the present work agree very well with valid K_{IC} tests performed on these materials and published in the literature (References 335-338). Both "W/A" and "Secant" methods have been employed in the analysis of the data generated in the present work and these are compared in Table 14. A comparison between "valid"

AFWAL-TR-81-4068

TABLE 13
TENSILE* DATA

<u>Material</u>	<u>U.T.S.</u>	<u>(MPa)Y.S.</u>	<u>%E1.</u>	<u>%R of A</u>
I/M-L	572	503	13	18
I/M-LT	517	462	13	13
P/M-L	543	476	14	32
P/M-LT	510	468	13	21

(average of two tests)

* ASTM E8-69

TABLE 14
TOUGHNESS* DATA

<u>Material</u>	<u>(MPa) Modulus (E)</u>	<u>K₀ Toughness (MPa√m)</u>	
		<u>Secant Method</u>	<u>W/A Method</u>
I/M-LT	73000	32	32
I/M-TL	70000	26	25
P/M-LT	71000	30	34
P/M-TL	69000	24	21

(average of two tests)

* ASTM E399-78

K_{IC} CTS vs. "valid" slow-bend, pre-cracked Charpy data for 7075-T7351 Al alloy indicated good correlation (within $\pm 20\%$) for ratios of toughness to yield strength up to $1/\sqrt{m}$ (Reference 339). For "valid" K_{IC} testing, ASTM Standard E399 (Reference 340) requires:

$$a, B > 2.5 \frac{(K_{IC})^2}{\sigma_{y.s.}} \quad (3)$$

where; a is the crack length
 B is the specimen thickness
 $\sigma_{y.s.}$ is the yield strength
 K_{IC} is the fracture toughness

For the specimens tested in the present work, " a " was approximately equal to 1/2cm and " B " was approximately equal to 1cm. From Tables 13 and 14, one has merely to select the appropriate values to discover that in no case was the crack length requirement met. In addition, the referenced standard requires that the ratio of maximum load (P_{max}) to load for toughness calculations (P_Q) be less than 1.1. From load-deflection, "x-y" recorder data plots generated during the testing (not shown), it was noted that this requirement also was not met. Because the specimen geometry of the Charpys tested in the present work did not meet the requirements that guarantee "plane strain", "triaxial stress" conditions, the "plastic zone size" can be considered to have been as much as three times larger than would have been appropriate for a "valid" K_{IC} test. When calculated, this contribution is found to be quite small in comparison to the total crack length. In fact, the difference between plastic zone size for the two conditions would be the difference between .005cm and .015cm for plane strain and plane stress respectively for 7075-T6. This difference is merely a consequence of the equations:

$$\text{plane strain plastic zone size} = \frac{1}{6\pi} \frac{(K_{app})^2}{\sigma_{y.s.}} \quad (4)$$

$$\text{plane stress plastic zone size} = \frac{1}{2\pi} \frac{(K_{app})^2}{\sigma_{y.s.}} \quad (5)$$

where; K_{app} is the applied stress intensity (Reference 341). Hence, the tests could not be considered truly conservative because of the existence of this slightly larger plastic zone size which increases the "critical" crack length for failure and reduces the effective stress concentration (K_{eff}) experienced by the material (Reference 342).

Plane strain fracture toughness (K_{IC}) testing is desirable because it is dependent only upon material properties; whereas, plane stress fracture toughness is dependent upon geometry factors as well (Reference 343). Investigators have generally found that K_{IC} and K_{ISCC} (the value of K_{IC} for a material subjected to stress in a stress corrosion environment) for 7075-T6, are approximately equivalent (Reference 344). This last factor provides added incentive for K_{IC} evaluation. The mode I or "opening" mode is not only the most severe, but is also the only deformation mode of any practical engineering significance except for the case of torsion (mode III or "tearing") (Reference 345). Unfortunately, the values obtained in the present work are useful for qualitative comparison purposes only. Again, for relatively high strength materials like these, the maximum plastic zone size possible is small to begin with and so the magnitude of change in effective crack length is quite small. For this reason, the difference between plane strain and plane stress fracture toughness is not likely to be very large (Reference 346). In fact, the data obtained in the present work does agree quite well with published values of valid K_{IC} data in the literature (References 347-351).

Another method of toughness evaluation sometimes used for relatively brittle materials like 7XXX Al alloys, is notched tensile testing. For such a test, the ratio of ultimate tensile strength to yield strength is observed to increase as toughness increases. Other investigators testing 7075-T6 and CT-91-T7 have found ratios of approximately 1.2 to 1.3 in TL and LT orientations respectively for both of these materials (References 352, 353). These ratios have been shown to correspond to K_{IC} 's of approximately 28 and 33 MPa \sqrt{m} respectively (Reference 354), slightly more optimistic than the present results.

Generally, materials with $K_{IC}/\sigma_{y.s.} \leq 1/\sqrt{m}$ are considered brittle and materials with $K_{IC}/\sigma_{y.s.} > 1/\sqrt{m}$ are considered ductile. The load-deflection records obtained for the materials tested in the present work indicated "Type 1" (brittle) behavior. For such materials, correlations based on load (P_Q) are recommended rather than correlations based on crack opening displacement (COD) (Reference 355). Percentage elongation is more the measure of a materials ability to strain harden and restrict void coalescence than it is the measure of toughness (Reference 356). The area under a load-deflection curve, immediately in energy units is instantly more appealing in a pedagogical sense as the measure of toughness. The so-called "W/A" method is the outgrowth of this concept. Unfortunately, the value of K_Q obtained from the W/A method can, except for the most brittle of materials, depend on the LVDT, the X-Y recorder, and extraneous deflections in the fixturing. The factor of 2 in the denominator in the expression for K_{IC} from W/A given in Appendix B may not be appropriate for all materials. To decide on the appropriate area under the load-deflection curve to be measured, the end of the fracturing process must be assumed (References 357, 358). For ductile materials or simply plane stress conditions for brittle materials, the W/A method should be non-conservative since the total energy absorption contribution of the relatively large, plane stress, shear lips formed, overshadows the contribution from the relatively small, plane strain, flat fracture. Obviously, the validity of the W/A method as a measure of K_{IC} decreases as the percentage of shear lip area increases. For such material conditions, the so-called "Secant" method, which relies only upon the initial fracturing load, is no doubt more appropriate and representative of a valid K_{IC} calculation. Because the Secant method is insensitive to shear lip formation, it should be fairly consistent for materials of any ductility and therefore, a more conservative estimate of fracture toughness. In fact, for the evaluation of plane stress fracture toughness (K_C), the W/A method should be preferred to the Secant method.

This calls to mind the importance of testing and qualifying the same sizes and configuration that will be used in actual design and fabrication. The W/A method would certainly be the more useful in this regard in defining optimum thicknesses for structural efficiency.

Obviously, sections too thin to develop complete shear lips do not utilize the full potential of a given material, as maximum energy absorption from their formation is not realized.

From the data in Table 14, it can be seen that the W/A method results in overly conservative predictions of fracture toughness for the TL orientations and either overly nonconservative or inconsistent estimates of K_{IC} for the LT orientations. On the other hand, the values obtained with the Secant method all appear fairly reasonable for these materials. Note that the absolute differences in toughness between the 7075-T6 (I/M) and CT-91-T7 (P/M) materials seem merely to reflect differences in their ultimate strengths (Reference 359). But even more notably, in normalizing the data with either ultimate or yield strengths, the TL orientation remained inferior to the LT orientation for both I/M and P/M materials.

c. Fractography of Tensile & Toughness Specimens

Figures 26 and 27 are SEM fractographs comparing the macroscopic fracture appearances of the four material orientations tested in smooth, round bar, monotonic tension. It is significant in these figures that the P/M feature details appear finer. Optical comparison of macroscopic differences in Charpy specimens (Figure 28) also suggest finer features for the P/M (right-hand side columns) material. Note that the shear lip size of the P/M material is deceptively large due to greater contrast from the finer structure. Both tensile and Charpy fractographs display pronounced differences between orientations. For the tensile specimens, the longitudinal orientations of both P/M and I/M materials exhibit greater amounts of ductile shear than the long transverse orientations. Such differences are consistent with expectations (Reference 360). For the Charpy specimens, the TL-orientation (upper two rows of Figure 28) is obviously more flat than LT-orientation (lower two rows of Figure 28). Again, these observations are in keeping with expectations because in the TL-orientation, crack travel is parallel to the material flow direction. In contrast, crack travel is perpendicular to the material flow direction and so must cross more grain boundaries requiring more energy in the LT-orientation (Reference 361).

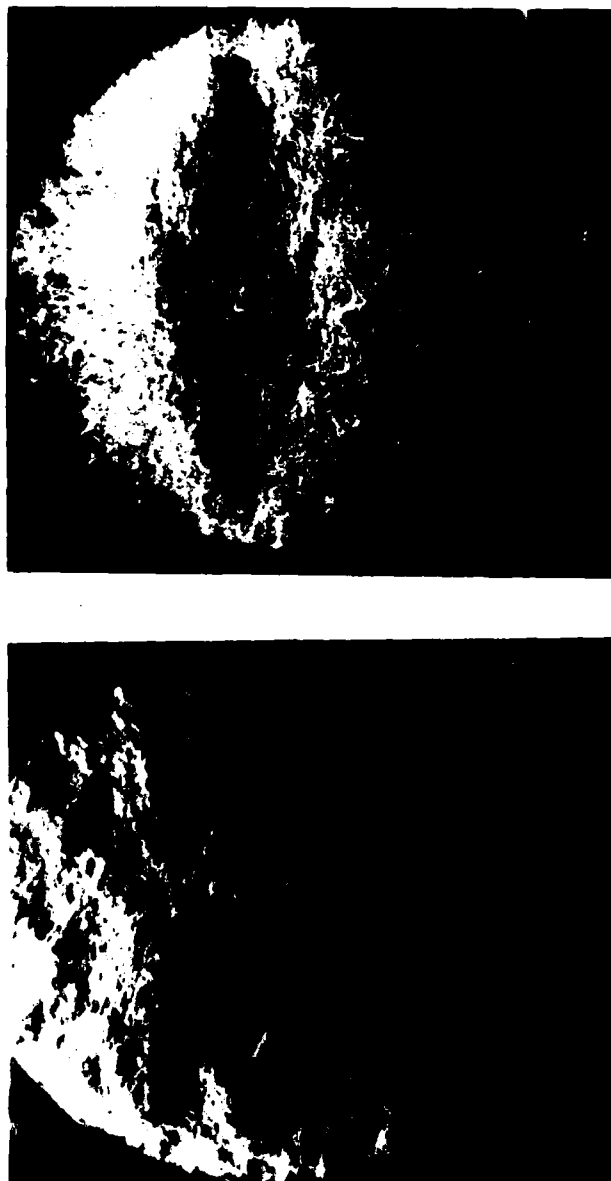


Figure 26. SEM Macrofractographs of Longitudinal I/M (Left) and P/M (Right) Monotonic Tension Test Specimens.



Figure 27. SEM Macrofractographs of Long Transverse I/M (Left) and P/M (Right) Monotonic Tension Test Specimens.



Figure 28. Optical Macrofractographs of Charpy Toughness Fracture Surfaces, the Two Left Columns are I/M, the Two Right Columns are P/M, the Upper Two Rows are TL and the Lower Two Rows are LT Orientation Specimens.

Figures 29 and 30 compare the microscopic appearances of the I/M and P/M, L and LT tensile specimen fracture surface conditions. These SEM micrographs more clearly display feature size and orientation effects. Notably, Figure 30 shows that the pronounced flow direction (horizontal) was perpendicular to the loading axis (out of the plane of the paper) for the transverse (LT) orientation specimens. Note that even though both of these materials can be considered relatively brittle, they do not cleave. Instead, the "dimples" formed from "microvoid coalescence" are simply small. Cleavage occurs only for brittle constituents or for materials that undergo ductile-to-brittle transitions, like steels (References 362, 363).

If plastic replicas had been made of the mating fracture surface halves and examined in the TEM, it would have been possible to observe the difference between dimples formed by shear or tearing and those formed by "normal" (perpendicular pulling) rupture. Those formed by normal rupture are equiaxed. Those formed by shear would be elongated parabolic cones with apexes pointing in opposite directions for shear, and in the same direction for tearing (References 364-367). Such conditions existed on the "slant", "vee" and "shear lip" faces of tensile and toughness specimen fracture halves. But even without such replicas, it is obvious from just macroscopic appearance that the L-orientation fractures exhibited a higher degree of shear than the LT-orientation. All microfractographs were obtained from the flat (normal rupture) portions of all the specimens so that fair comparison of dimple size would be possible. Figure 31 compares normal rupture dimples (left) with shear lip dimples (right) from the final overload area of a P/M fatigue fracture surface. Note the similarity between these micrographs and those of Figures 29 and 30.

Investigators proved years ago, that increased dimple size, depth and spacing increases toughness. It was also learned that the number of dimples per unit area decreased as the number of particles per unit area decreased because particles are nearly always the nucleation sites for dimple formation (References 368-373). Note that dispersoid size and distribution is only important to FCP at high ΔK 's ($>16\text{MPa}\sqrt{\text{m}}$) implying a

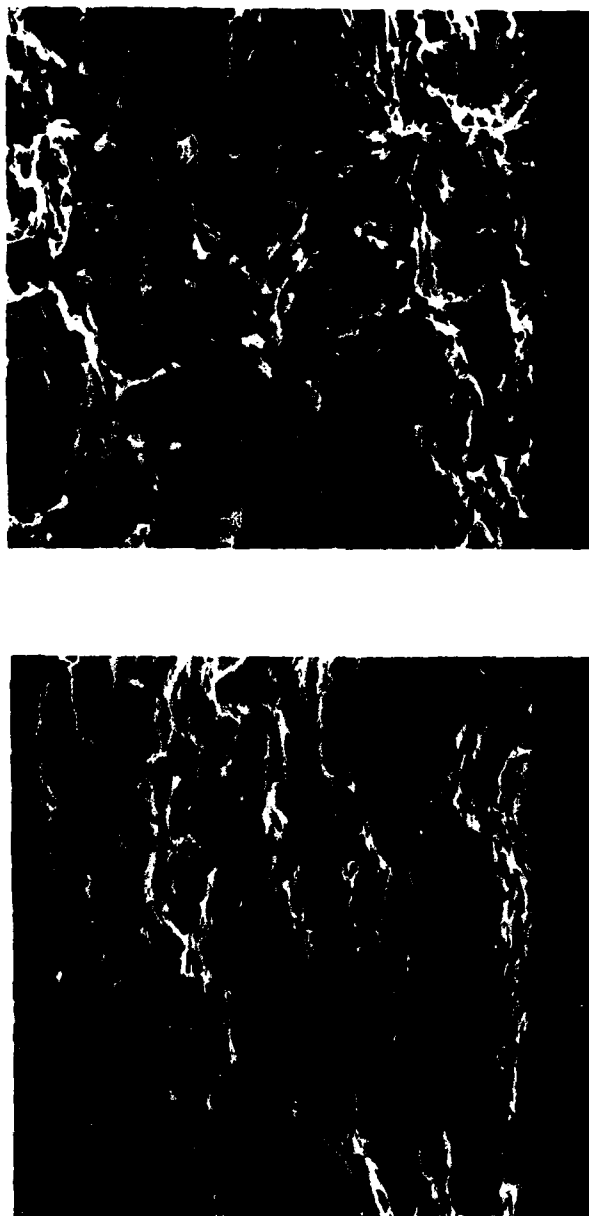


Figure 29. SEM Fractographs Obtained from the Flat Fracture Areas of Longitudinal I/M (Left) and P/M (Right) Monotonic Tension Test Specimens.

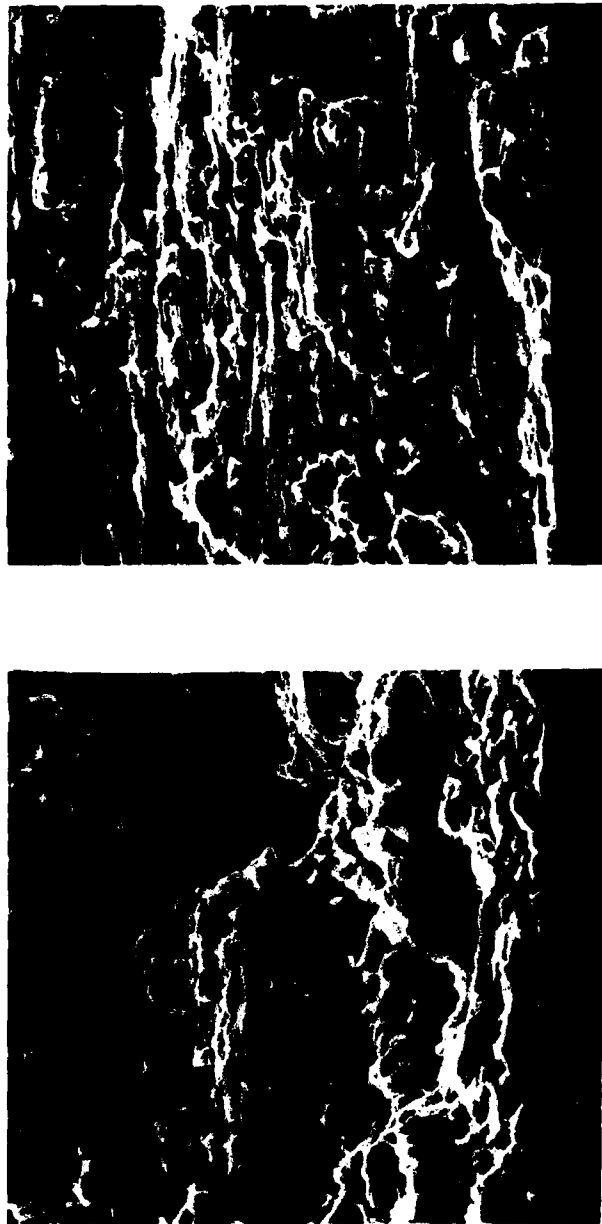


Figure 30. SEM Fractographs Obtained from the Flat Fracture Areas of Long Transverse I/M (Left) and P/M (Right) Monotonic Tension Test Specimens.

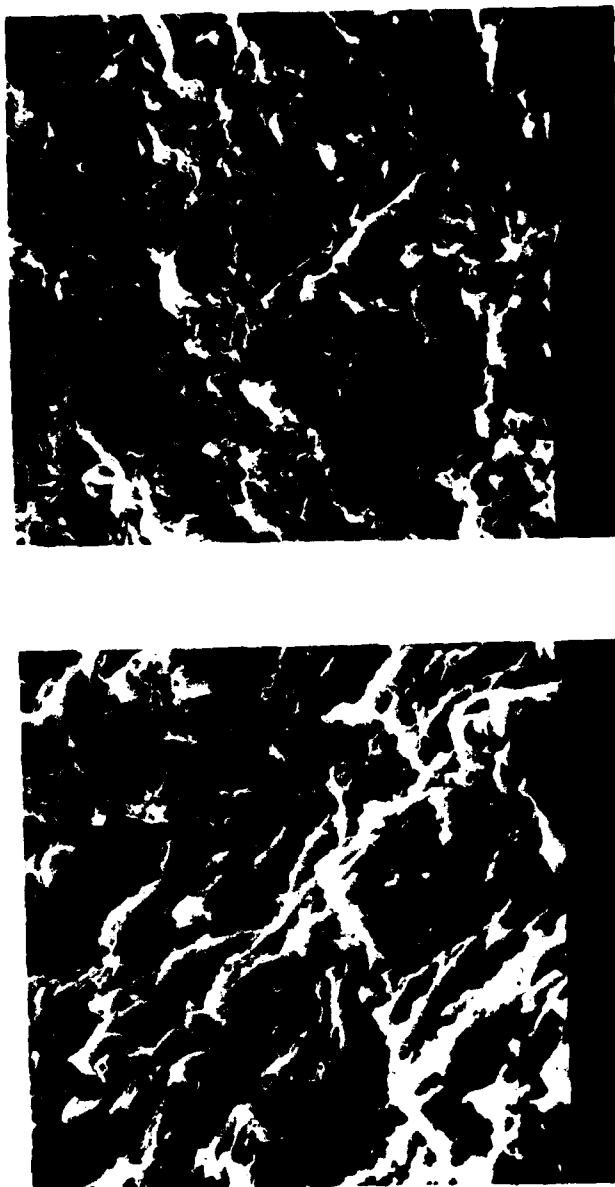


Figure 31. SEM Fractographs Obtained from the Flat (Left) and Shear Lip (Right) Fracture Areas of a P/M Notched Fatigue Test Specimen.

greater effect on toughness than on fatigue properties (Reference 374). SEM fractographs (Figures 32 and 33) suggest that the greater size and depth of dimples in the fast fracture portion of the LT-orientation Charpy specimens is indicative of the higher toughness observed. This is consistent with the smaller distances between grain boundaries in the LT direction. Dimple size is observed to increase as grain size and yield strength decrease and temperature increases (References 375-379). Others have shown that dimple spacing correlates with center-to-center spacing of inclusions in aluminum alloys and that higher toughness is the direct result of larger spacing (References 380-383).

Figures 34 and 35 clearly show fairly large voids in which cleaved facets of large constituent inclusions (probably $(\text{CuAl}_2)_2\text{FeAl}_3$) (Reference 384) are visible in the ingot metallurgy (I/M) material. In contrast to these are the smaller submicron dimples in both I/M and P/M materials probably associated with dispersoids and incoherent hardening precipitates (Reference 385). Research has shown that ductility increases as the volume percent of large irregularly-shaped clusters of second phase particles decreases (References 386, 387). The smaller dimples apparently contribute to decreasing fracture energy by linking-up with the larger voids. Dispersoids in both I/M and P/M materials probably serve to decrease toughness (References 388-390). Considering the equivalence in toughness for both LT and TL orientations of I/M and P/M materials (see Table 14), and the similarity in micro-fracture appearances (Figures 29 through 35), it would seem that the effect of large constituents in the I/M material was relatively insignificant to the effect of the dispersoids.

Note that especially in Figures 34 and 35, some areas of the fracture surfaces appear quite smooth and nearly free of dimples. These are probably the result of the removal of poorly bonded constituents from grain boundaries. But the fact that some few dimples are present, rules out the possibility of intergranular failure (Reference 391).

The only significant segregation in P/M materials is due to the oxide formed in powder atomization. As can be seen from TEM micrographs in Figures 16 and 24, the approximate 2 micron size, amorphous, segregated,

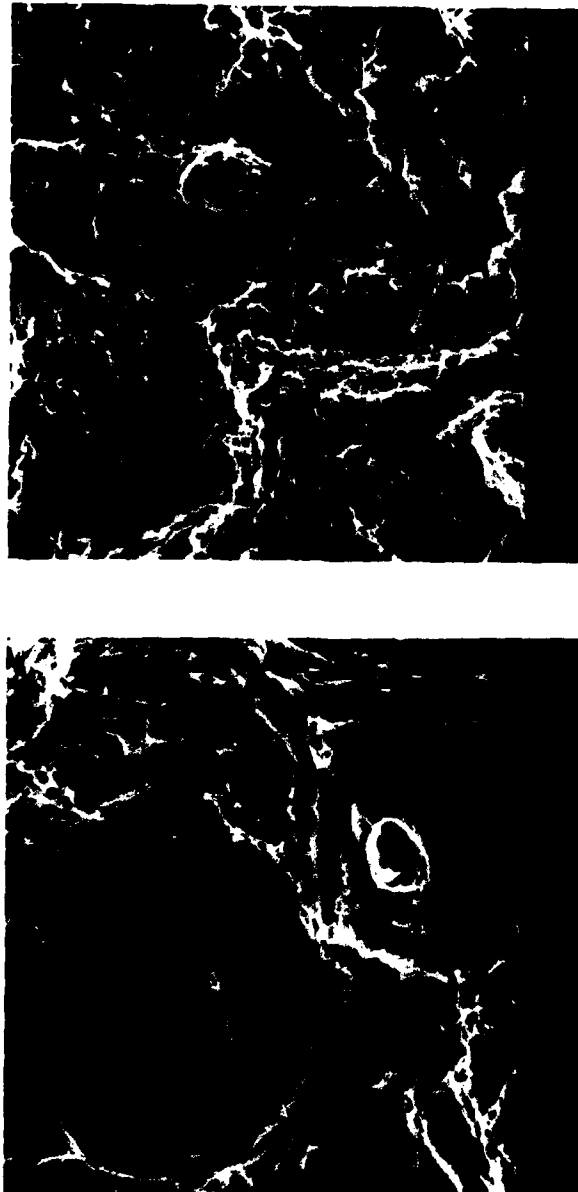


Figure 32. SEM Fractographs Obtained from the Flat Fracture Areas of LT I/M (Left) and P/M (Right) Slow-Bend Charpy Toughness Test Specimens.

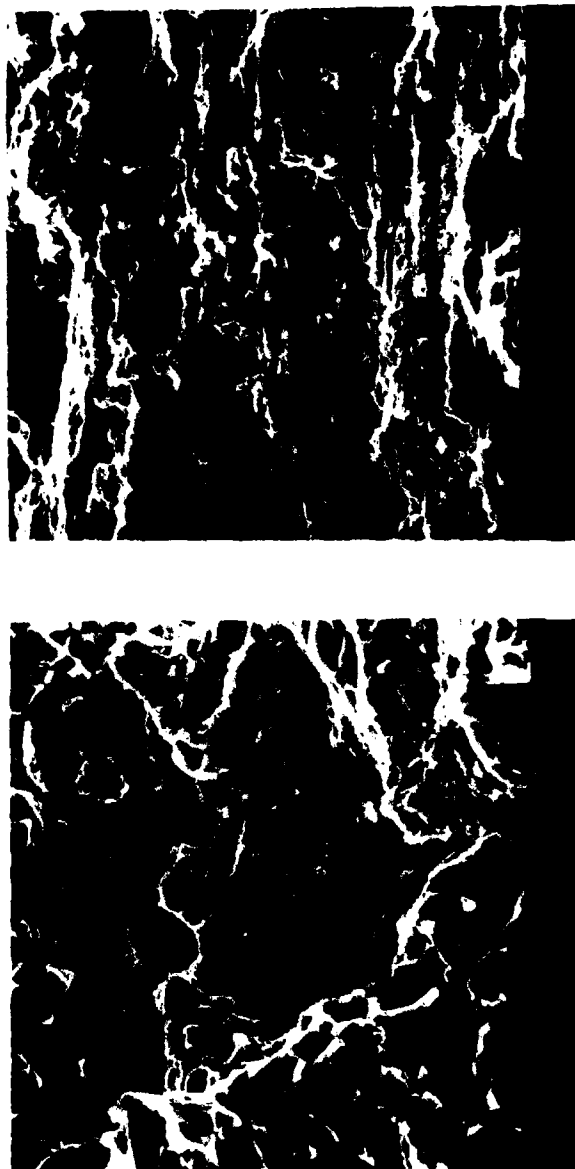


Figure 33. SEM Fractographs Obtained from the Flat Fracture Areas of TL I/M (Left) and P/M (Right) Slow-Bend Charpy Toughness Test Specimens.



Figure 34. Higher Magnification SEM Fractographs Obtained from the Flat Fracture Areas of LT I/M (Left) and P/M (Right) Slow-Bend Charpy Toughness Test Specimens.

AFWAL-TR-81-4068

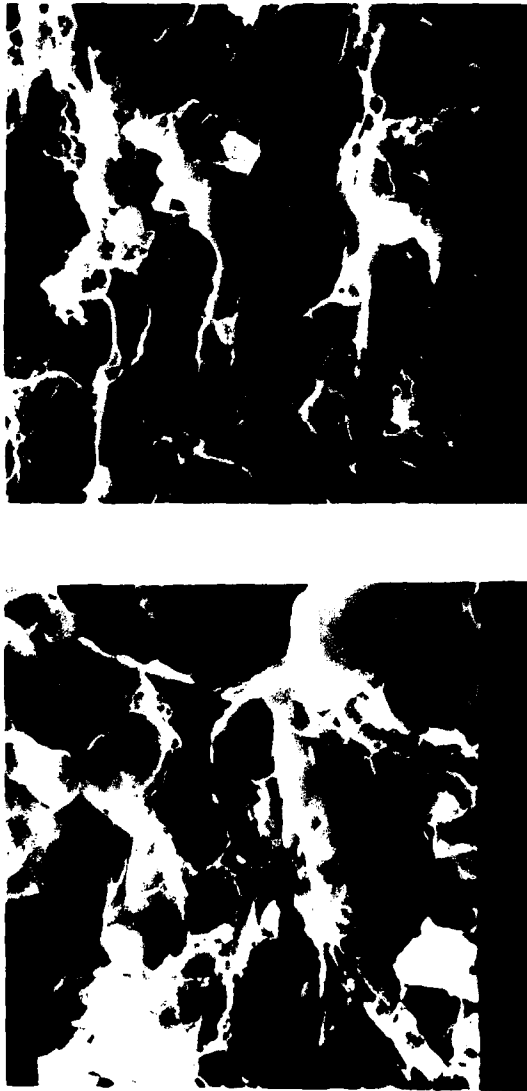


Figure 35. Higher Magnification SEM Fractographs Obtained from the Flat Fracture Areas of TL I/M (Left) and P/M (Right) Slow-Bend Charpy Toughness Test Specimens.

AD-A118 280

AIR FORCE WRIGHT AERONAUTICAL LABS WRIGHT-PATTERSON AFB OH F/G 11/6
A COMPARISON OF MICROSTRUCTURE AND PROPERTIES OF EQUIVALENT STR--ETC(U)
AUG 81 S H DOERR

UNCLASSIFIED

AFWAL-TR-81-4068

NL

2-2



END
DATE
FILMED
9 82
DTIC

oxide particles, associated with the envelope of a prior powder particle, become more uniformly distributed from the deformation and therefore less likely to serve as crack initiation sites which probably account for the increase in toughness observed in worked P/M material as compared with as-compacted P/M material (Reference 392). However, in conjunction with that toughness increase, indicating more metal-to-metal bonding from additional deformation, anisotropy also increases (Reference 393). Considering the response of I/M materials, such an observation, this should not come as a surprise. A simple concept of crack path "tortuosity", despite gross differences in its relative magnitude between P/M and I/M materials, should nonetheless apply equally if one considers grain boundaries as effective barriers or crack tip energy absorbers like so many laminates (Reference 394). Obviously, many more boundaries are encountered in the LT-orientation than in the TL-orientation. Therefore, toughness and ductility anisotropy are to be expected equally from P/M and I/M materials with such pronounced orientations.

A similar but different argument could account for the observed anisotropy in strength. That is, particles serve as the nucleation sites for void creation leading to rupture. Therefore, if aligned such that a larger cross-sectional area is affected by the applied stress, resulting strength should be lower than if a smaller cross-sectional area is affected. Overaging heat treatments and fine grain size have historically been credited with improved toughness in I/M materials (Reference 395). Considering the data in Table 14, such relations are apparently inappropriate for P/M materials.

As noted earlier, the grain size of the P/M material is roughly an order of magnitude smaller than that of the I/M material. It is known that grain size is not a predominant metallurgical feature controlling strength or fracture toughness in 7XXX aluminum alloys. Plane strain (K_{IC}) toughness is even less dependent on grain size than plane stress testing (References 396, 397). These facts are well supported in the present work. Another obvious fact in these comparisons is that the size of the second phase constituent particles (much larger in the I/M material) does not affect strength or toughness. These facts have been observed by others (Reference 398).

d. Fatigue

(1) Stress Concentrations

The Neuber (K_N) relationship referred to earlier, is based on grain size, and would predict a higher sensitivity for a fine-grained material such as a P/M material. Considering the available data (References 399, 400) and the data generated in the present work (see Figure 36 and Tables C-1 and C-2), which indicate less and not more notch sensitivity for P/M materials, such a prediction is clearly inaccurate and so the Neuber relation will not be further considered. Estimates of fatigue strengths based on these data would not be as conservative as the majority of published values (References 401-408). However, other investigators have tested both of the materials evaluated in the present work, under nearly identical conditions and proposed similar estimates of notched fatigue strengths (Reference 409).

Unlike the case for steels, K_f cannot be determined analytically for aluminum alloys as no straightforward relationship between notch geometry and any other material property is known to exist. Hence, both smooth and notched fatigue tests on aluminum alloys must be conducted in order to empirically determine K_f (References 410, 411). The value in calculating Q is in knowing how sensitive a given material is to scratches, dents, pores, and inclusions. Although only notched fatigue testing was performed in the present work, others have reported both smooth and notched fatigue data for both 7075 I/M and CT-91 P/M Al alloys tested under very similar conditions. Those data suggest a nearly equal notch sensitivity for the two materials of $Q \sim 6$ (References 412, 413), which results in an effective fatigue notch concentration factor (K_f) of approximately 2 for a $K_t \sim 3$ as calculated from Equation 2. All that is suggested here is that if the smooth fatigue strengths (σ_N 's) at 10^7 cycles of the two materials tested in the present work had been evaluated, they should have been approximately twice those obtained from the notched testing. Perhaps the most important conclusion to draw from these considerations is that high strength Al alloys are fairly notch-sensitive and hence, might best be evaluated in notched conditions (References 414, 415, 416). In fact, a much sharper notch would no doubt

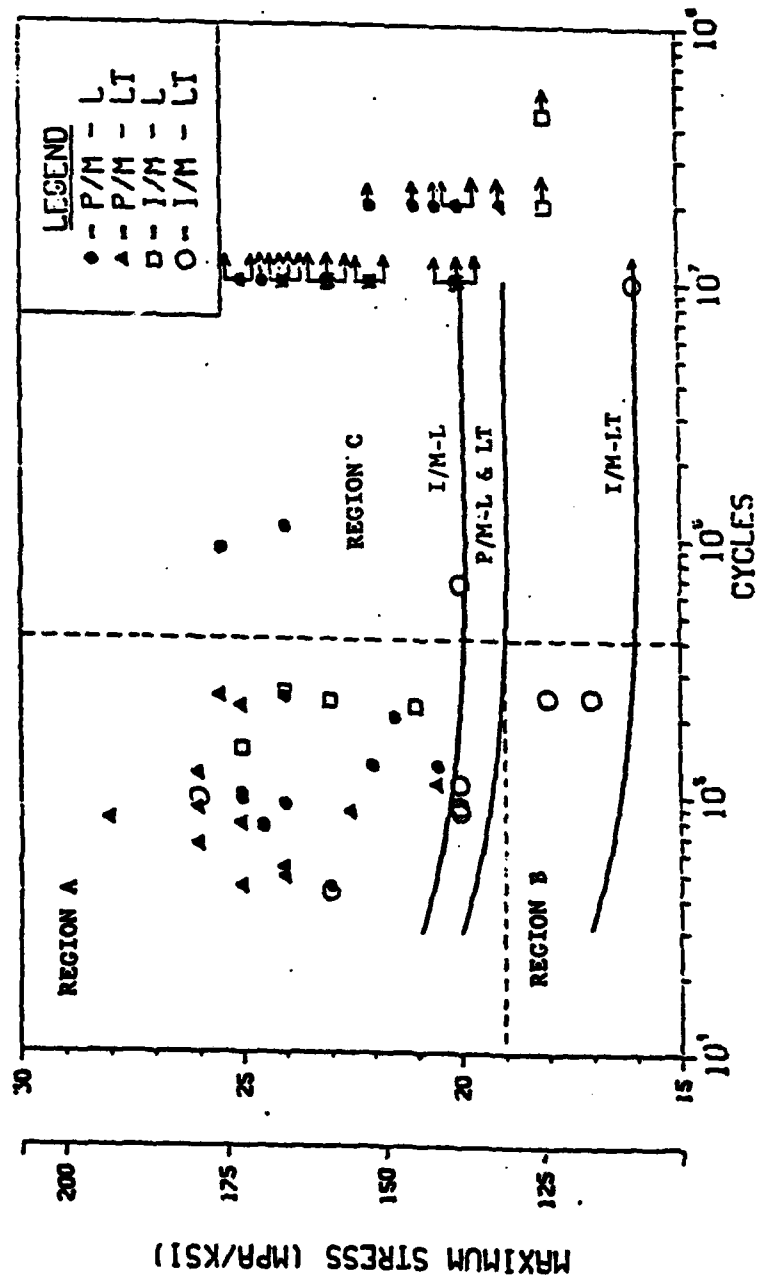


Figure 36. Region A Represents Initiation at Electropolishing Pits, Small Constituents, or Oxide Particles. Region B Represents Initiation at Large Constituents. Region C Represents Initiation at Scratches. Curves Drawn are Intended Merely to Suggest a General Trend for Comparison. Arrows Represent Runouts (no failure).

have resulted in a higher K_f ; that is, even lower fatigue strengths as obtained for these materials (References 417-419).

Another reason for the comparatively higher fatigue strength apparent in the data generated in the present work as depicted in Figure 36 and Tables C-1 and C-2, could be the consequence of the so-called "size effect". Unlike smooth bars, notched bars display a significant size effect, especially when axially loaded as was the case in the present work (Reference 420). A decreasing volume fraction of defects with decreasing cross-sectional area constitutes a definition of the "size effect". Another interpretation of its statement could be that a reduced notch perimeter reduces the probability of encountering defects and hence, reduces the probability of failure (Reference 421). Other work has shown that the size effect is greater for notched than for smooth specimens, but moreover, that notches tend to reduce differences in fatigue behavior between different 7XXX Al alloys (Reference 422). This last consideration obviously outweighs the negative aspects of a size effect enhancement from notched testing. The generation of design data was neither the object nor within the scope of the present work and accordingly, the non-conservative values obtained are of little consequence in themselves. More importantly, comparison of the two materials was obviously expedited by the use of notched specimens.

If one were to pursue the application of the data developed in the present work, one might consider the use of a failure theory first proposed by Goodman, which today bears his name. This theory is intended to enable conservative prediction of fatigue failure from data not generated under the most severe loading condition; that is, data not generated with a zero mean stress. This most severe condition is sometimes called "completely reversed" loading, and is designated by what is known as an "R-ratio" of negative unity. This simply means that the ratio of the minimum to the maximum stress is equal to -1. Under such a condition, zero is the average or "mean" stress. Obviously then, the magnitude of the maximum positive or "tensile" stress is equal to that of the maximum negative or "compressive" stress. Now taking the value for Q and whence for K_f obtained previously, and noting that ductility

of both materials as measured by percentage elongation (see Table 13) exceeds three percent; the Goodman theory defines these materials to be "ductile" and so the approach to selection of fatigue design stresses requires that K_f be applied only to the average change in the value of stress which is known as "alternating" stress (σ_a), and not to the maximum tensile stress endured. This value is then simply added to the average or "mean" stress (σ_m) and their sum is considered to be the "effective" stress for the component as indicated here:

$$\sigma_{\text{eff}} = \frac{\sigma_{\text{max}} + \sigma_{\text{min}}}{2} + K_f \frac{(\sigma_{\text{max}} - \sigma_{\text{min}})}{2} \quad (6)$$

Recall that the fatigue strength (σ_N) of a smooth specimen can be approximated by multiplying the value obtained for a notched specimen by K_f . That value, as well as the ultimate tensile strength ($\sigma_{\text{u.t.s.}}$) and yield strength ($\sigma_{\text{y.s.}}$) are also needed. In HCF, with a positive value of mean stress; that is, a positive "R-ratio" (as was employed in the present work), the Goodman theory offers the following criterion for failure in fatigue (Reference 422):

$$0 \leq \sigma_{\text{mean}} \leq \frac{\sigma_{\text{y.s.}} - \sigma_N}{1 - \frac{\sigma_N}{\sigma_{\text{u.t.s.}}}} \quad (7)$$

and failure is predicted to occur for:

$$\sigma_{\text{eff}} - \left(1 - \frac{\sigma_N}{\sigma_{\text{u.t.s.}}}\right) \sigma_{\text{mean}} \geq \sigma_N \quad (8)$$

Then selecting as an example, the longitudinal orientation of the 7075-T6 material tested with an R-ratio of .1 at a maximum stress of 210 MPa (30Ksi), and plugging in the values for $\sigma_{\text{u.t.s.}}$, $\sigma_{\text{y.s.}}$ from Table 13, the other appropriate values for K_f , σ_{mean} , σ_{alt} , and σ_N one calculates:

$$114 + 2(93) - \left(1 - \frac{276}{572}\right) 114 < 276 \text{ MPa}$$

Therefore, failure is not predicted to occur. Considering the data obtained, this approach certainly does not result in a conservative prediction. The reason for this, is not the inadequacy of the Goodman approach, but rather the failure of K_f to account for the effect of defects present. As noted earlier, an accurate value for K_f cannot be determined without the testing of smooth specimens and so no further use will be made of the Goodman theory.

A particularly intriguing observation made in some investigations, that the transition from slip band initiation (at higher stresses) to grain boundary/pore/particle initiation (at lower stresses) depended on Fe and Si content in 2XXX Al alloys merits further discussion (References 424, 425). It seems reasonable that the local threshold stress for initiation (by whatever mechanism) to begin at particles in the matrix or in grain boundaries, would be similar for any similar constituent level aluminum alloys. This might be expected because the fracture and/or matrix bond strengths; for example of any given incoherent, second phase constituent particle of $(\text{CuAl}_2)_2\text{FeAl}_3$ or Mg_2Si , probably do not change significantly from one solid solution aluminum alloy matrix chemistry to another (Reference 426). If the transition in the referenced (References 427, 428) experiments occurred at 140MPa nominal stress and a theoretical stress concentration factor (K_t) equal to 4.5 with a resultant effective fatigue stress concentration factor of about 2.6 from a notch sensitivity (Q) equal to .6 (typical of all precipitation-strengthened aluminum alloys), then the effective stress for the transition was approximately 140MPa x 2.6 or ~358MPa. Noting that fatigue strengths for 7XXX and 2XXX aluminum alloys do not greatly differ; and that fatigue life in HCF is primarily initiation; it would seem reasonable to expect similar fatigue crack initiation mechanism transitions for 7XXX and 2XXX Al alloys. Continuing in this fashion with a theoretical stress concentration factor (K_f) of $2.6 \times .6 \sim 1.6$ should result in a similar transition from pore/particle FCI to slip band FCI at a nominal stress of 358 MPa/1.6 ~ 220 MPa. Therefore, no slip band initiation might be expected for any of the specimens tested in the present work since all were tested at nominal stress levels less than 195 MPa. In fact, no such slip band could be found in the course of SEM fractographic examination despite the fact that

all specimens had been electropolished to a smooth finish prior to testing. A sort of transition between large constituents and small pores/particles (see Figure 36) seemed to suggest itself in the results of the present work. The initiation of failure at pores or particles observed in the present work agrees well with the experimental results of others (References 429-439).

The gross specimen stress to initiate cracks from second phase constituent particles in monotonic tension tests of high strength aluminum alloys has been observed to range between 400 and 600 MPa for 6 to 2 μ m particle sizes respectively (Reference 440). Extrapolating this data to a 12 μ m size particle, a stress as low as 200 MPa should be sufficient to initiate a crack; and for a 20 μ m size particle, a stress of only 140 MPa might initiate a crack and so forth. These magnitudes appear quite reasonable considering the sizes of the features (5 to 15 μ m) that initiated cracks and eventually caused failure of the 20 fatigue specimens observed in the present work. The lives of these specimens did not correlate very well with the sizes of the features causing crack initiation. In the present work, fatigue crack initiation always occurred after approximately 98% of total life as determined by the load drop of the fatigue machine and always at the surface at sites on the order to 5 to 10 μ m. This is consistent with currently accepted theories of fatigue and fracture, and especially valid under very low stress (elastic) and sub-creep (room temperature) conditions (Reference 441). Recall that in HCF, it is neither the size nor population density of such particles, but rather their geometry that determines fatigue response severity. Large electropolishing pits, regardless of shape are apparently less severe than large inclusions not removed by the electropolishing action. This also is understandable since an inclusion remains to resist and focus deformation, while a void can only yield to deformation. This hypothesis is supported by recent evidence for Ni-base alloys tested in LCF for which a smaller percentage of the more numerous defect (voids) initiated a lower percentage of fatigue failures than the less numerous defect (inclusions) (Reference 442).

(2) Fatigue Strength Anisotropy

In addition to the microstructural instability phenomena which lead to decreased strength under cyclic loading, many investigators have shown that any improvements exhibited in smooth S-N (stress vs. logarithm of number of cycles to failure) fatigue may be absent in notched S-N fatigue (References 443, 444). Figures 37 and 38 show that when static strength is taken into account, the slight apparent advantage of I/M over P/M material in the longitudinal orientation is eliminated. The long transverse orientation of the I/M material remains inferior despite normalization. The improvement in notched S-N fatigue for the transverse orientation of the P/M material as compared with the transverse orientation of the I/M material, is therefore significant.

Particles in P/M material are smaller than those in I/M material and therefore, the P/M material does not suffer a corresponding decrease in fatigue strength in the transverse loading orientation. That is, the FCI resistance of the P/M material; which is determined by the notch concentrations of the features contained within the material itself, and which in turn determine total HCF life, is approximately equal for P/M material in the L and LT orientations but not for the I/M material.

It has been shown that FCP is nearly independent of all microstructural features except at very high and very low ΔK levels (References 445-447). The equivalence in fatigue life of I/M and P/M materials tested in the longitudinal orientation confirms the fact that their fatigue crack growth rates over the relevant, linear or "Paris Law" (6 to 16 MPa \sqrt{m}) range are equivalent. This is also considered the relevant range for aircraft spectrum fatigue loading (References 448-454).

Investigators have found no significant differences in FCP for L and LT orientations or for constituent volume fractions in 7XXX aluminum alloys at low and intermediate ΔK levels. The difference in toughness between L and LT orientations is responsible for the difference in FCP at high ΔK levels (References 455-457). The differences in fatigue strength between L and LT orientations in I/M material are not as easily explainable. The expectation that defects in the L orientation would be

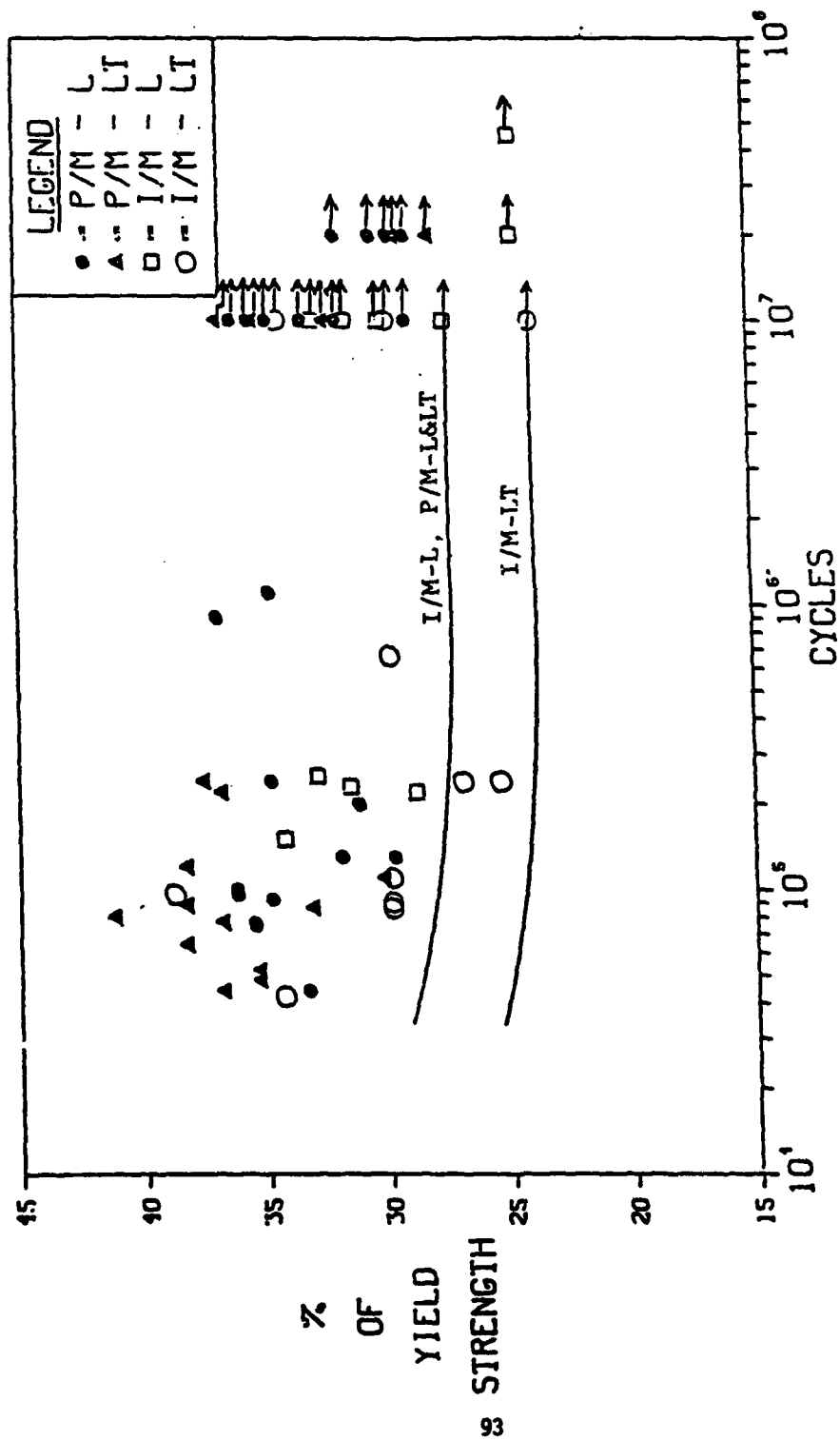


Figure 37. Data of Figure 36 Normalized to Yield Strength.

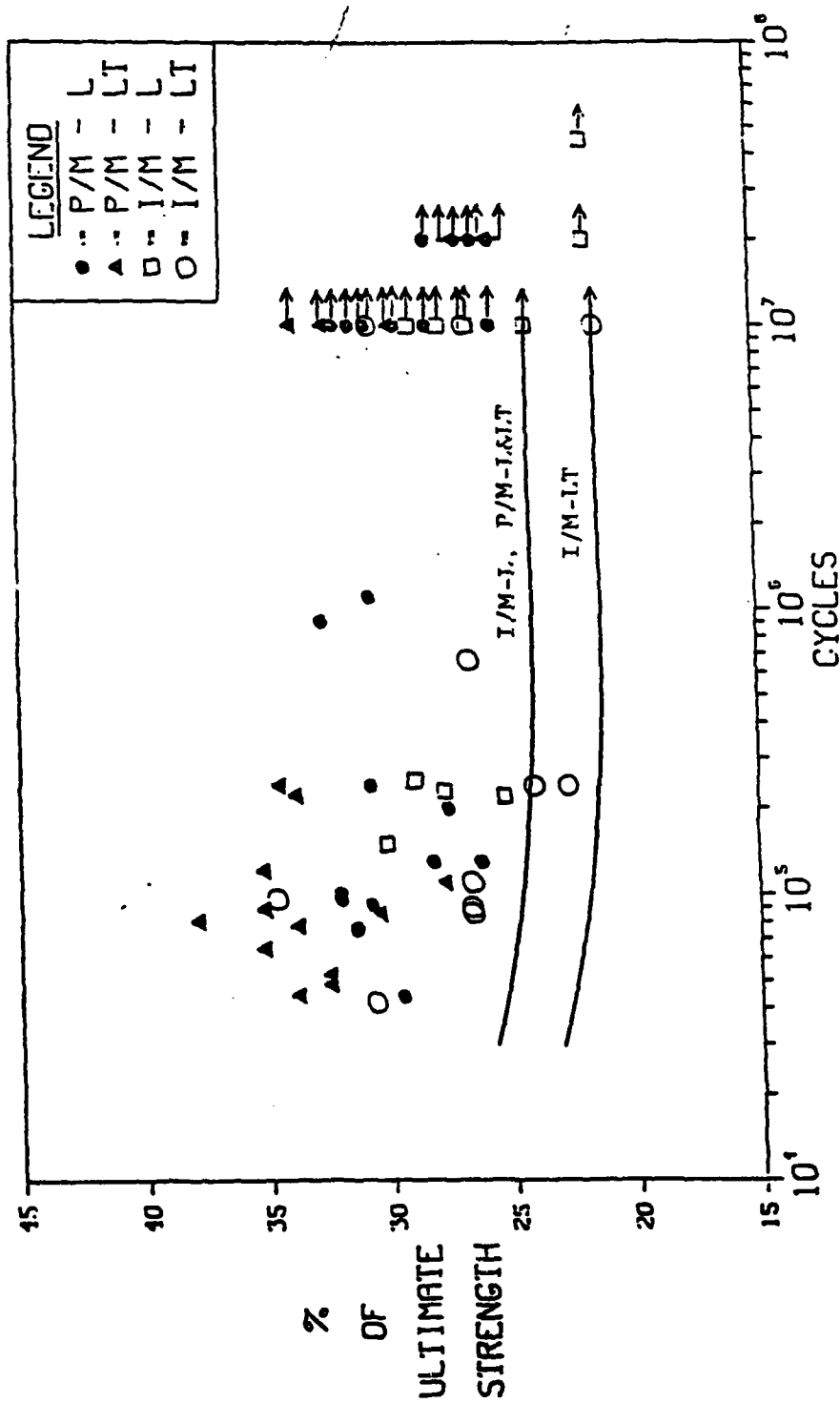


Figure 38. Data of Figure 36 Normalized to Ultimate Strength.

aligned parallel to the stress axis while defects in the LT-orientation would be either perpendicularly or randomly aligned with respect to the stress axis is strongly supported by the data of the present work. The significant inferiority of the LT I/M condition to the LT P/M condition is explainable in terms of relative defect size. SEM examinations of 20 initiation sites did in fact reveal that the size of defects in P/M material was consistently on the order to 1 to 5 μ m while the size of defects in the I/M material ranged as high as 10 μ m. FCI then and not FCP, is the more dominant factor in HCF life (Reference 458). Only this concept can explain the difference in fatigue behavior between I/M LT and P/M LT conditions. The fact that both I/M and P/M experience equivalent deterioration in toughness in the transverse orientation; yet the P/M material does not correspondingly sacrifice fatigue strength in the transverse orientation; supports the hypothesis that FCI and not FCP determines HCF behavior which is superior for the P/M material. The fact that investigators have even found negative R-ratios beneficial to fatigue crack growth behavior in 7075-T6 (Reference 459), makes the entire concept of FCP evaluation of materials suspect.

If the effect of material flow from deformation processing on the mechanical properties of the L, LT and ST orientations in I/M materials is determined by second phase constituent particle distribution and grain boundary alignment, then the ST orientation in I/M materials, whether or not it is the least flow direction (cf. e.g., rolled plate) should be and is in fact, always inferior than the L and LT orientations. For P/M materials, however, the degree of metal-to-metal bonding, as determined by the extent of oxide break-up, as well as grain boundary alignment establish the effect of flow. The inferior orientation is either LT or ST depending on which experienced the least flow.

For a material constrained to flow in one direction, as it was in the present work by means of uniaxial compression in a channel die with walls contiguous with the material being forged from the onset of deformation, the amount of flow that can occur in the LT direction is considerably reduced. In fact, the amount of flow in the ST direction was actually less than that in the LT direction. This can be understood

if one visualizes that the maximum LT flow is probably less than halfway from the center to the edge of the channel ($1/2 \times 1/2 \times 3-1/2" = 7/8"$); while the maximum ST flow is obviously from the top of the starting material to the top of the finished forging ($2 - 2/3" = 1-1/3"$) (see Figure 1). In view of these considerations, it is apparent that while the lowest property orientation of the P/M material was tested, an orientation of intermediate properties was tested for the I/M material. Therefore, the equivalent strength, ductility and toughness, and superior notched HCF performance of the P/M LT condition with respect to the I/M LT condition is significant indeed.

Work done by others has similarly shown little difference between L and LT orientation for axial, $R=.1$, LCF in air and salt fog of single axis forgings (60% reduction in height) of CT-91 Al P/M alloy (Reference 460). Compression testing done by Voss (Reference 461) on both P/M and I/M extrusions of commercial 7075 alloy chemistry indicate agreement with the findings of the present work that I/M processing results in greater anisotropy. Limited notched HCF testing of L and LT orientation CT-91 P/M extrusions had previously suggested this same result (Reference 462).

The results of the statistical analysis applied to the fatigue life data of the present work are contained in Figures C-1 through C-6.

In Figure C-2, it can be seen that the P/M slopes are not quite as steep as the I/M slopes. That is, for equal increases in stress, the probability of failure for the P/M material does not increase as rapidly as for the I/M material. The slope of the probability vs. percent of UTS curve (Figure C-3) is an indication of data scatter. The steeper the slope, the less the scatter and vice-versa. Figure C-3 indicates that the scatter is greater for transverse orientations than for longitudinal orientations. This observation is consistent with the generally more random distribution of second phase constituent particles in the transverse orientations as well as their greater potential for randomness in shape alignment with the applied stress axis. For the longitudinal orientations, particles are aligned more parallel to the tensile axis and hence, their distribution is the only factor affecting the probability

of failure. For the LT orientation, particles are randomly oriented and hence, their affect on probability of failure is dependent upon both distribution and orientation within the gage section. The stress dependence is greater for the L orientation probability of failure than for the LT orientation as evidenced by the steeper slopes for both I/M and P/M L orientation data in comparison to the slopes for the LT orientation data.

e. Fractography of Fatigue Specimens

(1) Macroscopic Features

A comparison of macroscopic fracture appearances of I/M (left) and P/M (right) notched fatigue failures is presented in Figure 39. The relatively flat, brittle topography over most of the fracture surfaces is characteristic of the sharply notched, low nominal stress, uniaxial tension-tension fatigue loading conditions experienced (References 463, 464). The difference in degree of surface relief between the I/M and P/M materials is merely a reflection of the relative coarseness of I/M grain size as was observed with tensile and Charpy specimens. The equatorial line observable only in P/M specimens for the abovementioned reason, is merely the record of test interruption automatically produced by the fatigue machine as it sensed a minute decrease in the load immediately prior to final failure. Figure 40 displays a magnified view of this area. Note the presence of small secondary cracks (parallel to the load arrest band), which are evidence of imminent fast fracture. Figure 41 focuses on the classic "thumbnail" shape of the fatigue initiation site most readily seen in the coarser grained ingot metallurgy products (Reference 465).

(2) Initiation Sites

Figure 42 is a higher magnification view of initiation sites in I/M material. The relatively small size of these initiation sites are evidence of a relatively low level of second phase constituents in the I/M materials (Reference 466) as supported by its chemical analysis (Table 8). The cleavage-like appearance of the area is the result of the very low stress intensity at which fracturing began (References 467-471). Comparing the right-hand micrographs in Figures 42 and 43 taken at

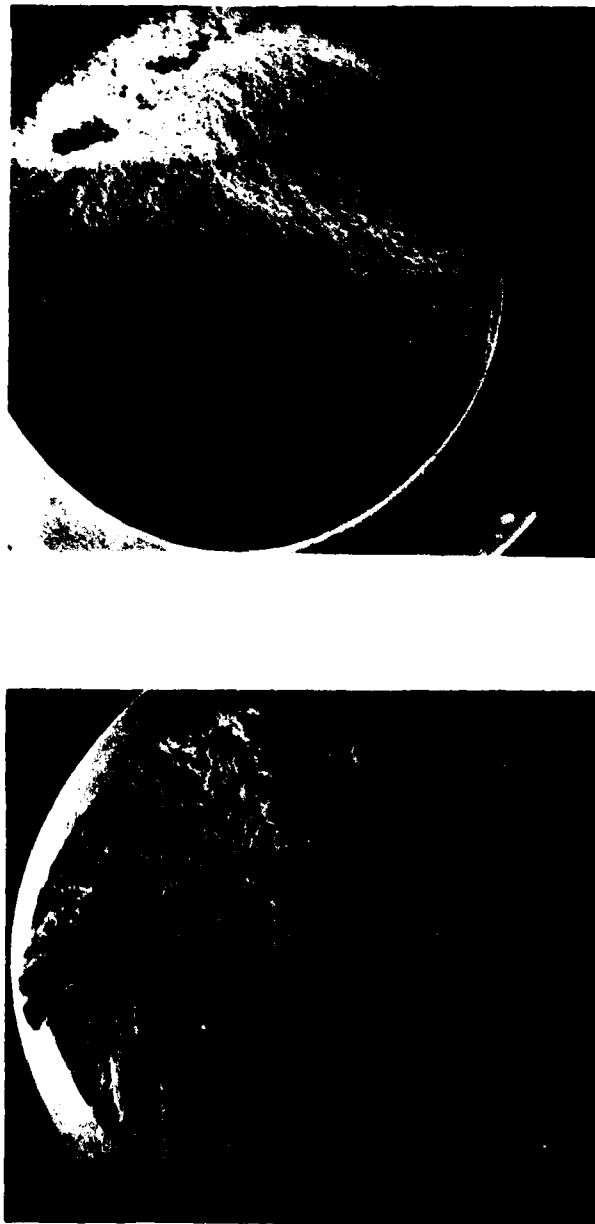


Figure 39. Typical SEM Macrofractographs of Notched Fatigue I/M (Left) and P/M (Right) Specimens. Initiation Sites of Both Specimens are at Nine O'Clock.

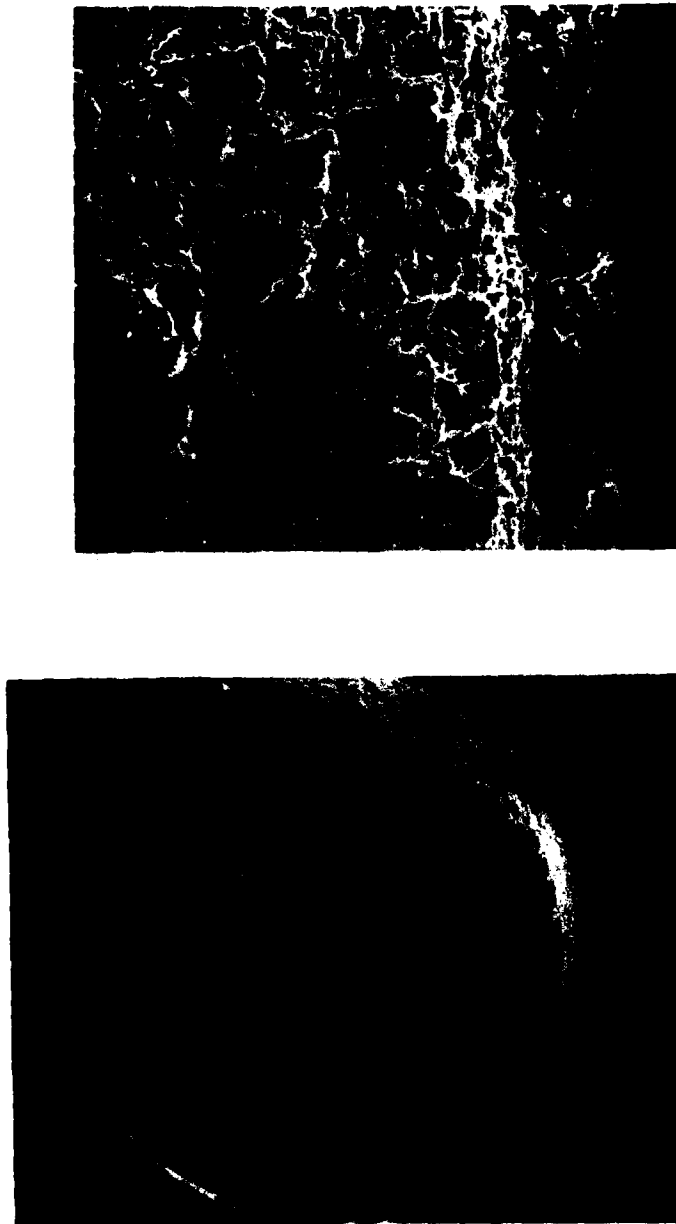


Figure 40. SEM Macrofractograph (Left) of Notched Fatigue P/M Specimen with Initiation Site at Twelve O'Clock and Diametrical Load Arrest Line Between Nine and Three O'Clock; and Close-Up (Right) of Load Arrest Line with Secondary Cracking Evident.

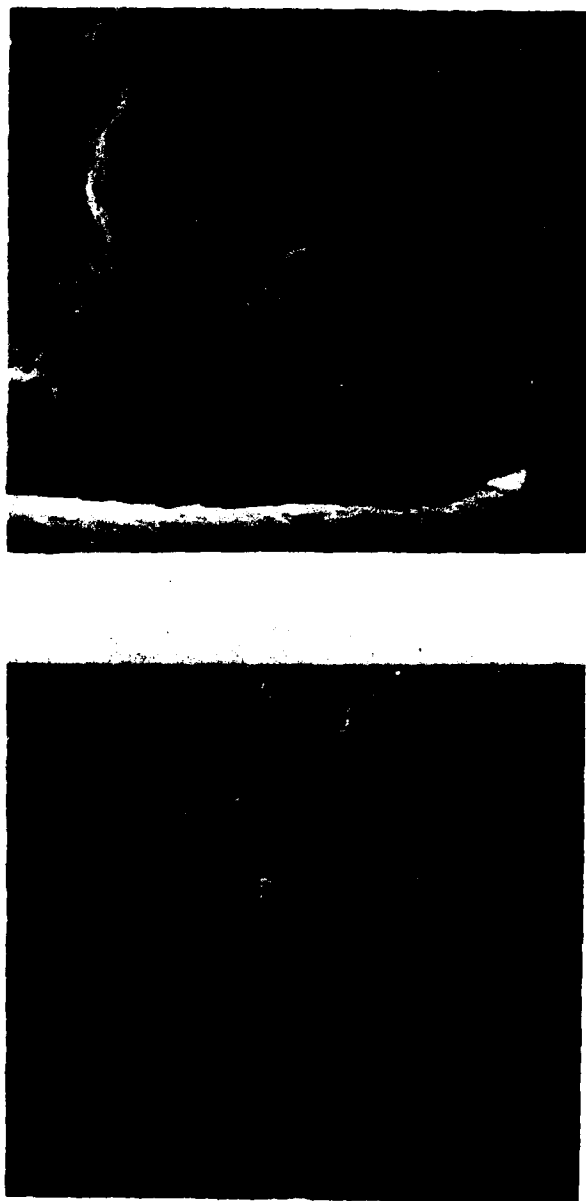


Figure 41. SEM Fractographs of Low Stress Failure I/M LT Notched Fatigue Initiation Sites at Large CuAl_2 (Left) and Mg_2Si (Right) Constituents (Six and Nine O'Clock Respectively).



Figure 42. SEM Fractographs of Intermediate Stress Failure I/M LT Notched Fatigue Initiation Site (Left) and Close-Up (Right) of Mg_2Si Constituent (Nine O'Clock) Clearly Displaying Stage I Crack Propagation Ripples Emanating from Initiation Site.



Figure 43. SEM Fractographs of Typical Intermediate Stress Failure Notched Fatigue Initiation Site (Left) and Close-Up (Right) at Electro-Polishing Pit (Nine O'Clock) in P/M Material.

the same magnification, one can see that these river-like plateaus are smaller in P/M than in I/M materials. This is no doubt due to the grain size difference. Some authors have identified these facets by X-ray diffraction as occurring on {100} planes but proposed that they are formed by "restricted-slip" and not cleavage (Reference 472). While the precise mechanism of their formation is not known, it is generally believed that they are associated with some sort of slip mechanism and represent the transition between Stage I and Stage II crack growth (References 473-478). Again, it has been proposed that decreasing size of this cleavage-like area is evidence of relatively high levels of second phase constituents in I/M material (Reference 479), but which claim is not readily proven by the fractographs obtained in the present work.

Because of incoherent phase segregation at the grain boundaries and their inherently lower bond strengths, strain localization and crack initiation are most likely to occur at large particles in grain boundaries. This should not be mistaken for intergranular failure (Reference 480). Other investigators have even tested smooth specimens of 7075-T6 I/M Al alloy material under axial HCF conditions in an aqueous NaCl environment and observed no intergranular failure (Reference 481). Crack initiation is intergranular by grain boundary shear (45° to tensile axis) but crack propagation is transgranular (90° to tensile axis) for both I/M and P/M materials (References 482-485). Crack growth rates have generally been observed to be faster when proceeding intergranularly, but a transition to intergranular failure does not occur as the result of change in stress intensity level or a decrease in grain size (References 486, 487). The fracture mode for Figures 39 through 43 is strictly transgranular despite any appearances to the contrary. The P/M material being of very fine grain size, does not appear to fracture in a strictly transgranular mode because grain boundaries are never very distant from one another hence making crack paths sometimes appear to follow them. But the fact that such appearance does not represent intergranular failure is brought out by good fatigue behavior in both L and LT orientations for the P/M material.

The relatively featureless, cleavage-like Stage I fracture area forms at very low growth rates just at or above the threshold stress intensity (ΔK_{th}). This region typically extends only a few grain diameters on {111} planes in $\langle 110 \rangle$ directions, but makes up most of the total life time in HCF loading conditions. The transition to "river-like" ripples radiating from this region and forming flat parallel, plateaus perpendicular to the tensile axis, marks the onset of Stage II fracture at some slightly higher ΔK level. Slight deviations in orientation signify grain boundary intersections. As evidenced by the debris on these fracture surfaces, the presence of inclusions does not interfere with plateau formation or advance. At still higher stress intensity levels, lines advancing perpendicular from the origin called "striations" are formed (see Figure 44). Finally, at relatively high ΔK 's, strain rate approaches monotonic loading rate for tensile or toughness testing and striations are succeeded by microvoid coalescence (dimple formation) which results in final overload failure (References 488-491). But this will be discussed more fully in the next section.

Returning to the topic of fatigue crack initiation, it is important to understand that subsurface origins are generally only observed in fatigue when large, internal inclusions or imperfections are present (Reference 492). Some interesting observations were made in examining the origins of fatigue fractures of the present work. First, both of the really low stress failures, (region B of Figure 36), were associated with very large inclusions not removed by the electropolishing (see Figures 42-45). By contrast, the three "long" life failures (region C of Figure 36) were all associated with what appears to be mechanical polishing scratches not removed by the electropolishing (see Figures 46 and 47). The remainder of relatively high stress, short life failures (region A of Figure 36) were all associated with small inclusions or small to large pits presumably created by the removal of inclusions during electropolishing (see Figures 43 and 48). Similar to the case with Ni-base alloys, no surface slip FCI was observed (Reference 493). Other fractographic studies in 7XXX Al alloys have failed to observe any FCI by slip-band formation (Reference 494). Others have shown fairly conclusively that large inclusions are by far the most prevalent

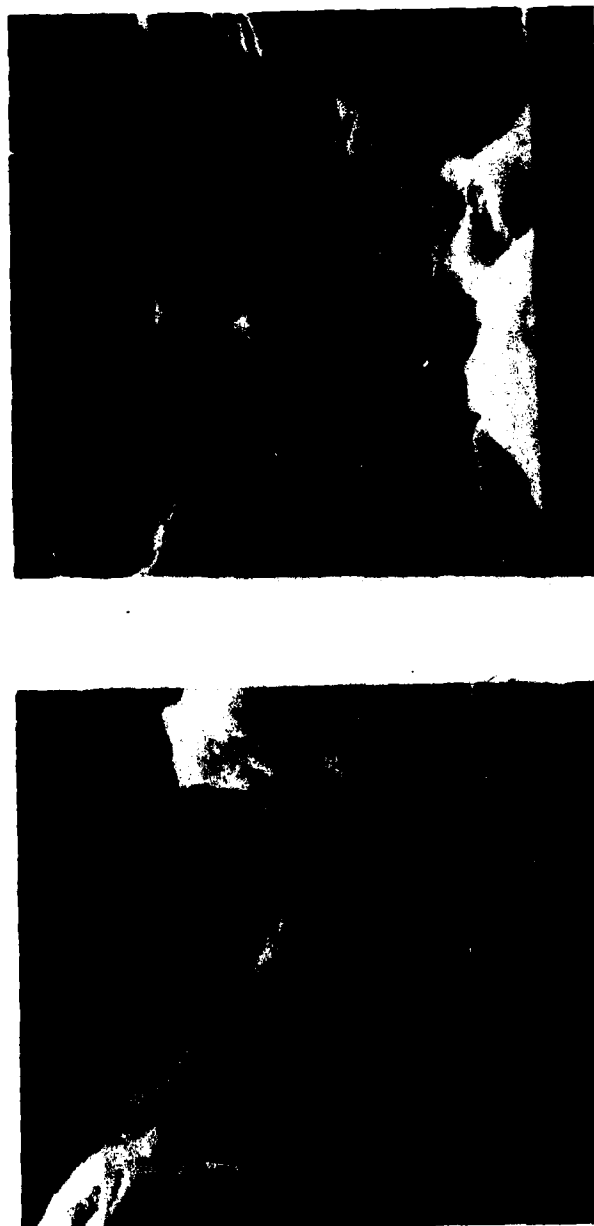


Figure 44. SEM Fractographs of Striations on P/M Fatigue Fracture Surface Advancing Away from Initiation Site (Bottom to Top) in Ever-Increasing Incremental Steps as Crack Length Increases (Left to Right). The .15 to .35 μ m (Left) and .5 μ m (Right) Striation Spacings Suggest Local Stress Intensities of 7 to 9 and 11 to 13 MPa \sqrt{m} respectively. Ridges between Striae Probably Indicate Grain Boundaries.

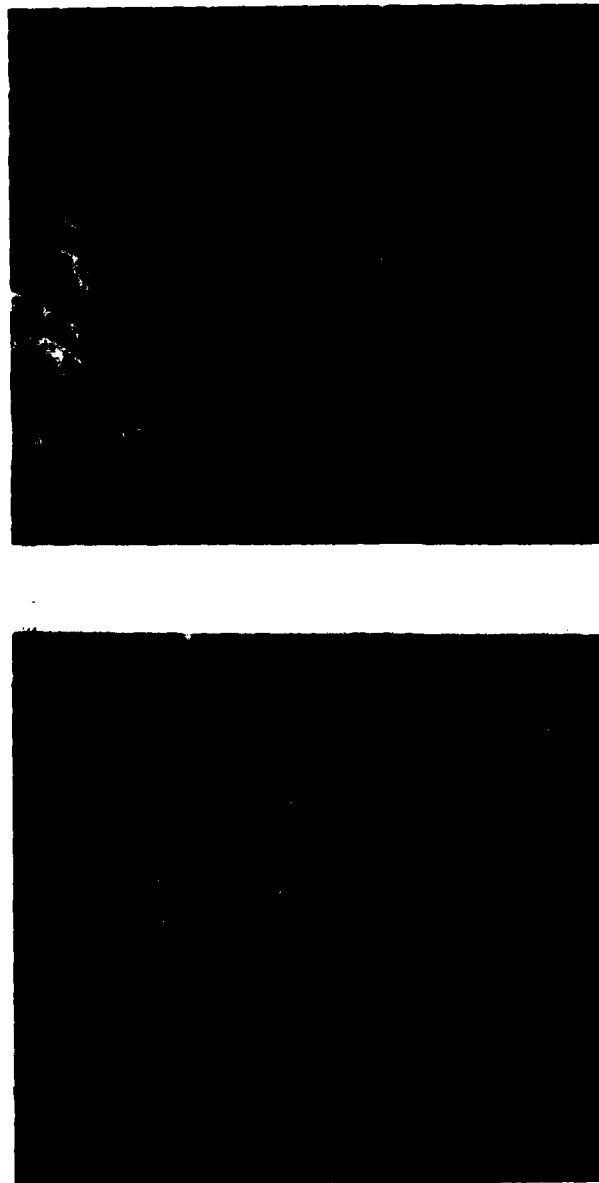


Figure 45. SEM Fractographs of Lowest Stress Failure I/M LT Notched Fatigue Initiation Site (Left) and Close-Up (Right) at Large CuAl_2 constituent Inclusion at Six O'Clock Clearly Displaying Stage I Crystalllographic Plateaus of Crack Advance.

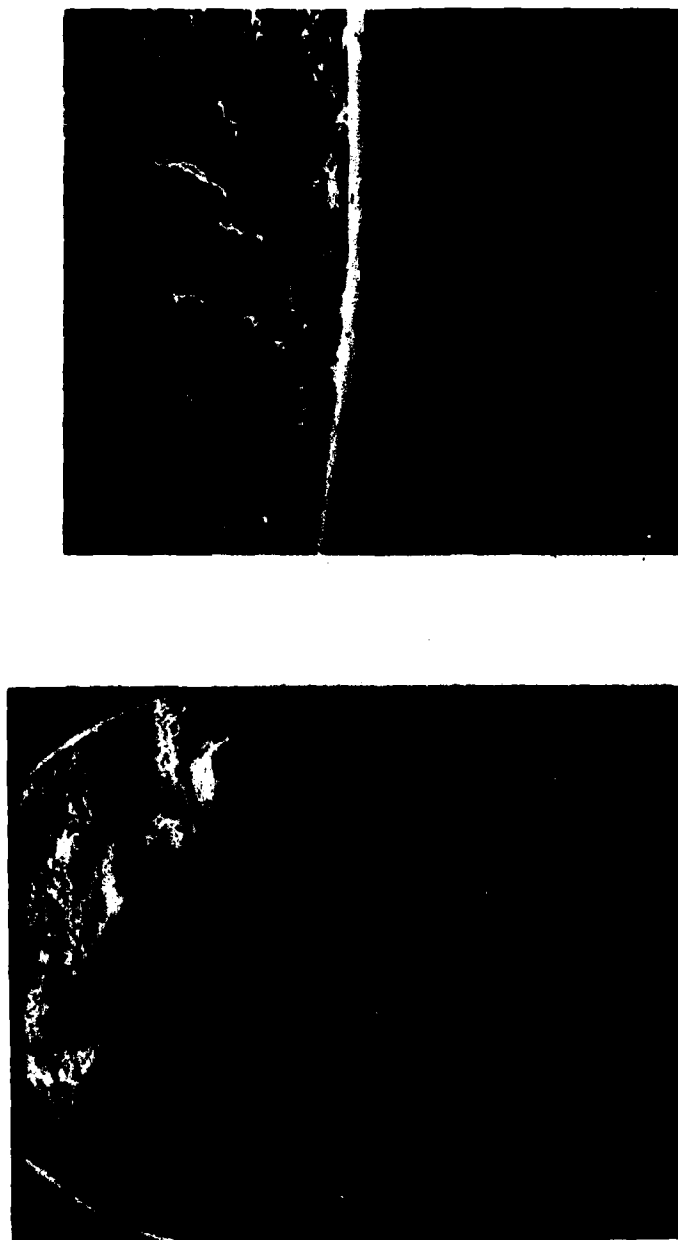


Figure 46. SEM Macrofractograph (Left) of Typical Long-Life Notched Fatigue Specimen and Close-Up (Right) of Polishing Scratch Initiation Site at Six O'Clock.



Figure 47. SEM Fractographs of Typical Long-Life Failure Notched Fatigue Initiation Site (Left) and Close-Up (Right) at Carbide Polishing Scratch (Six O'Clock).



Figure 48. SEM Fractographs of Typical Intermediate Stress Failure Notched Fatigue Initiation Site (Left) and Close-Up (Right) at Electro-Polishing Pit (Twelve O'Clock).

sites for FCI (References 495, 496). Mg_2Al_3 , $MgZn_2$ and $CuMgAl_2$ are anodic with respect to aluminum and hence, likely to be leached out, e.g., during electropolishing; Mg_2Si , $CuAl_2$, $FeAl_3$ and Si on the other hand, are cathodic with respect to Al and hence, are likely to serve as sites for peripheral attack of the surrounding matrix. If anything, they might fall out during electropolishing depending upon their shape. Of course, pits can develop randomly within the grains themselves (Reference 497). But the importance of these considerations is that the cathodic constituents could be expected to serve as initiation sites in electropolished specimens whereas only the pits from leached out anodic constituents should be expected to serve as initiation sites. This, in fact, is precisely what was observed (see Figures 41, 42, 43, 45, 48 and 49). Moreover, the severity of their effects should depend upon their characteristic sizes and shapes. Unfortunately, insufficient numbers of such constituents were observed to fully investigate this premise. Other investigators have also observed the absence of the anodic constituent phases in aluminum alloys following electropolishing (Reference 498). One investigator has observed only Mg_2Si as an initiation site inclusion in 7075 I/M Al alloy (Reference 499). In the present work, both $CuAl_2$ and Mg_2Si (Figures 41, 42, 45 and 49) phases were observed to initiate failure. In agreement with the present work, it has been observed that for electropolished specimens of 7XXX aluminum alloys, pits are the most often observed initiation sites (see Figure 48) (Reference 500). The deleterious effect of coarse second phase particles on fatigue behavior has long been recognized and made the subject of numerous and extensive researches. The results of these have been unanimous in suggesting that such inclusions provide preferential sites for FCI (Reference 501). In P/M Al alloys, the sizes of inclusions are inherently reduced and their distribution uniformly homogeneous. Improved behavior should be the result. However, recent investigations of Fe, Ti and Ni alloy P/M products indicate significant reductions in fatigue life from equivalent wrought (I/M) alloys. The diminished fatigue behavior has been attributed to contamination of powders with extraneous particles, or voids resulting from insufficient compaction (References 502-504). The Air Force has initiated an effort to discern the potential deleterious effects of similar contamination in Al alloy P/M products (Reference 505). The results of the investigation being

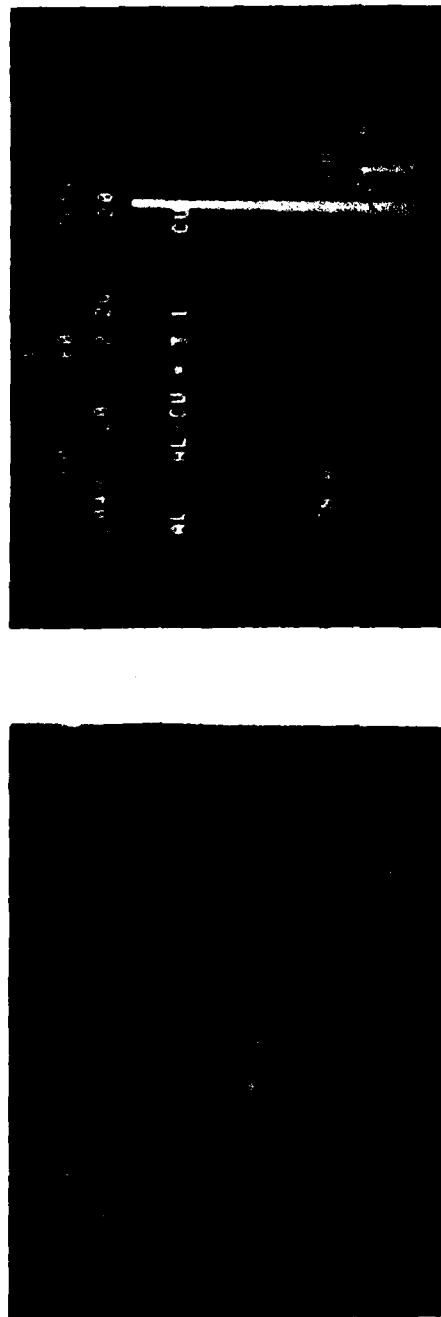


Figure 49. Photographs of EDAX Displays of Qualitative Chemical Analyses of Mg_2Si (Left) and $CuAl_2$ (Right) Initiation Sites of Figure 41.

reported here, though inconclusive, suggest that a similar degradation in mechanical behavior of Al P/M products due to extraneous particles does not, in fact, occur. Of course, a systematic investigation of the effects of defects (as will be performed in the referenced Air Force contract) should better establish any such effects.

(3) Striations

It has been shown that in FCC metals, in accordance with the theoretical predictions, slip can accumulate as transgranular crack front arrest lines called "striations" in the close-packed crystallographic planes $\{111\}$ and directions $\langle 110 \rangle$ (Reference 506). But it is also important to note that cyclic deformation need not accumulate in the form of striations and that any of the other possible deformation mechanisms for a given material loaded in fatigue may be observed. For many materials, striations are almost never found except under certain special loading conditions or in certain crystallographic orientations (Reference 507). Figure 50 illustrates the low magnification appearance of a Stage II fatigue region containing striations. The crack growth direction is left to right in the left-hand micrograph of Figure 50 and bottom to top in the right-hand micrograph. Note that striations are more or less perpendicular to crack advance direction. Striation advance itself is noncrystallographic and nonintersecting and has even been observed in amorphous materials (References 508-510). Striations are not observed at all for materials fatigued under vacuum or inert gas which suggests that some environmental effect is responsible for their appearance. Striations are eventually obliterated with exposure to air and so fracture surfaces which are intended to be examined must be stored in evacuated desiccators until examination.

Under corrosive environmental conditions, embrittling effects cause striations to appear distorted and broken. The striations appearing in Figures 51 and 52 were obviously produced by a ductile mechanism. Note also that crack growth rates may become a factor of 3X faster in such environments and so striation spacings tend to be larger for a given applied load (References 511-517). Local tear ridges and changes in the direction and spacing of striations, as seen in Figures 51 and 52, are

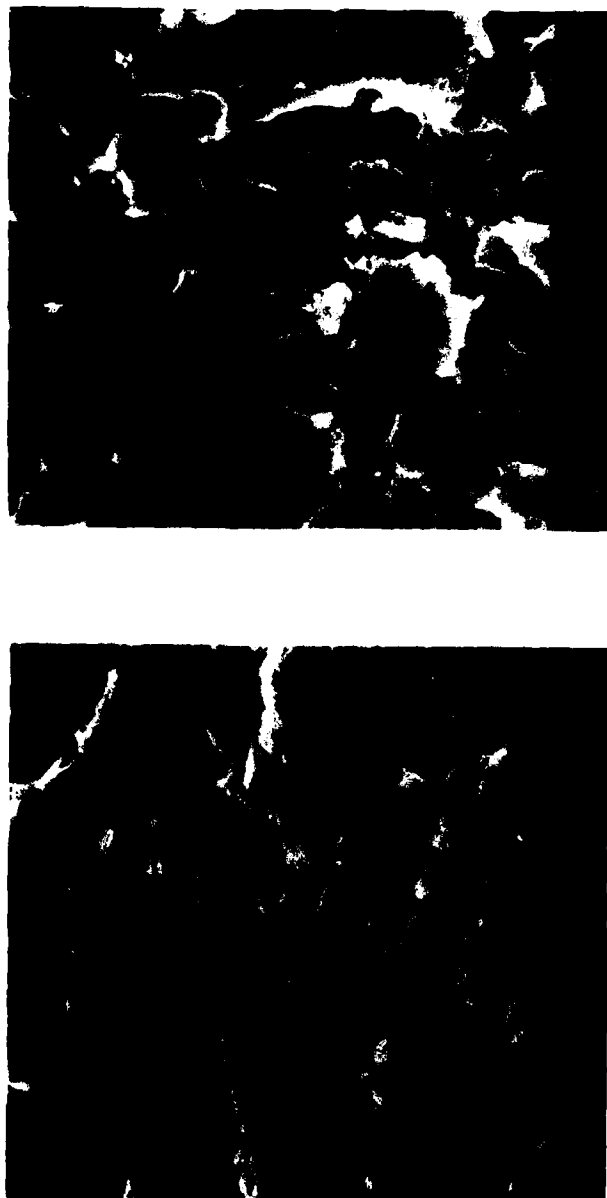


Figure 50. Low Magnification SEM Fractographs of Areas Containing Striations on Fatigue Fracture Surfaces. Crack Advance Direction is from Left to Right (Left) and Bottom to Top (Right).

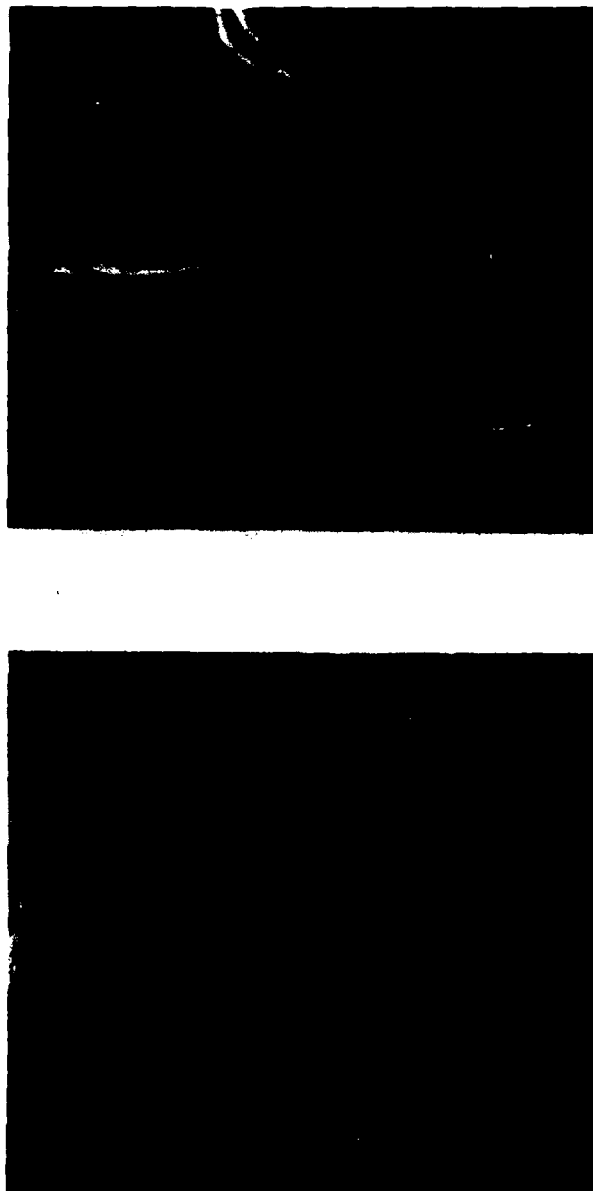


Figure 51. SEM Fractographs of Typical Stage II Fatigue Crack Propagation. Ductile Transgranular Striations in I/M Specimens; Advancing Left to Right (Left) and Bottom to Top (Right) Away from Their Respective Initiation Sites at Nine O'Clock (Left) and Six O'Clock (Right).

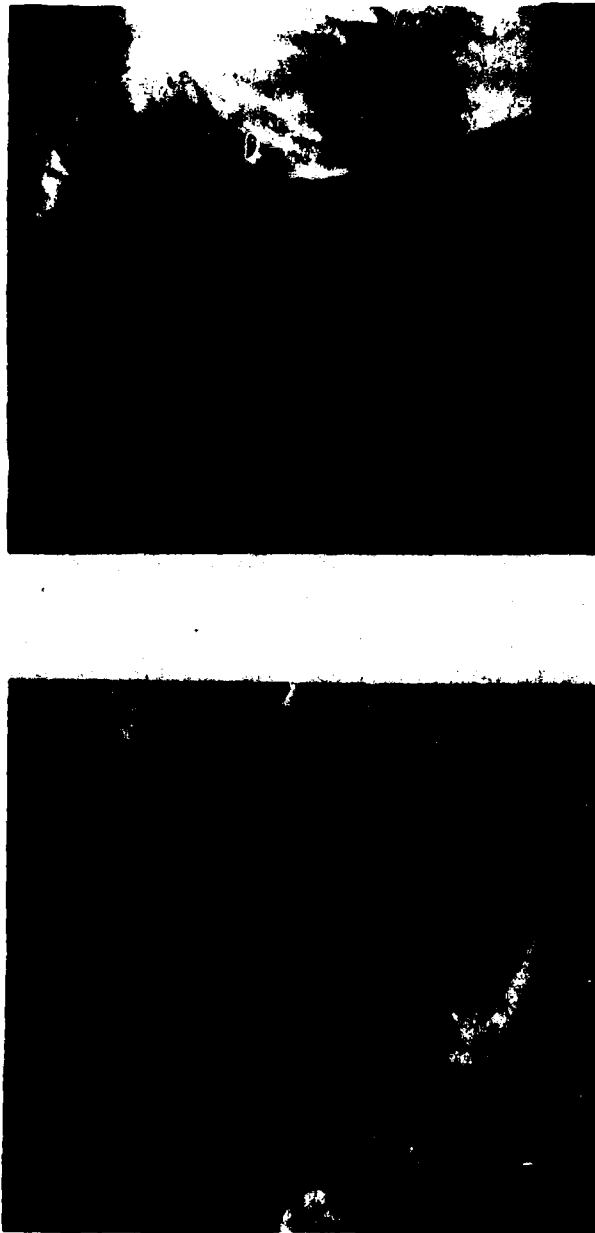


Figure 52. SEM Fractographs of Striations on P/M Fatigue Fracture Surface Advancing Away from Initiation Sites (Bottom to Top) Indicating Little or no Effect from Particles on their Progress.

are the result of motion across differently situated crystallographic grain orientations with respect to the predominant noncrystallographic crack path (Reference 518). This sort of speculation can be and has been fully verified (but not without great experimental difficulty) with the use of SEM electron channeling contrast techniques (Reference 519) or by means of TEM of thin foils taken from the fracture surface (Reference 520). Striation spacing does not change upon traversing a particle (see Figures 51 and 52). Neither Cr nor Co dispersoids in I/M and P/M materials respectively seem to have any significant interaction with the striation crack advance mechanism. Others have agreed with this conclusion in the case of the I/M material at least, (Reference 521). The small spherical particles sometimes visible on striae of the P/M fatigue fracture surfaces (Figures 44, 50 and 52) are approximately $1/4\mu\text{m}$ and are very likely Co_2Al_9 . Unfortunately, EDAX analysis could not sufficiently enhance the Co signal to determine this with certainty. Since these particles seem neither to be always present nor affect the striation path, they probably do not affect crack advance. The reason EDAX analysis cannot determine chemistry of submicron particles is that electron beam penetration and divergence happen to be on the order of one micron. At least $3/4$ ths of the detected signal will actually be from the underlying matrix material. If the striations containing the particle of interest could be preserved in sectioning and thinned from one side to a thin foil and examined in a scanning transmission electron microscope (STEM), beam penetration and divergence limitations could be largely eliminated (References 522, 523). Alternately, Auger electrons, by nature weaker and more superficial, could possibly detect the presence of Co in situ. Resolution at sufficient magnifications to find the particles becomes the limiting factors in AES. If all the Co is tied up with Al in the form Co_2Al_9 (and this is a very reasonable assumption considering all of the possible compounds that might form), then, .35 wt% Co in the CT-91 P/M alloy should combine with .9 wt% Al. Then, this .9 wt% represents roughly 1 vol% of Co_2Al_9 in the 89 wt% Al alloy CT-91. Such a conclusion has been reached by others (Reference 524). Therefore, given that there is no particular reason not to expect homogeneous distribution of the Co_2Al_9 dispersoid particles by the very nature of the P/M process, 1% of the area of any metallographic

or fractographic surface could be expected to contain Co_2Al_9 dispersoids. Considering SEM Figures 44 (right), 52 (left) and 53 all at 5000x magnification and showing an area roughly 300 square microns, the dozen odd spherical particles visible and covering an area of approximately three square microns support the above conclusions quite well. Therefore, the occurrence of Co_2Al_9 spherical particles with the frequency of 1% does not suggest that these particles are concentrated or in any way account for or contribute to the presence of fatigue fracture on these surfaces.

Fatigue crack propagation in high SFE materials is always associated with deformation by cross-slip. Cross-slip is more extensive within grains than along grain boundaries and so crack advance is interrupted by grain boundaries. These interruptions cause short-lived decreases in growth rate. As the crack length increases, the change in stress intensity (ΔK) increases and so the striation spacing increases (Reference 525). Wavy striations, secondary cracking and the appearance of dimples are indicative of a more elevated stress state and consistent with the larger striation spacings observed (Figure 53) (Reference 526). When these features are simultaneously present, the spacing may not correlate well with macroscopic crack growth rates. Microscopic crack growth rates determined by striation spacing and total crack length measurement would most likely underestimate the macroscopic crack growth rate and stress intensity (References 527, 528).

It has been conclusively demonstrated that each striation represents a single cycle of loading. However, small magnitude cycles (low ΔK) or cycles following crack growth arrest from a large overload, may not result in striations. Estimates of crack growth rates do correlate well whenever uniform uninterrupted striations are present. At very low ΔK 's, striation spacing may overestimate bulk crack growth rate, while at very high ΔK 's when dimples are simultaneously present, striation spacing may underestimate crack growth rates. Total crack length from precise measurements of location on the surface must be known to arrive at accurate calculations of stress intensity levels (References 529-533).



Figure 53. SEM Fractographs Indicating Transition to a More Elevated Stress Intensity (Left to Right) on a P/M Fatigue Fracture Surface as Evidenced by the Onset of More Widely Spaced, Wavy (Right) Striations, Dimple Formation, and Secondary Cracking.

Only striations between .1 and 1 micron in width were observed in the SEM on specimen fatigue fracture surfaces from the present work. Others have concluded that striations are only obtained for crack growth rates between .02 and 2 $\mu\text{m}/\text{cycle}$ so that observations from the present work are well within these guidelines (Reference 534).

In general form, crack growth rate is directly proportional to stress intensity:

$$\frac{da}{dN} = \Delta K^m \quad (9)$$

where; da/dN is change in crack length (a) per cycle (N), ΔK is the stress intensity and (m) is a material constant. This equation describes only the linear portion of a log-log plot of da/dN and ΔK , and (m) becomes the slope of the line. The upper and lower ends of this straight line divert parabolically and become asymptotic to the fracture toughness (K_Q) at the upper end and to the threshold stress intensity (ΔK_{th}) at the lower end (Reference 535).

Given values from the literature for crack growth rates at known stress intensity levels for these materials, a simple proportionality can be used to approximate the local stress intensities from striation spacings measured:

$$\frac{\Delta K_{\text{known}}}{\frac{da}{dN}_{\text{known}}} \sim \frac{\Delta K_{\text{unknown}}}{\frac{da}{dN}_{\text{measured}}} \quad (10)$$

From the literature, 5 MPa $\sqrt{\text{m}}$ corresponds to a crack growth rate of only about .02 $\mu\text{m}/\text{cycle}$ which is just at the threshold of striation formation. 7 MPa $\sqrt{\text{m}}$ corresponds to about .2 $\mu\text{m}/\text{cycle}$, 10 MPa $\sqrt{\text{m}}$ to about .4 $\mu\text{m}/\text{cycle}$, 15 MPa $\sqrt{\text{m}}$ to about .5 $\mu\text{m}/\text{cycle}$, and 20 MPa $\sqrt{\text{m}}$ to about 1 $\mu\text{m}/\text{cycle}$ for both 7XXX I/M and P/M aluminum alloys (References 536-540). In Figures 44, 51, 52, 53 and 54, local ΔK levels can be similarly suggested by the striation spacings. Again, such ΔK 's might not be an accurate assessment of the prevailing stress intensities seen by the bulk specimens when these striations were produced. The width of the striae in Figure 53 (right), and Figure 54 (left), suggest that they represent the last striations formed.



Figure 54. SEM Fractographs of What are Probably the Last Striations (Left) Prior to the Transition to All-Dimple Fast Fracture (Right).

The size of the largest striation in Figure 54 (left), is sufficient to correspond to a stress intensity closely approaching the fracture toughness of the material. The simultaneous presence of dimples adds credence to this hypothesis. Figure 55 (left), is a lower magnification shot of the area from which the micrographs of Figures 53 (right) and 54 (left) were obtained. Crack growth direction was from left to right and the striation containing area terminates on the left side of the apex of the cone-shaped area. Figure 54 (right), was obtained in the area immediately to the right of this apex suggesting that striation formation has completely given way to faster crack growth by microvoid coalescence. Figure 55 (right), displays the brittle fracture in the center of the field of a large $(\text{CuAl}_2)_2\text{FeAl}_3$ constituent particle in the fast fracture portion of an I/M material fatigue fracture surface. Finally, for the sake of completeness, Figure 56 displays an area of high stress intensity containing dimples, cracked constituent particles and wide striation spacings on an I/M material fracture surface.

3. CORROSION RESISTANCE

a. Hardness

Though scarcely a direct measure of chemical activity, hardness has been employed as an indicator of the nature and extent of precipitation in aluminum alloys. As is the case with steels, empirical relationships between hardness and strength have also been made. But in the case of aluminum alloys which derive their strength from the precipitation of chemically active phases, hardness can be somewhat predictive of corrosion response as well. The values obtained in the present work and presented in Table 15 are typical for these materials and heat treatment conditions (Reference 541). The greater hardness of the T6 I/M and P/M material conditions suggest greater precipitate instability, with inferior corrosion resistance to the T7 heat treatment conditions as a consequence.

b. Electrical Conductivity

Since any soluble element addition to pure aluminum will decrease its electrical and thermal conductivities, the observed decreases following strengthening heat treatments indicate the presence of coherent zones and elements in solid solution (Reference 542). Electrical conductivity is

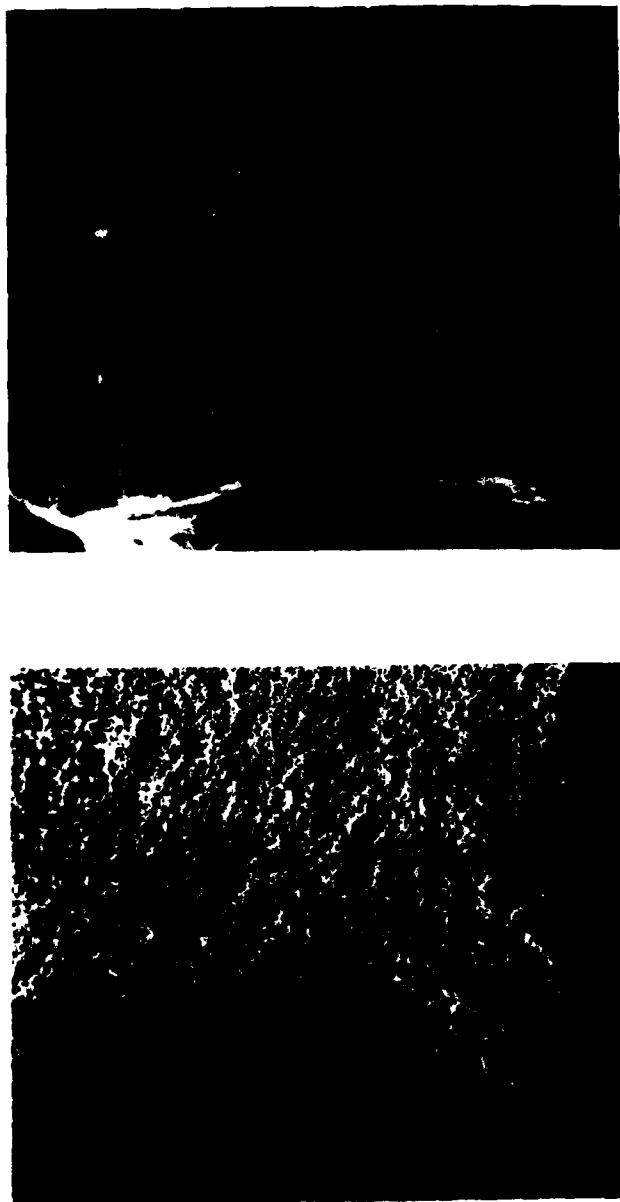


Figure 55. SEM Fractographs of the End of the Striation Containing Area (Left) and an Area Immediately to the Right of its Apex Containing a Large Fractured $(\text{CuAl}_2)_2\text{FeAl}_3$ Constituent Particle (Right).

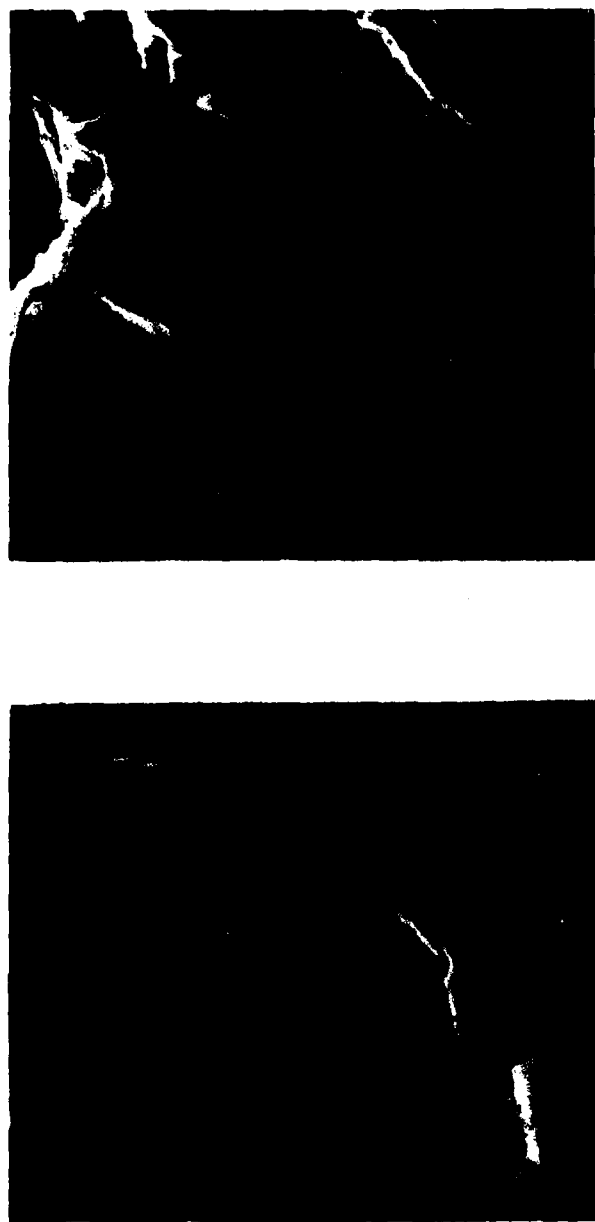


Figure 56. SEM Fractographs Indicating Transition to Higher Stress Intensity (Left to Right) on an I/M Fatigue Fracture Surface as Evidenced by the Onset of More Widely Spaced, Wavy (Right) Striations, Dimple Formation, and Secondary Cracking.

the most often used method of determining degree of aging of an alloy. As overaging results in additional precipitation removing soluble elements from solution and growth of G. P. zones to incoherency, conductivity is observed to increase (Reference 543).

Furthermore, it follows that an overaged heat treatment (T7) condition, which is of course known to ripen (increase size and spacing) such precipitates, should be superior to the fully "hard" (T6) condition. Some investigators have even suggested that minimum electrical conductivity values could be used as guidelines for determination of susceptibility to stress corrosion cracking. It is admitted, however, that small deviations in chemistry are seen to have large effects on electrical conductivity (Reference 544).

In any event, the values obtained in the present work and presented in Table 16, are typical (Reference 545) and suggest that the P/M material in either T6 or T7 condition should be less susceptible to corrosion than the I/M material in either T6 or T7 condition.

TABLE 15
ROCKWELL B* HARDNESS DATA

<u>Material</u>	<u>Hardness</u>
I/M-T6	89
I/M-T73	85
P/M-T6	88
P/M-T73	84

(average of five tests)

* ASTM E18-74

TABLE 16
CONDUCTIVITY* DATA

<u>Material</u>	<u>% IACS</u>
I/M-T6	32
I/M-T73	37
P/M-T6	39
P/M-T73	42

* % of the International Annealed Copper Standard, ASTM B342-63.

c. Exfoliation Corrosion

Another simple but more-to-the-point method of corrosion resistance measurement utilized in the present work, was testing for susceptibility to a form of intergranular corrosion commonly known as "exfoliation". "Pitting-type" corrosion is usually not affected by microstructural features. An exception is observed for material susceptible to pitting that first penetrates and then turns parallel to the grain flow direction. This process, termed "end-grain" attack is merely a more severe form of pitting and results in blisters (Reference 546). Nearly all wrought aluminum products exhibit the classic thin "pancake" grain shape; that is, considerably extended in one dimension (termed longitudinal or L), somewhat less extended or equiaxed in a second dimension (termed long transverse or LT), and rather contracted in the third dimension (termed short transverse or ST). This was clearly observed in Figure 12. It has been fully documented that stress corrosion susceptibility is more important than so-called "end-grain" or "pit-blistering" susceptibility. Nevertheless, specimens were machined diagonally on one face in order to expose a greater number of end grains. However, no difference was observed between either face (see Figure 57). It is important to note that the pancake-shaped grains in combination with grain boundary constituents, not only restrict susceptibility to one direction in the product (the ST direction) but actually improve overall stress corrosion cracking resistance. Artificially low constituent, equiaxed grain, laboratory alloys generally do not perform as well as the commercial products described (Reference 547).

The upper photograph of Figure 58 documents the differences in apparent initial aggressiveness of attack from the ASTM Standard exfoliation corrosion of "EXCO" solution on six different material and heat treatment conditions (see Tables 8 and 12). Other investigators have measured gas evolution during EXCO testing of these materials and found it to be greater for the cobalt-containing P/M alloy material suggesting that the presence of Co might be detrimental (Reference 548).

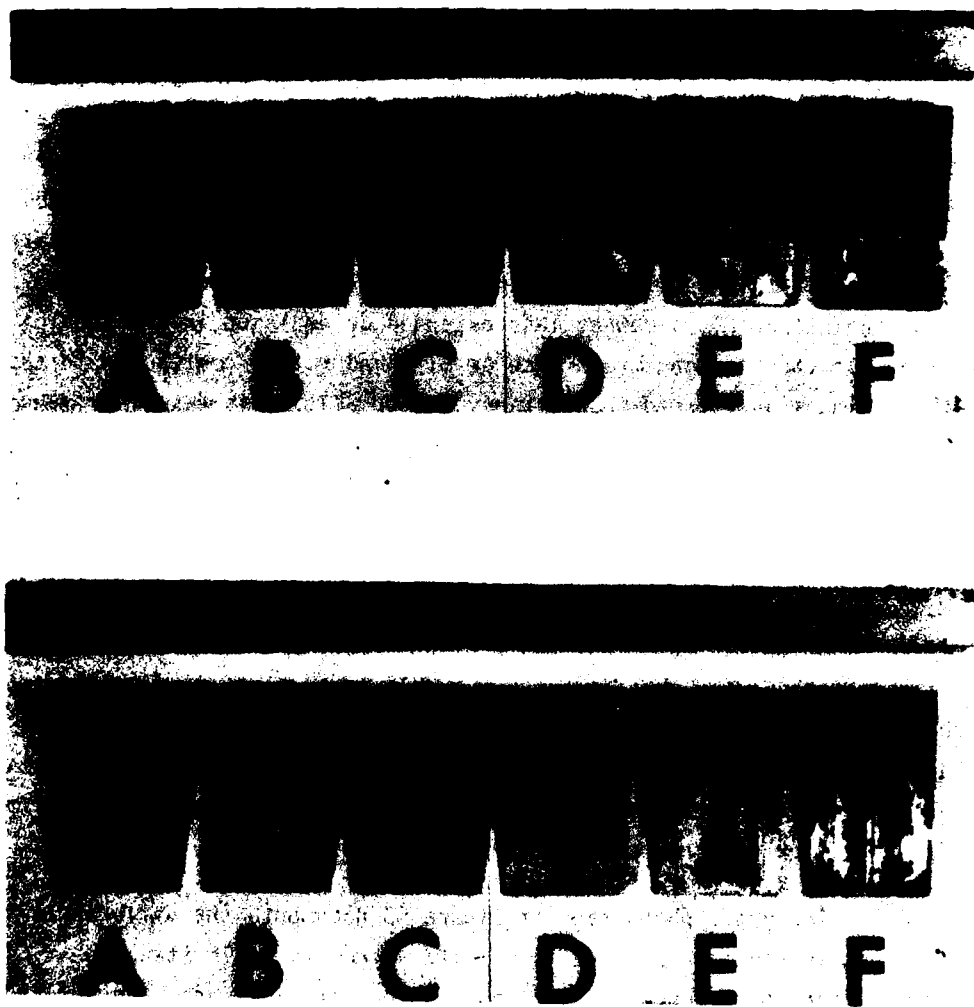


Figure 57. Photographs of Flat-Milled (Upper) and Diagonally-Milled (Lower) Sides of EXCO Coupons After Completion of Testing. The Left to Right (A to F) Order of Specimens is the same as that for the Beakers in Figure 58.



Figure 58. Photographs of EXCO Test Beakers Containing (Left to Right) CT-91-T7 (.4% Co), CT-91-T6 (0% Co), CT-91-T6 (.4% Co), 7075-T6, 7075-T73, CT-91-T7 (0% Co) Coupons at One Hour (Upper Set) and Six Hours (Lower Set) After Immersion in the Solution.

Notwithstanding such observations, one might suppose from these photographs that the 7075-T6 I/M material (4th beaker from the left) was not being any more severely attacked than the three CT-91 P/M materials in the beakers to its left. Closer examination of the beakers and test coupons displayed in Figures 57 and 58 indicated that for the P/M materials, corrosion was more uniform and deposited more material to the bottom of the beakers. In contrast, the I/M materials developed larger scale features but deposited less material to the bottom of the beakers. Figure 57 merely demonstrates the beneficial effects of residual stresses for resisting corrosive attack. Several of the shiny, unattacked patches still contain machining marks.

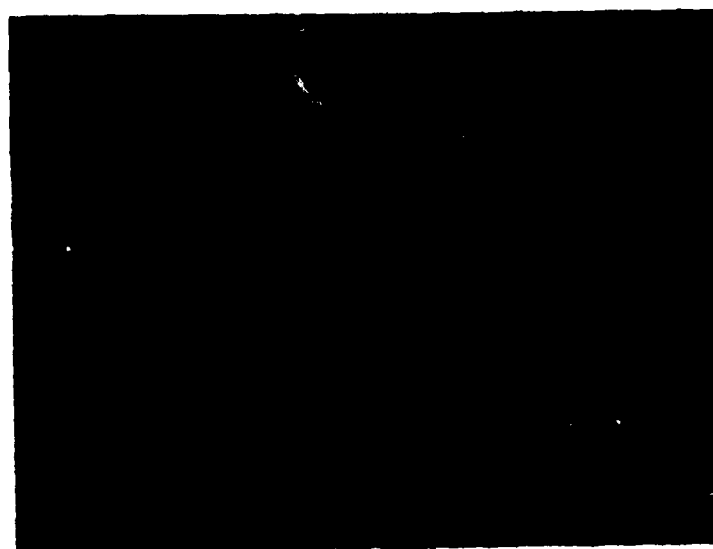
But proper assessment of the severity and extent of corrosion is only accomplished by mechanical testing or metallographic examination. The latter method revealed that, in fact, the 7075-T6 material actually performed the worst and ranking in order of performance is as follows: F, A, E, C, B, and D (see Figures 57 and 58). Figures 59 through 62 clearly substantiate this order of resistance to corrosion. The overaged P/M materials (F&A) suffered only pitting (ASTM EXCO Code N), which was indeed deeper for the Co-containing alloy (A). The fully hardened P/M and overaged I/M alloys (E, C, and B) suffered the more severe pit-blistering (ASTM EXCO Code P) attack. But note that in this case, the severity of attack was greater for the non-Co-containing alloy (B). The T6 I/M condition suffered true exfoliation (ASTM EXCO Code E, severity B) (Reference 549). It can be noted for the 7075-T6 materials that the unrecrystallized (darker, higher chromium and subgrain containing) grains seemed to be more preferentially attacked.

Both hardness and conductivity measurements were generally predictive of the outcome of the exfoliation corrosion testing. The superiority of the P/M materials over the I/M materials, as well as the other observations made in the present work, are consistent with the findings of all other investigators to date (References 550-554). The P/M material has also been compared in actual stress corrosion to I/M materials and found to maintain its position of superiority (Reference 555).

AFWAL-TR-81-4068



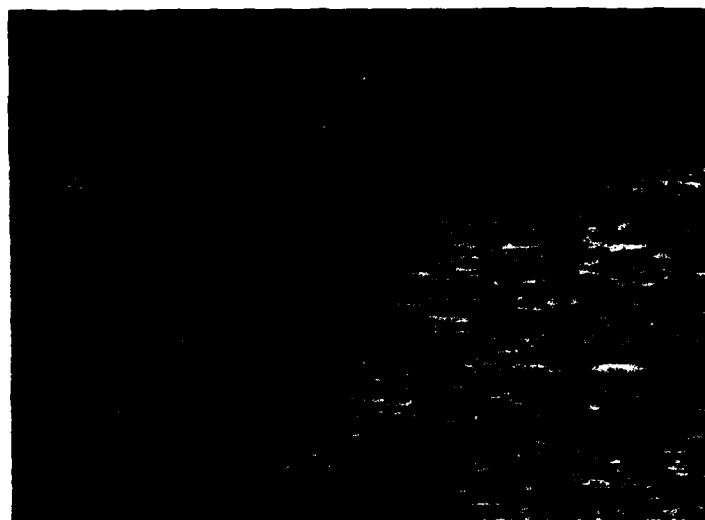
500µm



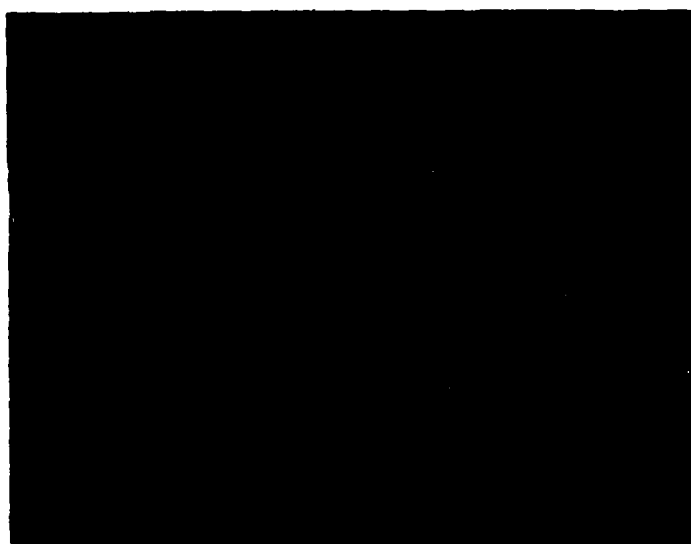
500µm

Figure 59. Optical Micrographs of Sectioned CT-91-T7 0% Co (Upper) and .4% Co (Lower) EXCO Test Specimens.

AFWAL-TR-81-4068



500 μ m



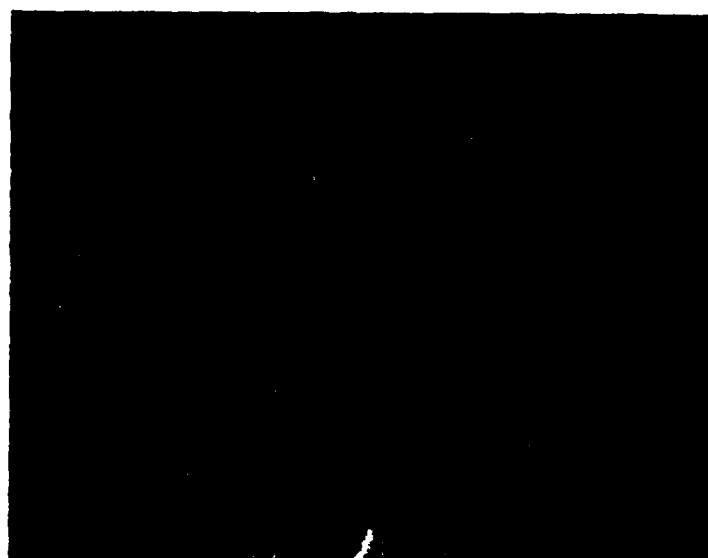
500 μ m

Figure 60. Optical Micrographs of Sectioned CT-91-T6 .4% Co (Upper) and 7075-T73 (Lower) EXCO Test Specimens

AFWAL-TR-81-4068



500 μ m



500 μ m

Figure 61. Optical Micrographs of Sectioned CT-91-T6 0% Co (Upper) and 7075-T6 (Lower) EXCO Test Specimens

AFWAL-TR-81-4068



125μm



125μm

Figure 62. Higher Magnification Views of the Preceding Two Micrographs.

SECTION V
SUMMARY AND CONCLUSIONS

A comparison of microstructure, notched high cycle fatigue, toughness and exfoliation corrosion behavior in longitudinal and transverse orientations of equivalent strength 7075-T6 I/M and fully dense CT-91-T7 P/M aluminum alloys was made. Optical and electron microscopy procedures, round electropolished tension-tension fatigue, slow-bend fatigue pre-cracked Charpy toughness, and wedge-shaped corrosion specimens; all machined from die forgings were employed in the testing. Conclusions drawn from this work are as follows:

1. Unlike Al I/M alloys, P/M alloys do not suffer deterioration in fatigue strength in the transverse orientations.
2. Fatigue crack initiation rather than fatigue crack propagation determines high cycle fatigue life.
3. Al P/M alloys in any condition of heat treatment are more resistant to exfoliation corrosion than even the overaged condition of heat treatment of equivalent I/M alloys.
4. At a constant constituent volume, grain flow direction rather than constituent particle size, distribution, or orientation, determines the toughness of a given orientation.
5. Smaller constituent particle size in P/M alloys produces the observed equivalence in longitudinal and transverse fatigue behavior.

SECTION VI
RECOMMENDATIONS FOR FUTURE WORK

1. Explore the relationship between elastic or shear modulus and fatigue crack growth rate.
2. Explore the effects of residual stress on fatigue behavior.
3. Optimize the heat treatment of P/M aluminum alloys.
4. Investigate the significance of anisotropy (crystallographic texture) by means of X-ray pole figure analysis.
5. Measure stacking fault energies of various microstructural features in aluminum alloys.
6. Utilize analytical surface techniques to discover the differences in chemical bonding and the role of oxides in P/M microstructure.
7. Examine polarization corrosion kinetics of the various second phase constituents in aluminum alloys.
8. Theoretically determine the stress concentrations of characteristic second phase constituents as a function of their sizes, shapes, locations and orientations with respect to the stress axis.

APPENDIX A
SAMPLE CALCULATIONS FOR TENSIL DATA

$$\text{U.T.S.} = \frac{P_{\max}}{A_0}$$

$$\text{V.S.} = \frac{P_{0.2\% \text{ offset}}}{A_0}$$

$$\% \text{ El.} = \frac{l_f - l_0}{l_0} \times 100$$

$$\% \text{ R of A} = \frac{D_0^2 - D_f^2}{D_0^2} \times 100$$

where; P_{\max} = max. load from Instron load deflection chart
 $P_{0.2\%}$ = load at 2% offset from Instron load deflection chart
 $l_f - l_0$ = total plastic strain approximated from Instron load deflection chart divided by the effective gage length of the specimen.
 l_0 = initial effective gage length
 D_0 = initial gage diameter
 D_f = final minimum gage diameter in necked region of specimen.

APPENDIX B
SAMPLE CALCULATION FOR TOUGHNESS DATA

$$K_Q = \frac{P_Q - g(a_{avg}/w)}{B \cdot \sqrt{w}} \quad \text{"Secant"}$$

$$K_Q = \frac{E}{n(1 - \nu^2)} \cdot \frac{W}{B-a \cdot w} \quad \text{"W/A"}$$

(assumed n (a constant) = 2 & ν (Poisson's ratio) = .33)

$$E = \frac{P_{el.}}{\delta_{el} \cdot B} \cdot h(a_{avg}/w)$$

E = elastic modulus

K_Q = estimated fracture toughness

$P_{el.}$ = 10% of P_Q from x-y recorder

δ_{el} = deflection from x-y recorder for $P_{el.}$

B = thickness

w = width

W = in-lbs. (total area inside P- curve measured with K&E model 620000 Polar Area Tracing Planimeter)

$g(a/w)$ → from J. Srawley, International Journal of Fracture, 12, (1976), 475.

$h(a/w)$ → from G. Succop et.al., ASTM STP 632, (1977), p. 177.

K_Q ("Secant Method") → from T. Ronald et.al., AFML-TR-70-311, p. 6.

APPENDIX C

The "staircase" or "up and down" method is widely used but allows determination only of the "median" fatigue life because of its approach to stress level selection; that is, the middle-most value in an ordered array. The arithmetic "mean" or average value is typically close to this value. This test provides little or no information regarding the fatigue strength distribution. In fact, determining the true shape of this distribution is virtually impossible. Nonetheless, some form is usually assumed; for example, symmetrical "normal" (Gaussian) or non-symmetrical Weibull.

Mean values are obviously less valuable than; for example, 10% probability of failure values. The reason for this is immediately obvious upon recognizing that a design engineer must use a much more conservative estimate in selecting operating stresses for a service component.

The Boundary technique provides such a means to allow reasonable approximation of minimum rather than mean values. Unfortunately, in the case of the present data, the reliability of this method is actually no greater than the Staircase method simply because the ratio of $N_{\max} : M_{\min}$ (maximum number of cycles to failure to minimum number of cycles to failure ratio) at a given stress level is greater than 30 to 1. Note however, that a mere doubling of the number of specimens tested (according to Maennig) would achieve improved enough statistical accuracy to predict such minimum values of fatigue life.

As noted by Voss, the probability of failure below 10% or above 90% is almost entirely dependent upon the distribution function employed. Therefore, only probabilities between 10 and 90% have any consistent relevance in such statistical treatments, and the reader is cautioned against any extrapolations of the lives drawn in Figures C-1 through C-6, which would exceed those boundaries (Reference Voss Diss. p. 83).

Sample calculations of each method are as follows:

Sample Calculations for Statistical Treatment
Boundary Method

$$P = \frac{3r - 1}{3n + 1} \times 100$$

P = probability of failure at a certain life

r = failed before that life

n = total number of tests in a given stress range

Staircase Method

Stress at which runouts (less frequent event) occurred.

<u>S(MPa)</u>	<u>Order</u>	<u># of Runouts</u> (less freq. event)	<u>Order x</u> <u># of Runouts</u>	<u>(Order x#)</u> <u>of Runouts</u>
S _{min} = 138	0	2	0	2
141	1	1	1	1
145	2	1	2	4
152	3	2	6	18
159	4	1	4	16
165	5	1	5	25
169	6	1	6	36
172	7	1	7	49
		Sum N=10	Sum A=31	Sum B=149

$$\begin{aligned} \hat{\mu}_{est} &= \text{Estimated Mean Fatigue Strength} \\ &= S_{min} + (A/N - d) \cdot d \end{aligned}$$

where; d = average change in stress level

$$c = \frac{NB - A^2}{N^2} > .3 \text{ therefore,}$$

$$\begin{aligned} \hat{\sigma}_{est} &= \text{Estimated Standard Deviation of Mean Fatigue Strength} = \\ &1.62 (\sigma) (c + .029) \end{aligned}$$

$$\frac{d}{\hat{\sigma}_{est}} = x$$

AFWAL-TR-82-4068

then, from plot of G vs. $\frac{d}{\hat{\sigma}_{\text{est}}}$ (where; G = confidence limit function of

$\frac{d}{\hat{\sigma}_{\text{est}}}$)

$\hat{\sigma}$ = standard deviation of mean fatigue strength = $\frac{G\hat{\sigma}}{\sqrt{N}}$ and,

$$S_{\min} = \hat{\sigma} - 1.96(\hat{\sigma}) \leq \hat{\mu} \leq S_{\min} + \hat{\sigma} + 1.96(\hat{\sigma})$$

where, 1.96 is factor from table of standards normal distribution for $\alpha = .05$; that is, 95% confidence interval, and $\hat{\mu}$ is the mean fatigue strength.

TABLE C-1
P/M FATIGUE** DATA

P/M - L		P/M - LT	
Stress MPa	Cycles	Stress MPa	Cycles
141	$2 \times 10^{7*}$	165	10^{7*}
141	1.3×10^5	172	10^{7*}
145	$2 \times 10^{7*}$	179	8.8×10^4
152	$2 \times 10^{7*}$	172	10^7
159	4.4×10^4	172	4.4×10^4
138	$2 \times 10^{7*}$	165	10^{7*}
165	9.2×10^4	172	2.2×10^5
165	1.1×10^6	193	8×10^4
172	9.6×10^4	179	1.2×10^5
169	7.6×10^4	155	8.6×10^4
172	10^5	141	1.1×10^5
169	7.5×10^4	172	7.7×10^4
152	1.3×10^5	179	6.4×10^4
138	10^{7*}	152	10^{7*}
152	10^{7*}	165	4.8×10^4
159	10^{7*}	165	5.2×10^4
148	2×10^5	176	2.4×10^5
165	10^{7*}	131	$2 \times 10^{7*}$
172	2.4×10^5	138	$2 \times 10^{7*}$
169	10^{7*}		
172	10^{7*}		
176	9×10^5		

* Test Interrupted - No Failure

** ASTM E466-72T

TABLE C-2
I/M FATIGUE** DATA

I/M - L		I/M - LT	
Stress MPa	Cycles	Stress MPa	Cycles
159	2.3×10^5	138	6.6×10^5
145	2.2×10^5	138	10^{7*}
124	$4.5 \times 10^{7*}$	159	10^{7*}
165	10^{7*}	179	9.6×10^4
138	10^{7*}	138	8.6×10^4
165	2.5×10^5	159	4.2×10^4
152	10^{7*}	138	9×10^4
159	10^{7*}	138	1.1×10^5
172	1.5×10^5	124	2.4×10^5
124	$2 \times 10^{7*}$	110	10^{7*}
		117	2.4×10^5

* Test Interrupted - No Failure

** ASTM E466-72T

TABLE C-3
COMPARISON OF 95% CONFIDENCE INTERVAL MEAN FATIGUE STRENGTH AT 10^7
CYCLES FOR STAIRCASE AND BOUNDARY METHODS (MPa)

Material	Staircase Method	Boundary Method
I/M-L	$145 \leq \mu \leq 159$	$159 \leq \mu \leq 172$
I/M-LT	$114 \leq \mu \leq 176$	$138 \leq \mu \leq 159$
P/M-L	$131 \leq \mu \leq 166$	$159 \leq \mu \leq 179$
P/M-LT	$138 \leq \mu \leq 166$	$166 \leq \mu \leq 179$

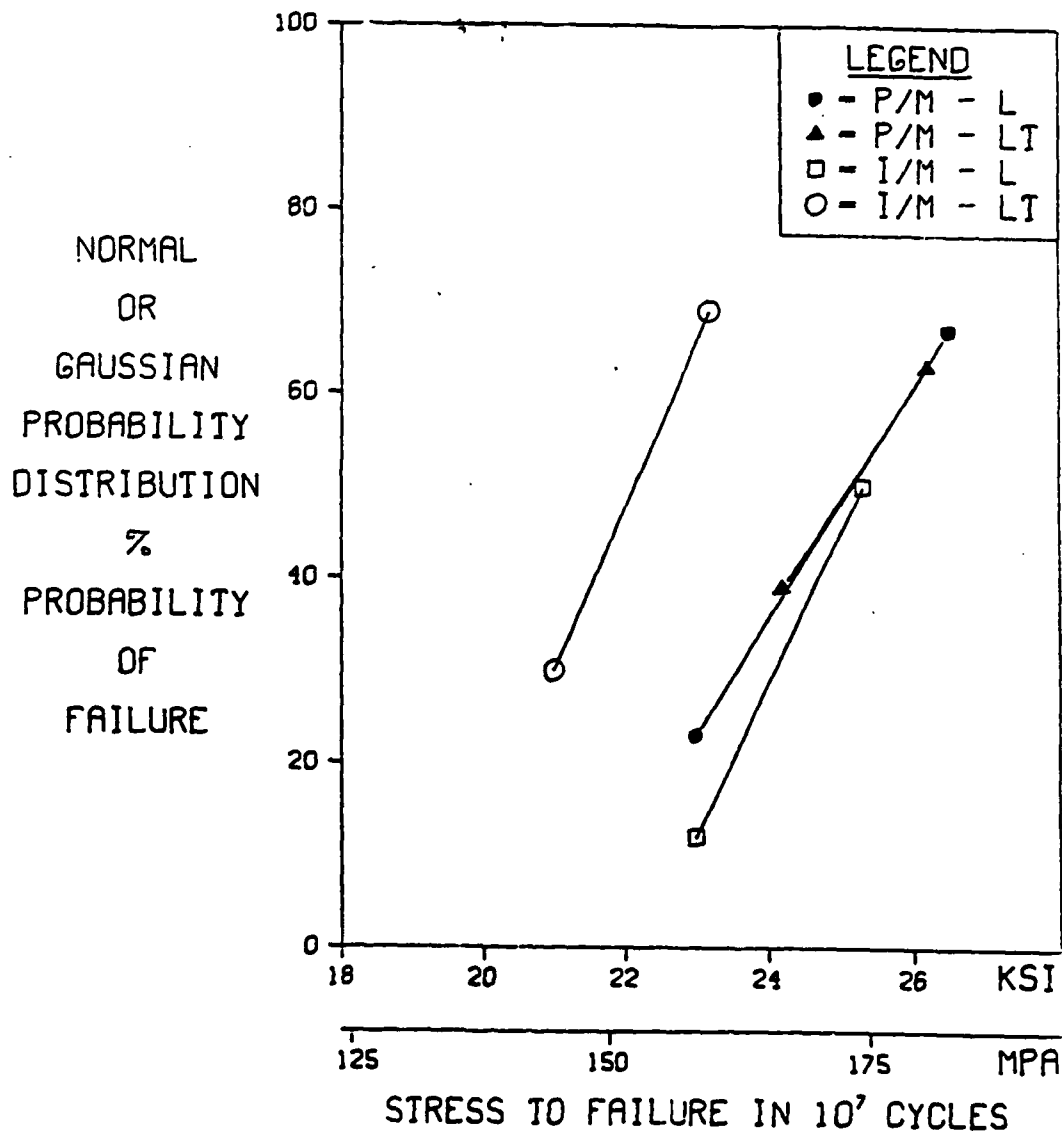


Figure C-1. Boundary Method Statistical Treatment of Fatigue Data in Tables C-1 and C-2.

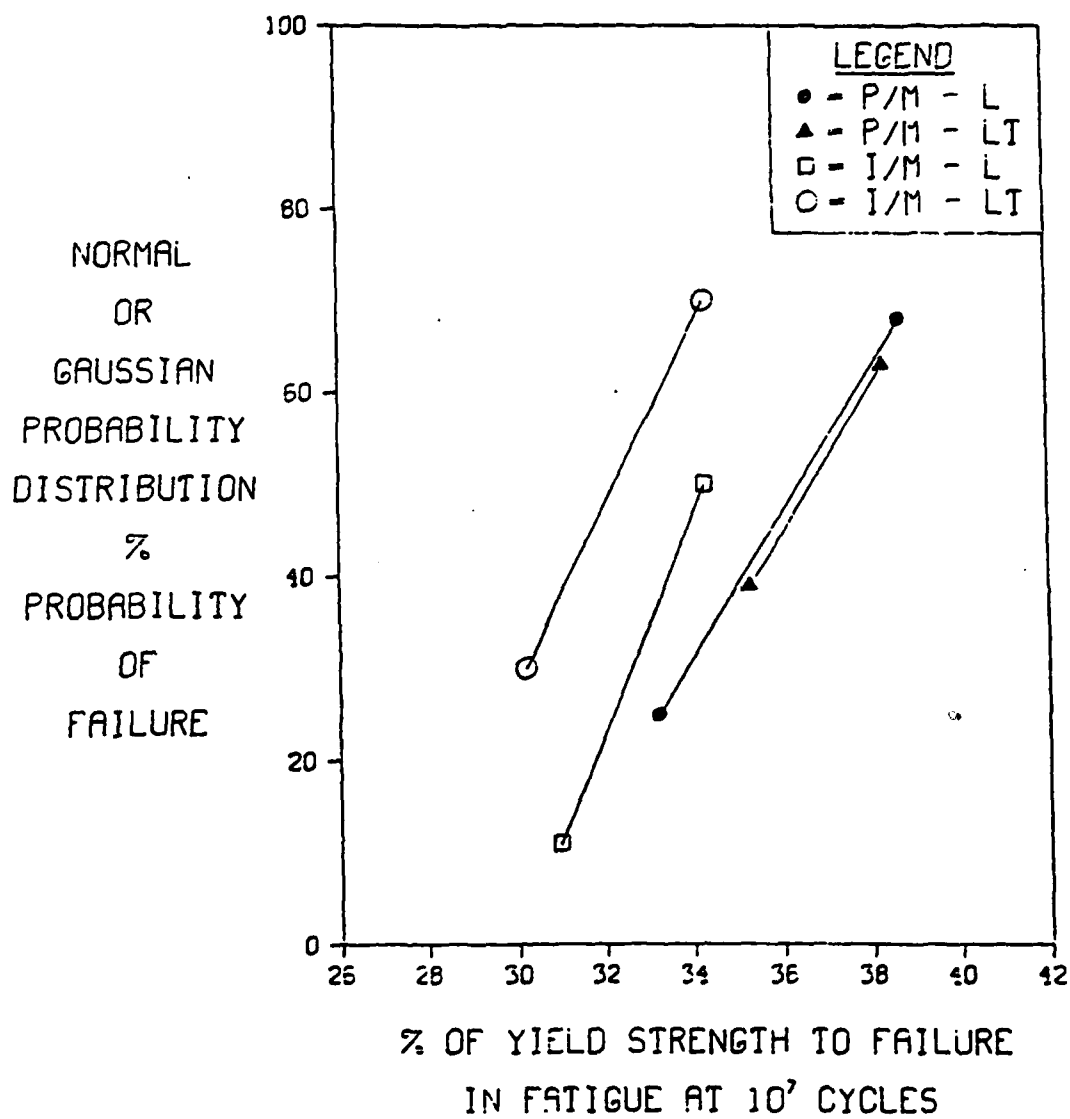


Figure C-2. Data of Figure C-1 Normalized to Yield Strength.

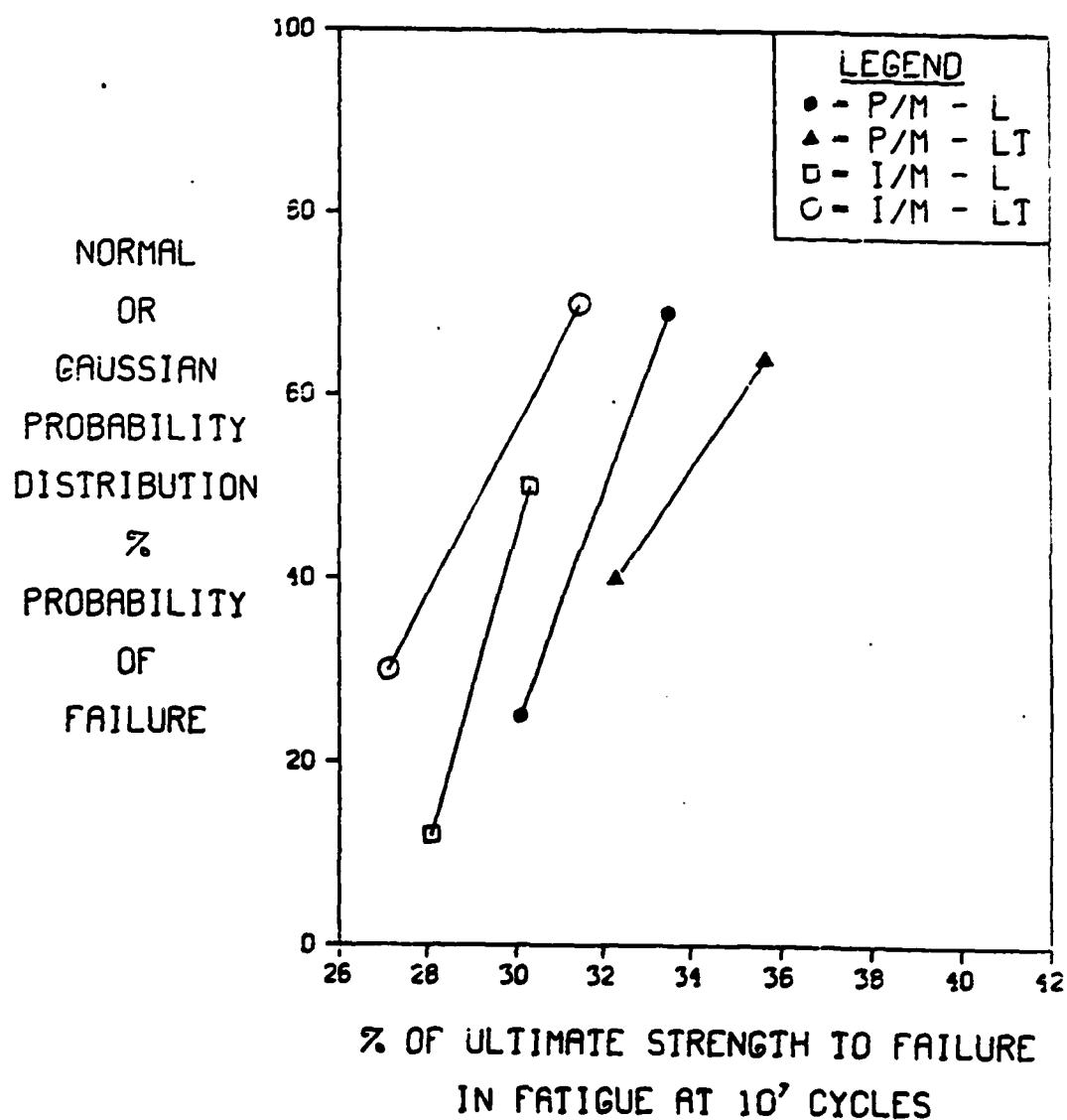


Figure C-3. Data of Figure C-1 Normalized to Ultimate Strength.

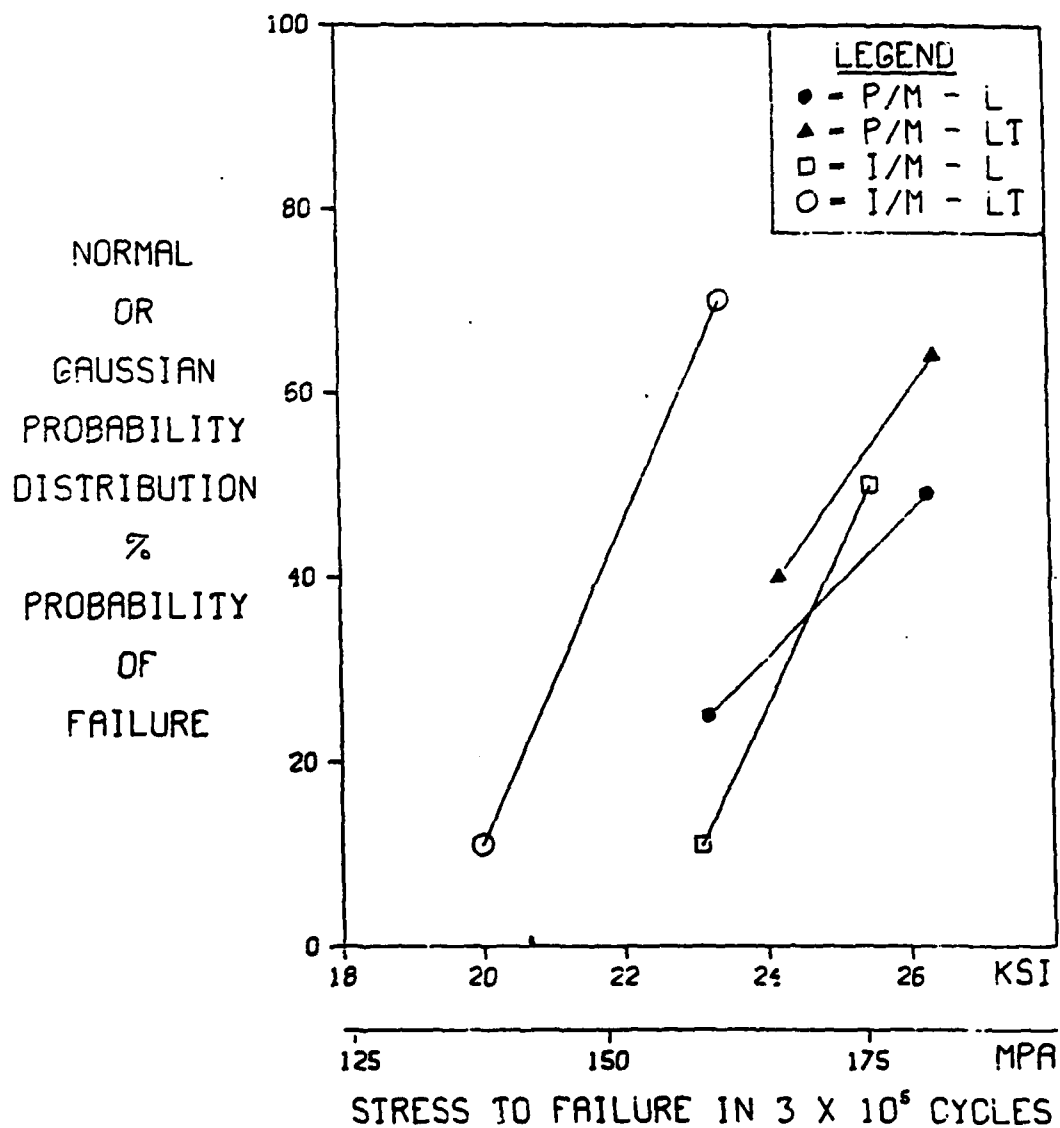


Figure C-4. Boundary Method Statistical Treatment of Fatigue Data in Table C-1 and C-2.

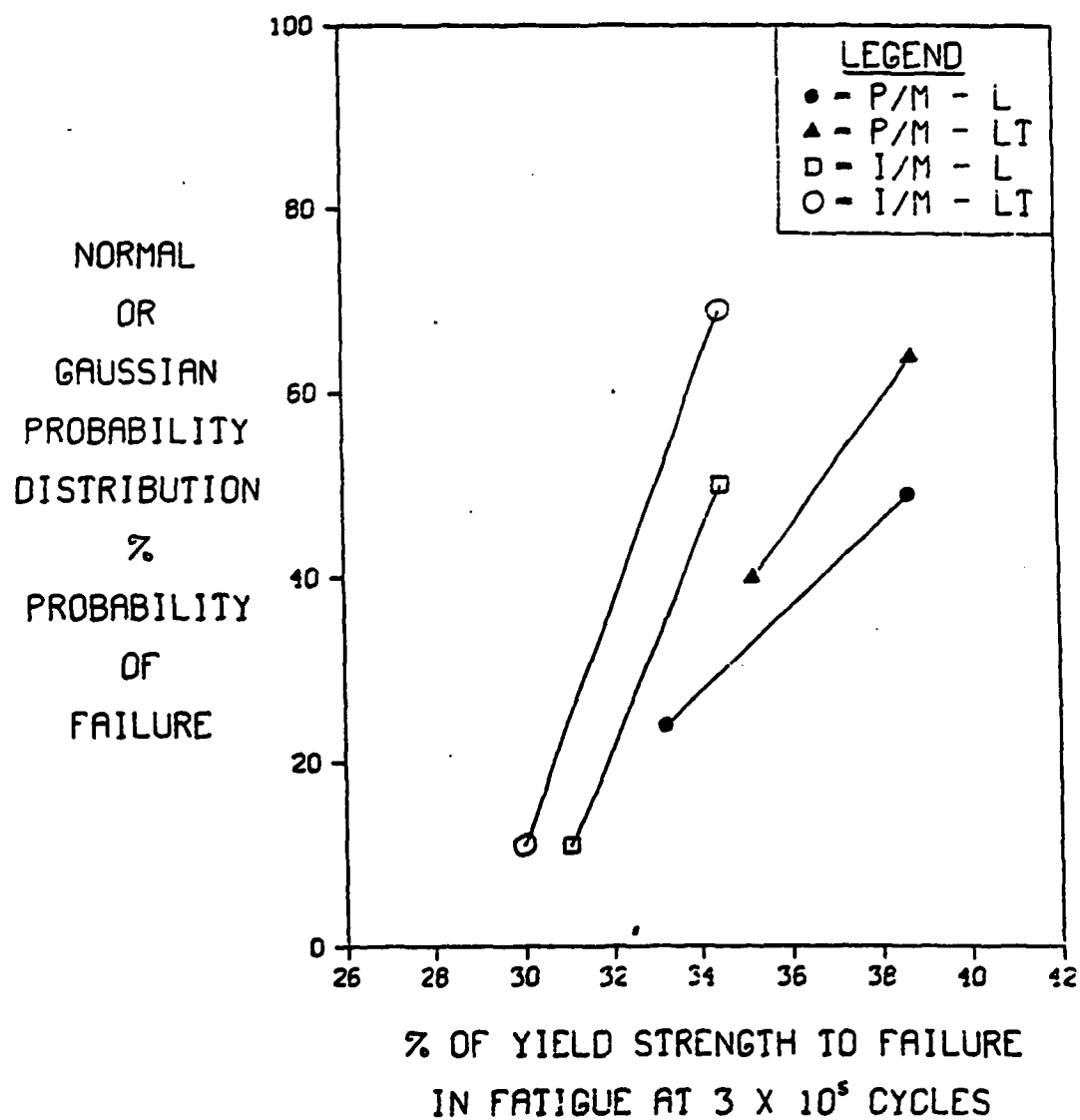


Figure C-5. Data of Figure C-4 Normalized to Yield Strength.

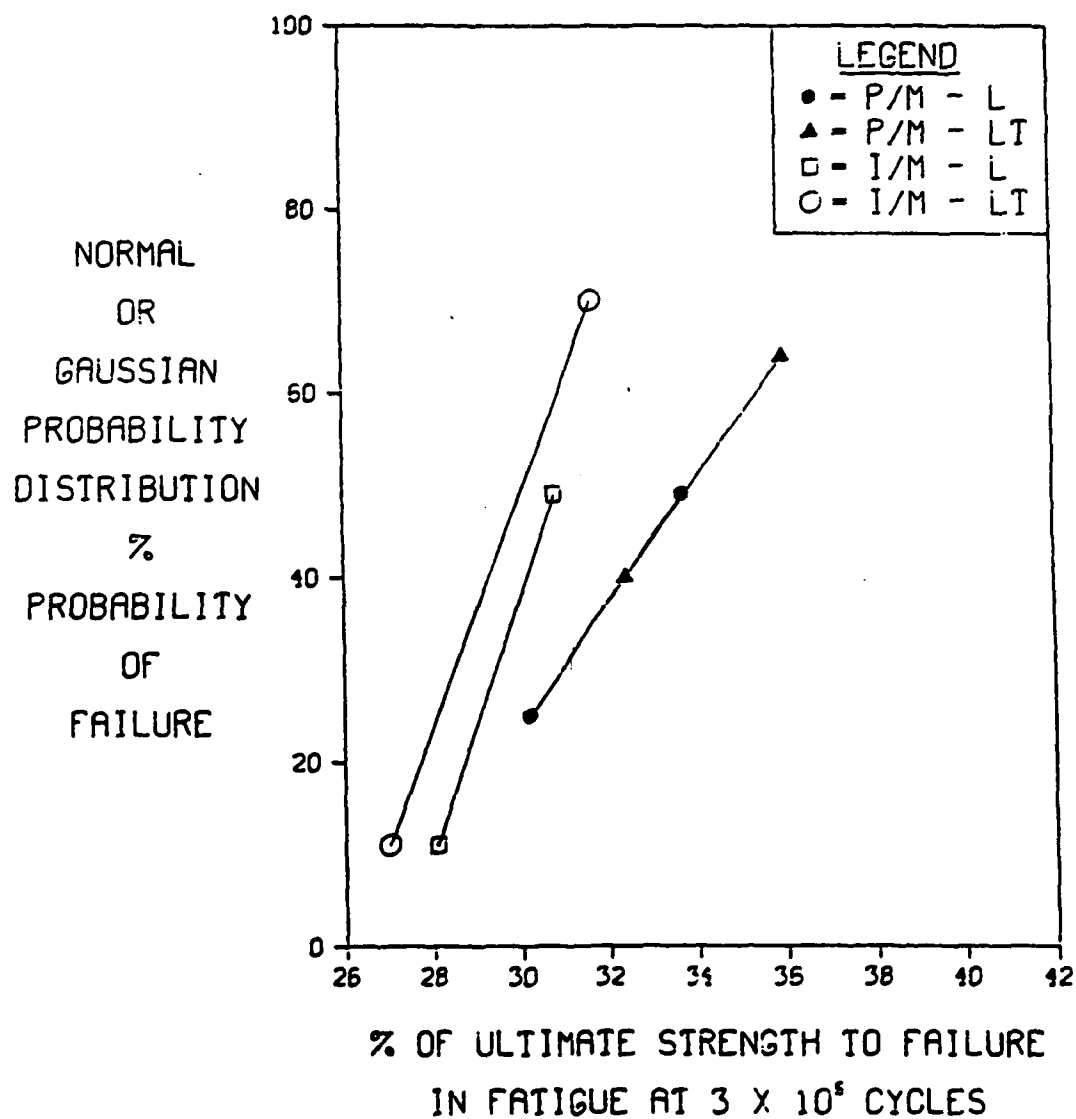


Figure C-6. Data of Figure C-4 Normalized to Ultimate Strength.

REFERENCES

1. N. Petch, JISI, 174, (1953), 747.
2. B. Watts et.al., Metal Sci., 10, (1976), 189.
3. B. Park and J. Vrugink, "Thermomechanical Processing of Al Alloys", J. Morris (ed.), Met. Soc. AIME, Warrendale, PA., (1979), 25-49.
4. W. Reimann and A. Brisbane, Engr. Fract. Mech., 5, (1973), 67.
5. M. Hyatt, AFML-TR-73-224, Air Force Materials Laboratory, (AFML), Wright-Patterson Air Force Base (WPAFB), Ohio, (1973).
6. D. Thompson et.al., AFML-TR-73-247, AFML, WPAFB, Ohio, (1973).
7. J. Waldman et.al., Met. Trans., 5, (1974), 573.
8. H. Antes, Progress in P/M, 28, MPIF, Princeton, N.J., (1972), 5-40.
9. D. Evans and D. Malley, AFML-TR-186-7T, AFML, WPAFB, Ohio (1978).
10. W. Cebulak, FA-TR-76067, Frankford Arsenal, Phila. PA, (1977).
11. D. Voss, "Correlation of Processing Parameters, Microstructure and Mechanical Properties of High Strength P/M Al Alloys", Ph.D. Diss., Aachen Univ. W. Ger., (1979).
12. A. Clauer et.al., AFML-TR-77-107, AFML, WPAFB, Ohio, (1977).
13. D. Voss, op. cit., 18.
14. T. Bower, H. Brody and M. Flemings, TAIME, 236, (1966), 624.
15. W. Cebulak et.al., Int'l J. of P/M and P/T, 12, (4), (1976), 306.
16. Air Force Wright Aeronautical Laboratories (AFWAL), WPAFB, Ohio, on-going R&D contract F33615-76-C-5136 with Pratt and Whitney A/C, Florida.
17. AFWAL, WPAFB, Ohio, on-going R&D contract F33615-80-C-5005 with P&WA, Florida.
18. J. Kaufman, AGARD Conference Proceedings #185, (1976), 2-1.
19. T. Sanders and J. Staley, "Fatigue and Microstructure", ASM, Metals Park, Ohio, (1979), 467.
20. R. Hertzberg, "Deformation and Fracture Mechanics of Engineering Materials", Wiley, N.Y., (1976), 355.
21. G. Dieter, "Mechanical Metallurgy", McGraw-Hill, N.Y., (1976), 455.

REFERENCES (Continued)

22. R. Sanders et.al., AFML-TR-79-4131, AFML, WPAFB, Ohio (1979), 93.
23. M. Hyatt, *op. cit.*
24. D. Thompson et.al., *op. cit.*
25. R. Sanders et.al., *op. cit.*, 17.
26. AFWAL-TR-80-4089, AFWAL, WPAFB, Ohio, (1980).
27. R. Sanders et.al., *op. cit.*, 38.
28. AFWAL, WPAFB, Ohio, on-going R&D contract F33615-80-C-5098 with Alcoa, Pittsburgh, PA.
29. A. Tetelman and A. McEvily, "Fracture of Structural Materials", Wiley, N.Y., (1967), 156-74, 352-80.
30. R. Hertzberg, *op. cit.*, 45, 72, 93, 243.
31. A. McEvily and T. Johnson, Int'l J. of Fract. Mech., 3, (1967), 45.
32. C. Wells, Acta Met., 17, (1969), 413.
33. J. Grosskreutz and G. Shaw, Acta Met., 20, (1972), 523.
34. C. Laird, ASTM STP 415, Amer. Soc. for Testing and Materials, Phila, PA., (1967), 131.
35. C. Laird, ASTM STP 637, (1977), 47.
36. ASM Handbook, Vol. 9, "Fractography and Atlas of Fractographs", 8th Edition, ASM, Metals Park, Ohio, (1974), 43, 68-89, 249-260.
37. R. Hertzberg, *op. cit.*, 248.
38. P. Forsyth, Acta Met., 11, (1963), 703.
39. J. McMillan and R. Hertzberg, ASTM STP 436, (1968), 89.
40. J. Santner, "Microstructural Effects on the Fatigue Crack Propagation in Al-Cu Alloys", Ph.D. Diss., Northwestern Univ., Chicago, IL., (1975).
41. D. Thompson et.al., Met Trans., 2, (1971), 1971.
42. I. Kirman, *ibid.*, 1971.
43. E. Hondros and M. Seah, Scripta Met., 6, (10), (1972), 1011.
44. G. Dieter, *op. cit.*, 193.

REFERENCES (Continued)

45. J. Santner, op. cit., 91.
46. J. Grosskreutz and G. Shaw, loc. cit.
47. A. Tetelman and A. McEvily, op. cit.
48. J. Grosskreutz, ASTM STP 495, (1971), 5.
49. C. Laird and G. Smith, Phil. Mag., 7, (1962), 847.
50. S. Manson, Exper. Mechs., 5, (1965), 193.
51. W. Truckner et.al., AFML-TR-76-169, AFML, WPAFB, Ohio (1976), 162.
52. M. Fine and O. Ritchie, "Fatigue and Microstructure", ASM, Metals Park, Ohio, (1979), 262.
53. D. Duquette, *ibid.*, 360.
54. G. Miller, D. Avery and W. Backofen, TAIME, 236, (1966), 1967.
55. C. Kung and M. Fine, Met. Trans., 10A (1979), 609.
56. W. Morris et.al., Met. Trans., 8A, (1977), 1079.
57. J. Low, "Fracture of Solids", D. Druckner and J. Gilman (eds.), Wiley, N.Y., (1963), 213.
58. N. Thompson, N. Wadsworth and N. Louat, Phil. Mag., 11, (1956), 113.
59. R. Pangborn, S. Weissman, and I. Kramer, Scripta Met., 12, (2), (1978), 129.
60. C. Wells and C. Sullivan, Trans. ASM, 61, (1968), 149.
61. C. Bowles and J. Schijve, Int'l J. of Fract., 9, (1973), 171.
62. Y. Kim, "Initiation and Growth of Fatigue Microcracks and Strain-Controlled Fatigue Properties in Steel Alloys: Microstructure and Mechanisms", Ph.D. Diss., Northwestern Univ., Chicago, ILL., (1979).
63. W. Morris, O. Buck and H. Marcus, Met. Trans., 7A, (1976), 1161.
64. C. Wells, loc. cit.
65. C. Feltner and P. Beardmore, ASTM STP 467, (1970), 77.
66. R. Sanders and E. Starke, Mat. Sci. and Engr., 28, (1977), 53.
67. C. McMahon, Fundamental Phenomena in Materials Science, 4, (1967), 247.

REFERENCES (Continued)

68. N. Palakowski and E. Ripling, "Strength and Structure of Engineering Materials", Prentice-Hall, N.J., (1966), 508.
69. G. Lutjering and J. Lindekeit, Acta. Met., 27, (11), (1979), 1717.
70. M. Nageswararao, V. Gerold and G. Kralik, J. Mat. Sci., 10, (1975), 515.
71. M. Ronay, "Fracture", Vol. 3., H. Liebowitz (ed.), Academic Press, N. Y., (1979), 149.
72. N. Eid and P. Thomason, Acta Met., 27, (1979), 1239.
73. C. Laird, "Fatigue and Microstructure", ASM, Metals Park, Ohio, (1979), 149.
74. M. Hunter and W. Fricke, Annual ASTM Proceedings, 54, (1954), 717.
75. S. Lynch, ASTM STP 675, (1979), 175.
76. M. Fine and D. Ritchie, loc. cit.
77. D. Duquette, loc. cit.
78. J. Grosskreutz, loc. cit.
79. G. Miller et.al., loc. cit.
81. MIL-STD-1530, USAF, "Military Standard Aircraft Structural Integrity Program", (1972).
82. C. Laird, (1967), loc. cit.
83. R. Sanders and E. Starke, loc. cit.
84. L. Karjalainen, Scripta Met., 7, (1973), 43.
85. A. Thompson and W. Backofen, Acta Met., 19, (1971), 597.
86. A. TeteIman and A. McEvily, op. cit.
87. W. Morris et.al., loc. cit.
88. J. Awatani et.al., Met. Trans., 10A, (1979), 503.
89. D. Holloway, "Determination of Threshold Stress Intensity Factors for 7175-T651 Al and Alcoa MA-87 Powdered Al Alloys", M.S. Thesis, Air Force Institute of Technology, WPAFB, Ohio (1977), 25.

REFERENCES (Continued)

90. R. Sanders et.al., op. cit.
91. D. Voss, op. cit.
92. R. Boetner, C. Laird and A. McEvily, TAIME, 233, (1965), 379.
93. W. Truckner et.al., op. cit., 6.
94. A. Thompson and W. Backofen, loc. cit.
95. A. Thompson, Scripta Met., 5, (1971), 859.
96. D. Hoepfner, ASTM STP 415, (1967), 486.
97. G. Birkbeck et.al., J. Mat. Sci., 6, (1971), 319.
98. G. Yoder et.al., ASME Trans., J. of Engr. Mat'ls and Tech., 101, (1), 1979), 86.
99. A. Thompson et.al., J. Mat. Sci., 9, (1975), 46.
100. G. Lutjering and J. Lindekeit, loc. cit.
101. R. Pelloux, ASME Trans., 57, (1964), 511.
102. D. Broek, "Fracture", P. Pratt (ed.), Chapman and Hall Publishers, London, (1969), 754.
103. J. Mulherin and H. Rosenthal, Met. Trans., 2, (1971) 427.
104. A. Hertzberg, op. cit., 335.
105. W. Anderson and W. Quist, U.S. Patent #3, 284, 193, (1966).
106. M. Hyatt, op. cit.
107. AFML-TR-74-1249, AFML, WPAFB, Ohio, (1974).
108. R. Sanders, "Compilation and Review of Available Fatigue Data for 7XXX P/M Alloys", Alcoa Internal Report 56-59-AFS2, Alcoa Center, PA., (1979), 15.
109. D. Voss, op. cit.
110. R. Sanders et.al., op. cit.
111. D. Voss, op. cit.
112. B. Kirby and C. Beevers, Fatigue of Engrg. Mat'ls and Structures, 1, (1979), 203.

REFERENCES (Continued)

113. D. Davidson, J. Lankford, T. Yokobori, and K. Sato, Int'l J. of Fract., 12, (1976), 155.
114. E. Starke and G. Lutjering, "Fatigue and Microstructure", ASM, Metals Park, Ohio, (1979), 205.
115. C. Laird, (1967), loc. cit.
116. J. Grosskreutz, loc. cit.
117. J. Schihve, ASTM STP 415, (1967), 415.
118. J. Hyzak, "The Effect of Defects of the Fatigue Initiation Process in Two Powder Metallurgy Superalloys", Ph.D. Diss., Carnegie-Mellon Univ., Pitts., PA., (1980).
119. J. Lankford, Engr. Fract. Mech., 9, (1977), 617.
120. W. Morris, O. Buck and H. Marcus, loc. cit.
121. J. Grosskreutz, loc. cit.
122. T. Sanders and J. Staley, loc. cit.
123. R. Hertzberg, op.cit., 428.
124. J. Hyzak, op. cit.
125. J. Meakin and N. Petch, "Fracture of Solids", D. Drucker and J. Gilman (eds.), Wiley, N.Y., (1963), 410.
126. G. Dieter, op. cit., 414.
127. ASTM STP 566, (1974), 44.
128. G. Harkegard, Engr. Fract. Mech., 6, (1974), 795.
129. C. Kung and M. Fine, loc. cit.
130. J. Hyzak, op. cit.
131. J. Grosskreutz and G. Shaw, AFML-TR-66-96, AFML, WPAFB, Ohio (1966).
132. A. Tetelman and A. McEvily, op. cit.
133. C. Kung and M. Fine, loc. cit.
134. J. Hyzak, op. cit.

REFERENCES (Continued)

135. J. Ryder and J. Van Orden, "Effect of Purity on Fatigue and Fracture of 7XXX-T76511 Al Extrusion", Internal Report 28612, Lockheed Aircraft Corp., Burbank, CA, (1978).
136. J. Santner, op. cit.
137. J. Grosskreutz, loc. cit.
138. N. Plakowski and E. Ripling, op. cit.
139. A. Tetelman and A. McEvily, op. cit.
140. J. Schijve, loc. cit.
141. A. Tetelman and A. McEvily, op. cit.
142. Y. Kim, op. cit., 154.
143. H. Abdel-Raouf et.al., Met. Trans., 10A, (1979), 449.
144. J. Santner, op. cit.
145. E. Imhof and J. Barsom, ASTM STP 536, (1973), 182.
146. J. Weber and R. Hertzberg, Met. Trans., 4, (1973), 595.
147. A. McEvily and T. Johnston, loc. cit.
148. F. Heiser and R. Hertzberg, ASME Trans., J. Basic Engrg., 93, (1971), 71.
149. A. Tetelman and A. McEvily, op. cit.
150. N. Polawkowski and E. Ripling, op. cit., 508.
151. J. Barsom and S. Rolfe, "Fracture and Fatigue Control in Structures". Prentice-Hall, N.J., (1977), 219.
152. G. Dieter, op. cit., 443.
153. R. Sanders et.al., op. cit.
154. R. Templin, ASTM Annual Proceedings, 54, (1954), 641.
155. G. Stickley and J. Lyst, Product Engrg., (Nov., 1964).
156. K. Sadananda and P. Shahinian, Int'l J. of Fract., 13, (1977), 585.
157. S. Pearson, Nature, 211, (1966), 1077.
158. S. Purushothama and J. Tien, Scripta Met., 9, (9), (1975), 923.

REFERENCES (Continued)

159. R. Bates and W. Clark, ASM Trans. Quart., 62, (2), (1969), 380.
160. G. Dieter, op. cit., 271.
161. J. Barsom and S. Rolfe, op. cit.
162. A. Wells, Engrg. Fract. Mech., 1, (1969), 399.
163. J. Weertman, Int'l J. of Fract., 5, (1969), 13.
164. T. Mura and C. Lin, Int'l J. of Fract., 10, (1974), 284.
165. M. Hyatt, op. cit., 36.
166. C. Feltner and C. Laird, Acta Met., 15, (1967), 1621.
167. B. Linder, "Extremely Low Fatigue Crack Growth Rates in Al Alloy 7075-T6", M.S. Thesis, Lehigh Univ. Bethlehem, PA., (1965).
168. F. Fouquet et.al., Acta Met., 27, (3), (1979), 315.
169. T. Sanders and J. Staley, loc. cit.
170. D. Raske, J. of Test. and Eval., 1, (1973), 394.
171. C. Gowda et.al., J. of Test. and Eval., 2, (1974), 57.
172. J. Crews and H. Hardrath, Exper. Mech., 6, (1966), 313.
173. ASTM STD E466-72T, Amer. Soc. for Testing and Mat'ls, Phila, PA.
174. N. Dowling, ASTM STP-677, (1979), 247.
175. ASTM STP 566, (1974), 44.
176. J. Grosskreutz and G. Shaw, op. cit.
177. H. Neuber, "Theory of Notch-Stresses", J.W. Edwards Publisher Inc., Ann Arbor, Michigan, (1946)(Translation of original 1937 German version).
178. T. Topper, R. Wetzel and J. Morrow, J. Mat'ls., 4, (1969), 200.
179. A. Kennedy, "Processes of Creep and Fatigue in Metals", Wiley, N.Y., (1963), 362.
180. G. Dieter, op. cit., 435.
181. *ibid.*
182. A. Tetelman and A. McEvily, op. cit.

REFERENCES (Continued)

183. R. Forman, V. Kearney and R. Engle, J. Basic Engrg., (1967), 459.
184. W. Illg and A. McEvily, NASA TND-52, NASA-Lewis Research Center, Cleveland, Ohio, (1959).
185. C. Hudson, NASA TND-5390, (1969).
186. W. Elber, ASTM STP 486, (1971), 230.
187. G. Dieter, op. cit., 435.
188. R. Hertzberg, op. cit., 420.
189. J. Hyzak, op. cit., 126.
190. J. Santner, AFML-TR-77-78, AFML, WPAFB, Ohio, (1977), 23.
191. M. Fine, Air Force Office of Scientific Research (AFOSR), Wash., D.C., on-going R&D Contract F33615-78-C-3732, (1979).
192. E. Starke, loc. cit.
193. L. James and R. Knecht, Met. Trans., 6A, (1975), 109.
194. *ibid.*
195. E. Starke, loc. cit.
196. L. James and R. Knecht, Met. Trans., 6A, (1975), 109.
197. "Metals Handbook", Vol. 1, American Society for Metals, Metals Park, Ohio, (1961), 916.
198. W. Anderson, "Precipitation from Solid Solution", ASM, Ohio (1959), 150.
199. J. Staley, Mets. Engr. Quart., 13, (4) (1973), 52.
200. *ibid.*
201. H. Hunsicker, J. Staley and R. Brown, Met. Trans., 3, (1972), 201.
202. J. Staley, R. Brown and R. Schmidt, Met. Trans., 3, (1972), 191.
203. "Metals Handbook", Vol. 1, loc. cit.
204. "Aluminum", K. Van Horn (ed.) ASM, (1967), 228, 240.
205. D. Thompson and S. Levy, AFML-TR-70-171, AFML, WPAFB, Ohio, (1970).

REFERENCES (Continued)

206. L. Otto, AFML-TR-76-60, AFML, WPAFB, Ohio (1976)
207. R. Brodei and L. Bakow, Naval Air Development Center (NADC), Warminster, PA, Final Report 78185-60, (1979), 32.
208. F. Ostermann and W. Reimann, ASTM STP 467, (1970), 169.
209. D. Sprowls and R. Brown, Metals Progress, 81, (4) (1962), 77.
210. *ibid.*
211. M. Hyatt, Corrosion, 26, (1970), 487.
212. P. Adler and R. DeIasi, NASA-Marshall R&D Contract 8-28986 Report 468, (1974).
213. A. Jacobs, ASM Trans., 58, (1965), 579.
214. H. vanLeeuwen, L. Schra and W. VanderVet, J. Inst. of Mets., 100, (1972), 86.
215. M. Speidel and M. Hyatt, "Advances in Corrosion Science and Technology", Vol. 2, Plenum Press, N.Y., (1972), 115.
216. W. Cebulak et.al., *loc. cit.*
217. M. Hyatt, AFML-TR-73-224, AFML, WPAFB, Ohio, (1973).
218. P. Adler and R. DeIasi, *loc. cit.*
219. W. Cebulak et.al., *loc. cit.*
220. R. Selines and R. Pelloux, Met Trans., 3, (1972), 2525.
221. T. Sanders et.al., NADC, Warminster, PA., Final Report N00019-76-C-0482, (1978), 45.
222. R. Sanders et.al., *op. cit.*, 17.
223. G. Chanani, ASTM STP 642, (1978), 51.
224. T. Sanders and J. Staley, *loc. cit.*
225. R. Wei, Engrg. Fract. Mechs., 1, (1970), 633.
226. M. Speidel, "Hydrogen in Metals", I. Bernstein and W. Thompson (eds.), ASM, Metals Park, Ohio, (1974), 249.
227. R. Brown et.al., ASTM STP 518, (1972), 87.
228. R. Parkins, Brit. Corr. Journ., 7, (1972), 15.

REFERENCES (Continued)

229. M. Speidel, Met. Trans., 6A, (1975), 641.
230. F. Furney, D. Abson and V. DePierre, Powder Metallurgy, 17, (33), (1974), 46.
231. H. Matayia et.al., J. Inst. Mets., 96, (1968), 30.
232. ASTM STD E12-70, Amer. Soc. for Testing and Mat'ls, Phila, PA.
233. J. Lyle and W. Cebulak, Met. Trans., 6A, (1975), 685.
234. L. Otto, op. cit.
235. R. Sanders et.al., op. cit.
236. L. Otto, personal communication.
237. AFML-TR-70-117, AFML, WPAFB, Ohio, (1970).
238. D. Voss, op. cit.
239. ASTM STD E385-73, Amer. Soc. for Testing and Materials, Phila, PA.
240. J. Wert, N. Patron, C. Hamilton and M. Mahoney, "Grain Refinement in 7075 Al by Thermomechanical Processing", submitted to Met. Trans., July, 1980.
241. G. Dieter, op. cit. 375.
242. *ibid*, 545.
243. "Aluminum", Vol. 1, K. Van Horn (ed.), ASM, Metals Park, Ohio, (1967), 135.
244. M. Hyatt, op. cit.
245. H. vanLeeuwen et.al., *loc. cit.*
246. D. Thompson and S. Levy, op. cit.
247. R. Sanders et.al., op. cit.
248. "Aluminum", Vol. 3, K. Van Horn (ed.), ASM, Metals Park, Ohio (1967), 355.
249. "Metals Handbook", Vol. 2, ASM, Metals Park, Ohio (1964), 274.
250. *ibid*.
251. "Aluminum" Vol. 1, *loc. cit.*
252. G. Dieter, op. cit., 557.

REFERENCES (Continued)

- 253. ASTM STD E8-69, ASTM, Phila. PA.
- 254. R. Hertzberg, op. cit., 3.
- 255. G. Dieter, op. cit., 7.
- 256. N. Polakowski and D. Ripling, op. cit., 49.
- 257. E. Wessel, W. Clark and W. Wilson, U.S. Army Tank and Automotive Command Contract DA-30-069-AMC-602(t) Final Report, (June, 1966).
- 258. E. Wessel, W. Clark and W. Wilson, USAT&AC, Contract DAAE-07-67-C-4021, Final Report, (November, 1968).
- 259. C. Freed, R. Goode and R. Judy, Engr. Fract. Mech., 2, (1971), 359.
- 260. C. Hartbower and C. Turner, ASTM STP 466, (1970), 93.
- 261. NMAC-Publication-328, National Academy of Sciences, Wash., D.C., (1976), 19.
- 262. ASTM STD E399-78, ASTM, Phila., PA.
- 263. C. Interrante and J. Filliben, ASTM committee E24.03.03 Phase I Report, (1979), 41.
- 264. *ibid*, 37.
- 265. J. Kaufman, ASTM STP 632, (1977), 3.
- 266. G. Succop et.al., ASTM STP 632, (1977), 177.
- 267. ASTM STD E466-72T, ASTM, Phila. PA.
- 268. Mil HDBK-5C, Dept of Defense, Wash., D.C., (1976), 3-284.
- 269. "Aluminum Standards and Data", Aluminum Association Inc., Wash., D.C., (1978), 32.
- 270. H. Grover, "Fatigue of Aircraft Structures", U.S. Govt. Printing Office, Wash. D.C., (1966), 317.
- 271. R. Brodie and L. Bakow, op. cit.
- 272. J. VanOrden, "Advanced Aluminum Alloy Evaluation", Lockheed Internal Report 25699, Lockheed Corp., Burbank, CA, (1973).
- 273. M. Hyatt, op. cit.
- 274. R. Peterson, "Stress Concentration Factors", Wiley, N.Y., (1974) pp. 50, 58, 79.

REFERENCES (Continued)

275. ASTM STD E466-72T, ASTM, Phila., PA.
276. T. Oberg, Metals Progress, (July, 1951).
277. ASTM STP-91-A, ASTM, Phila., PA., (1963).
278. ASTM STP 511, R. Heller (ed.), ASTM, Phila., PA., (1972).
279. R. Little and E. Jabe, "Statistical Design of Fatigue Experiments", Wiley, N.Y., (1975).
280. C. Lipson and N. Sheth, "Statistical Design and Analysis of Engineering Experiments", McGraw-Hill, N.Y., (1973).
281. ASTM STP 137, E. Epremian and R. Mehl (eds.), ASTM, Phila., PA., (1952).
282. G. Dieter, op. cit., 409.
283. D. Voss, op. cit., 83.
284. W. Maenning, Int'l J. of Fract., 11, (1), (1975), 123.
285. W. Maenning and M. Pfender, Engrg. Fract. Mech., 8, (1976), 39.
286. ASTM STD E18-74, Amer. Soc. for Testing and Mat'ls, Phila., PA.
287. ASTM STD B342-63. ASTM, Phila., PA.
288. ASTM STD G34-72, ASTM, Phila., PA.
289. "Aluminum", Vol. 1, K. Van Horn (ed.), ASM, Metals Park, Ohio, (1967), 231.
290. L. Otto, op. cit., 61.
291. R. Sanders et.al., op. cit., 17.
292. G. Dieter, op. cit., 557.
293. A. Cornish and M. Day, J. Inst. of Metals, 97, (1969), 44.
294. A. Kelly and R. Nicholson, Prog. in Mat. Sci., 10, (1965), 151.
295. G. Thomas and J. Nutting, J. Inst. of Metals, 86, (1956-57), 7.
296. A. Kelly, A. Lassila, and S. Sto, Phil. Mag., 4, (8), (1959), 1260.
297. J. Grosskreutz and G. Shaw, loc. cit.
298. D. Vos, op. cit., 56.

REFERENCES (Continued)

299. G. Thomas, "Transmission Electron Microscopy of Metals", Wiley, N.Y., (1962).
300. P. Hirsch et.al., "Electron Microscopy of Thin Crystals", Krieger, N.Y., (1977).
301. "Metals Handbook", Vol. 7, ASM, Metals Park, Ohio, (1972), 251.
302. H. Antes, "Role of Deformation Processing on the Fatigue Behavior of a High Strength Powder Metallurgy Aluminum Alloy", Ph.D. Diss., Drexel Univ., Phila., PA., (1979), 36.
303. J. Lyle and W. Cebulak, loc. cit.
304. "Aluminum", Vol. 1, loc. cit.
305. A. Cornish and M. Day., loc. cit.
306. A. Kelly and R. Nicholson, loc. cit.
307. D. Thompson and S. Levy, op. cit.
308. G. Thomas and J. Nutting, J. Inst. of Mets., 88, (1959-60), 81.
309. "Aluminum", Vol. 1, loc. cit.
310. P. Thackery, J. Inst. of Mets., 96, (1968), 228.
311. J. Holl, J. Inst. of Mets., 97, (1969), 220.
312. D. Thompson, S. Levy and B. Subramanya, Met. Trans., 2, (1971), 1971.
313. "Metals Handbook", Vol. 7, loc. cit.
314. I. Kirman, loc. cit.
315. M. Conserva and P. Fiorini, Met. Trans., 4, (1973), 857.
316. C. Babilon et.al., AFML-TR-73-83, AFML, WPAFB, Ohio, (1973).
317. S. El-Sondani and R. Pelloux, Metallurgy, 6, (1973), 37.
318. P. Adler and R. DeIasi, loc. cit.
319. AFML-TR-74-129, loc cit.
320. C. McAdam and L. Hogan, Acta Met, 23, (1975), 345.
321. J. Staley, ASTM STP 605, (1976), 71.
322. T. Sanders and E. Starke, Met. Trans., 7A, (1976), 1407.

REFERENCES (Continued)

323. T. Sanders et.al., op. cit., 7, 55, 80.
324. A. Kelly and R. Nicholson, loc. cit.
325. D. Thompson and S. Levy, op. cit.
326. R. Sanders et.al., op. cit., 98.
327. M. Hyatt, op. cit.
328. L. Otto, op. cit.
329. W. Truckner et.al., op. cit.
330. "Aluminum Standards and Data", loc. cit.
331. "Mil HDBK 5-C", QQ-A-367H, Dept. of Defense, Wash., D.C., (1976), 4.
332. Metals Progress, 118, (1), (1980), 58.
333. R. Sanders et.al., op. cit., 38, 54.
334. *ibid.*
335. G. Succop et.al., ASTM STP 632, (1977), 177.
336. P. Nehr, "7475 Plate", Alcoa Greenletter, Alcoa Center, New Kensington, PA., (1973), 31.
337. NMAB Publication, 328, loc. cit.
338. R. Brodie and L. Bakow, op. cit.
339. D. Rich, "Evaluation of Slow-Bend Test of Pre-Cracked Charpy Specimen for Fracture Toughness Determination", Internal Report A2210, McDonnell-Douglas Corporation, St. Louis, Mo., (a1973).
340. ASTM STD E399-78, loc. cit.
341. J. Kaufman and H. Hunsicker, ASTM STP 381, (1965), 295.
342. F. McClintock and G. Irwin, *ibid*, 84.
343. R. Hertzberg, op. cit., 289.
344. J. Campbell, W. Berry and C. Feddersen, "Damage Tolerant Design Handbook" Air Force Materials Laboratory/Air Force Flight Dynamics Laboratory, WPAFB, Ohio, (1972).
345. R. Hertberg, op. cit., 262.
346. *ibid.*, 273.

REFERENCES (Continued)

347. J. Kaufman and H. Hunsicker, loc. cit.
348. J. Campbell, W. Berry and C. Feddersen, op. cit.
349. J. Kaufman, P. Schilling and F. Nelson, Met. Engr, Quart., 9, (3), (1969), 39.
350. J. Kaufman, loc. cit.
351. ASTM STP 601, (1976), 178.
352. *ibid.*
353. L. Otto, op. cit.
354. ASTM STP 601, loc. cit.
355. ASTM STD E399-78, loc. cit.
356. A. Tetelman and A. McEvily, op. cit., 79.
357. NMAB Publication 328, op. cit., 127.
358. G. Succop et.al., loc. cit.
359. NMAB Publication 328, op. cit., 10.
360. "Metals Handbook", Vol. 9, loc. cit., 43, 68-89, 249-260.
361. *ibid.*
362. A. Tetelman and A. McEvily, op. cit., 42, 110, 153, 230.
363. R. Hertzberg, op. cit., 248.
364. *ibid.*
365. A. Tetelman and A. McEvily, op. cit.
366. R. Hertzberg, ASM Trans. Quart., (Sept 1963), 319.
367. C. Beachem and R. Pelloux, ASTM STP 381, (1965), 220.
368. A. Tetelman and A. McEvily, op. cit.
369. R. Hertzberg, op. cit.
370. D. Ryder and A. Smale, "Fracture of Solids", D. Drucker and J. Gilman (eds.), Wiley, N.Y., (1963), 258.
371. J. Meakin and N. Petch, *ibid*, 403.

REFERENCES (Continued)

- 372. A. Birkle, R. Wei and G. Pellisser, ASM Trans., 59, (1966), 981.
- 373. D. Passoja and D. Hill, Met. Trans., 5, (1974), 1851.
- 374. W. Truckner et.al., op. cit.
- 375. *ibid.*
- 376. C. Beachem and R. Pelloux, loc. cit.
- 377. T. Kawabata and D. Izumi, Acta Met., 24, (1976), 817.
- 378. C. Beachem, ASM Trans., 56, (1963), 318.
- 379. J. Kaufman, AGARD Conference Proceedings, loc. cit.
- 380. D. Broek, Engrg. Fract. Mechs., 5, (1973), 55.
- 381. G. Hahn and A. Rosenfield, Met. Trans., 6A, (1975), 653.
- 382. R. VanStone and J. Psioda, Met. Trans., 6A, (1975), 668.
- 383. R. VanStone and T. Cox, ASTM STP 600, (1976), 23.
- 384. C. Beachem and R. Pelloux, loc. cit.
- 385. "Metals Handbook", Vol. 9., loc. cit.
- 386. *ibid.*
- 387. S. Singh and M. Flemings, TAIME, 245, (1969), 1811.
- 388. J. Staley, loc. cit.
- 389. R. VanStone and J. Low, ASTM STP 556, (1974), 93.
- 390. D. Voss, op. cit.
- 391. "Metals Handbook", Vol. 9, loc. cit.
- 392. L. Otto, op. cit., 37, 52.
- 393. H. Antes, op. cit., 62, 74.
- 394. A. McEvily and R. Bush, ASM Trans. Quart., 55, (1962), 654.
- 395. AFML-TR-74-129, loc. cit.
- 396. E. Hornbogen and M. Graf, Acta Met., 25, (1977), 877.
- 397. J. Waldman et.al., loc. cit.

REFERENCES (Continued)

- 398. D. Voss, op. cit.
- 399. R. Peterson, op. cit., 9.
- 400. R. Sanders, loc. cit.
- 401. M. Hyatt, op. cit.
- 402. "Aluminum Standards and Data", loc. cit.
- 403. "Mil HDBK 5C", QQ-A-367H, loc. cit.
- 404. P. Mehr, loc. cit.
- 405. H. Moore, "Effect of Size and Notch Sensitivity on Fatigue of Two Metallic Materials", Air Force Tech. Report #5726, WPAFB, Ohio (1948).
- 406. H. Grover, op. cit.
- 407. J. Grant, "Alcoa Alloys 7075-T6 and 7178-T96", Alcoa Greenletter, Alcoa Tech. Center., New Kensington, PA., (1972), 19.
- 408. "Aerospace Structural Materials Handbook", Vol. 3, Dept. of Defense, Wash., D.C., (1979), Code 3207; 8, 26.
- 409. R. Brodie and L. Bakow, op. cit.
- 410. M. Mitchell, "Fundamentals of Modern Fatigue Analysis for Design", McGraw-Hill, N.Y., (1962).
- 411. T. Sanders and J. Staley, loc. cit.
- 412. R. Sanders, loc. cit.
- 413. R. Hertzberg, op. cit., 428.
- 414. A. Tetelman and A. McEvily, op. cit., 381.
- 415. D. Voss, op. cit., 236.
- 416. R. Sanders, loc. cit.
- 417. *ibid.*
- 418. "Mil HDBK-5C", loc. cit., 3-284.
- 419. "Aerospace Structural Materials Handbook", loc. cit.
- 420. R. Hertzberg, op. cit. 430.
- 421. A. Tetelman and A. McEvily, op. cit., 382

REFERENCES (Continued)

- 422. J. Viglione, NADC Report 72154-VT, Warminster, PA., (1973).
- 423. R. Juvinall, "Stress, Strain and Strength", McGraw-Hill, N.Y., (1967), 270.
- 424. M. Hunter and W. Fricke, loc. cit.
- 425. C. Kung and M. Fine, loc. cit.
- 426. T. Sanders and J. Staley, loc. cit.
- 427. M. Hunter and W. Fricke, loc. cit.
- 428. C. Kung and M. Fine, loc. cit.
- 429. T. Sanders and J. Staley, loc. cit.
- 430. D. Voss, op. cit., 62.
- 431. J. Grosskreutz, loc. cit.
- 432. C. Bowles and J. Scjijve, loc. cit.
- 433. D. Broek and C. Bowles, J. Inst. Mets., 92, (1971), 255.
- 434. J. Hyzak, op. cit.
- 435. J. Grosskreutz and G. Shaw, op. cit.
- 436. S. Pearson, Engrg. Fract. Mechs., 7, (1975), 235.
- 437. C. McMahon, loc. cit.
- 438. D. Broek, loc. cit.
- 439. J. Kaufman, AGARD Conference Proceedings, loc. cit.
- 440. R. VanStone and T. Cox, loc. cit.
- 441. ASTM STP 595, (1975), 75.
- 442. AFWAL, WPAFB, Ohio, on-going R&F Contract F33615-79-C-5074 with Pratt and Whitney Aircraft, Florida.
- 443. R. Templin, loc. cit.
- 444. D. Voss, op. cit.
- 445. R. Sanders, loc. cit.
- 446. AFML-TR-74-129, op. cit.

REFERENCES (Continued)

- 447. G. Lutjering and J. Lindekeit, loc. cit.
- 448. A. Tetelman and A. McEvily, op. cit.
- 449. D. Voss, op. cit.
- 450. R. Sanders, loc. cit.
- 451. R. Sanders et.al., loc. cit.
- 452. J. Santner, opl cit.
- 453. P. Irving and C. Beevers, Mat. Sci. and Engrg., 14, (1974), 229.
- 454. T. Sanders et.al., NADC Report, op. cit., 14.
- 455. J. Ryder and J. VanOrden, loc. cit.
- 456. D. Thompson and R. Zinkham, Engrg. Fract. Mechs., 7, (1975), 389.
- 457. W. Truckner et.al., op. cit.
- 458. D. Voss, op. cit., 246.
- 459. ASTM STP 595, (1975), 37.
- 460. A. Lawley and M. Koczak, AFOSR Contract Final Report 77-3247, Wash., D.C., (1980), 9.
- 461. D. Voss, op. cit., 235.
- 462. R. Sanders, loc. cit.
- 463. "Metals Handbook", Vol. 9, loc. cit.
- 464. A. Tetelman and A. McEvily, opl cit., 366.
- 465. ibid.
- 466. J. Santner, AFML-TR-77-78, op. cit.
- 467. "Metals Handbook", Vol. 9, loc. cit.
- 468. P. Forsyth and D. Ryder, Metallurgia, 63, (1961), 117.
- 469. L. Corsetti and D. Duquette, Met. Trans., 5, (1974), 1087.
- 470. M. Nageswararo and V. Gerold, Met. Trans., 7A, (1976), 1847.
- 471. J. Nelson and E. Pugh, Met. Trans., 6A, (1975), 1459.

REFERENCES (Continued)

- 472. G. Garrett and J. Knott, Acta Met., 23, (7), (1975), 841.
- 473. A. Tetelman and A. McEvily, op. cit.
- 474. J. Feeney and J. McMillan and R. Wei, Met. Trans., 1, (1970), 1741.
- 475. J. Santner, Ph.D. Diss., op. cit.
- 476. R. Hertzberg and W. Bills, ASTM STP 600, (1976).
- 477. C. Beachem and D. Meyn, ASTM STP 436, (1968), 59.
- 478. J. Santner and M. Fine, Met. Trans., 7A, (1976), 583.
- 479. J. Santner, AFML-TR-77-78, loc. cit.
- 480. M. Gräf and E. Hornbogen, loc. cit.
- 481. L. Corsetti and D. Duquette, loc. cit.
- 482. T. Kawabata and O. Izumi, loc. cit.
- 483. C Beachem, loc. cit.
- 484. D. Voss, op. cit.
- 485. M. Fine, AFOSR on-going R&D Contract op. cit.
- 486. G. Lutjering and J. Lindekeit, loc. cit.
- 487. J. Feeney, J. McMillan and R. Wei, loc. cit.
- 488. "Metals Handbook", Vol. 9, loc. cit.
- 489. R. Hertzberg, op. cit., 472.
- 490. K. Erhardt, R. Pelloux, N. Grant, AFML-TR-69-85, (1969).
- 491. L. Corsetti and D. Duquette, loc. cit.
- 492. "Metals Handbook", Vol. 9, loc. cit.
- 493. L. Burck, C. Sullivan and C. Wells, Met. Trans., 1, (1970), 1595.
- 494. L. Corsetti and D. Duquette, loc. cit.
- 495. J. Grosskreutz and G. Shaw, op. cit.
- 496. J. Grosskreutz and G. Shaw and D. Benson, AFML-TR-69-121, (1969).
- 497. "Aluminum", Vol. 1, loc. cit., 212.

REFERENCES (Continued)

498. C. Kung and M. Fine, loc. cit.
499. D. Voss, op. cit.
500. L. Corsetti and D. Duquette, loc. cit.
501. M. Hyatt, op. cit.
502. S. Williams and R. Haynes, Powder Metallurgy, 16, (1973), 387.
503. G. Scarich, G. Chanani, V. Petersen and D. Weaver, "P/M of Ti Alloys", Annual Conference Proceeding of the Metallurgical Society of the Aime, Las Vegas, NV, (1980), 103.
504. J. Hyzak, op. cit., 210.
505. AFWAL, WPAFB, Ohio, on-going R&D Contract F33615-80-C-5089 with Materials Research Laboratories, Chicago, IL.
506. R. Hertzberg, op. cit., 476.
507. R. Pelloux, ASM Trans. Quart., 62, (1), (1969), 281.
508. "Metals Handbook", Vol. 9, loc. cit.
509. R. Hertzberg, op. cit., 476.
510. *ibid.*
511. J. Grosskreutz and G. Shaw, op. cit., 25.
512. C. Beachem and R. Pelloux, loc. cit.
513. P. Forsyth, loc. cit.
514. J. McMillan and R. Hertzberg, loc. cit.
515. C. Stubbington, Metallurgia, 68, (1963), 109.
516. C. Laird and C. Feltner, TAIME, 239, (1967), 1074.
517. C. Laird, ASTM STP 415, loc. cit.
518. "Metals Handbook", Vol. 9, loc. cit.
519. J. Goldstein et.al., "Practical Scanning Electron Microscopy", Plenum Press, N.Y., (1975), 149-176.
520. J. Santner and D. Eylon, Met. Trans., 10A, (1979), 846.
521. R. Selines and R. Pelloux, loc. cit.

REFERENCES (Continued)

- 522. J. Goldstein, ASTM STP 557, (1974), 86.
- 523. J. Goldstein et.al., op. cit., 5, 11, 410.
- 524. W. Cebulak et.al., loc. cit.
- 525. C. Beachem and R. Pelloux, loc. cit.
- 526. J. Schijve, loc. cit.
- 527. C. Beachem and R. Pelloux, loc. cit.
- 528. "Metals Handbook", Vol. 9, loc. cit.
- 529. *ibid.*
- 530. R. Hertzberg, op. cit., 468.
- 531. P. Forsyth and D. Ryder, loc. cit.
- 532. P. Forsyth, C. Stubbington, and D. Clark, J. Inst. Metals., (London), 90, (1962), 238.
- 533. C. Beachen and R. Pelloux, loc. cit.
- 534. *ibid.*
- 535. P. Paris, "The Growth of Fatigue Cracks Due to Variations in Load", Ph.D. Diss., LeHigh Univ., Bethlehem, PA., (1962).
- 536. W. Truckner et.al., op. cit.
- 537. D. Voss, op. cit.
- 538. AFML-TR-74-129, op. cit.
- 539. H. Antes, op. cit.
- 540. R. Brodie and L. Bakow, op. cit., 75.
- 541. R. Sanders, et.al., op. cit., 98.
- 542. "Aluminum", Vol. 1, loc. cit.
- 543. D. Thompson and S. Levy, op. cit.
- 544. *ibid.*
- 545. R. Sanders, et.al., op. cit., 98.
- 546. "Aluminum" Vol. 1, loc. cit., 228.

AFWAL-TR-81-4068

REFERENCES (Concluded)

- 547. R. Brown, D. Sprowls and M. Schumaker, ASTM STP 518, (1972), 87.
- 548. H. Naranyan, Boeing Aircraft Co., Seattle, Wash., private communication.
- 549. ASTM STD G34-72, loc. cit.
- 550. "Metals Handbook", Vol. 7, loc. cit.
- 551. C. Babilon et.al., AFML-TR-73-83, AFML, WPAFB, Ohio, (1973), 127.
- 552. P. Blau, AFML-TR-75-43, AFML, WPAFB, Ohio, (1975).
- 553. L. Otto, op. cit.
- 554. R. Brodie and L. Bakow, op. cit., 32.
- 555. *ibid.*

DATE
FILMED
8